Astrophysics and Space Science Proceedings 39

Andrea Miglio
Patrick Eggenberger
Léo Girardi
Josefina Montalbán *Editors*

Asteroseismology of Stellar Populations in the Milky Way

Springer

Astrophysics and Space Science Proceedings

Volume 39

More information about this series at
http://www.springer.com/series/7395

Andrea Miglio • Patrick Eggenberger •
Léo Girardi • Josefina Montalbán
Editors

Asteroseismology of Stellar Populations in the Milky Way

Springer

Editors
Andrea Miglio
School of Physics and Astronomy
University of Birmingham
Edgbaston, Birmingham
United Kingdom

Patrick Eggenberger
Observatoire de Genève
University of Geneva
Sauverny
Switzerland

Léo Girardi
Osservatorio Astronomico di Padova
INAF
Padova
Italy

Josefina Montalbán
Institut d'Astrophysique et de Géophysique
University of Liège
Liège
Belgium

ISSN 1570-6591
ISBN 978-3-319-10992-3
DOI 10.1007/978-3-319-10993-0
ISSN 1570-6605 (electronic)
ISBN 978-3-319-10993-0 (eBook)
Springer Cham Heidelberg New York Dordrecht London

Library of Congress Control Number: 2014957645

Printed on acid-free paper

Springer is part of Springer Science+Business Media (www.springer.com)

Acknowledgements

We would like to heartily thank Annie Baglin, Jørgen Christensen-Dalsgaard and our sponsors CoRoT and SAC for the financial support that made this workshop, and the publication of this volume, possible.

We are grateful to the *Sexten Center for Astrophysics* and to Mrs Deconi, who helped us organise the workshop in such an enchanting place.

Many, many thanks to all the participants for their engagement in the discussions, and for having agreed to make their contributions available online[1] and "on paper" in this volume. A particular thanks goes to Arlette Noels, Angela Bragaglia, Bertrand Plez, Nicolas Grevesse, and Joris De Ridder for having actively chaired the discussion sessions during the workshop, and then reported questions & answers in these proceedings.

Andrea Miglio
Patrick Eggenberger
Léo Girardi
Josefina Montalbán

[1] http://www.sexten-cfa.eu/images/stories/conferenze2013/asteroseism/Asteroseismology_final.pdf.

Contents

List of Participants

Friedrich Anders Leibniz-Institut für Astrophysik Potsdam (AIP), Potsdam, Germany fanders@aip.de

Martin Asplund Australian National University, Canberra, Australia martin@mso.anu.edu.au

Diego Bossini University of Birmingham, Birmingham, UK diego.bossini@gmail.com

Angela Bragaglia INAF Bologna, Bologna, Italy angela.bragaglia@oabo.inaf.it

Alessandro Bressan SISSA, Trieste, Italy alessandro.bressan@oapd.inaf.it

Karsten Brogaard Aarhus University, Aarhus, Denmark kfb@phys.au.dk

Carla Cacciari INAF Bologna, Bologna, Italy carla.cacciari@oabo.inaf.it

Luca Casagrande Australian National University, Canberra, Australia luca@mso.anu.edu.au

Corinne Charbonnel Université de Genève, Sauverny, Switzerland Corinne.Charbonnel@unige.ch

Cristina Chiappini Leibniz-Institut für Astrophysik Potsdam (AIP), Potsdam, Germany cristina.chiappini@aip.de

Eric Depagne South African Astronomical Observatory, Cape Town, South Africa eric@saao.ac.za

Joris De Ridder KU Leuven, Leuven, Belgium Joris.DeRidder@ster.kuleuven.be

Patrick Eggenberger Université de Genève, Sauverny, Switzerland Patrick.Eggenberger@unige.ch

Courtney Epstein The Ohio State University, Columbus, OH, USA epstein@astronomy.ohio-state.edu

Ken Freeman Australian National University, Canberra, Australia kcf@mso.anu.edu.au

Sara Alejandra Sans Fuentes KU Leuven, Leuven, Belgium alejandra@ster.kuleuven.be

Léo Girardi INAF Osservatorio di Padova, Padova, Italy leo.girardi@oapd.inaf.it

Gerry Gilmore Cambridge University, Cambridge, UK gil@ast.cam.ac.uk

Nicolas Grevesse Université de Liège, Liège, Belgium Nicolas.Grevesse@ulg.ac.be

Jennifer Johnson The Ohio State University, Columbus, OH, USA jaj@astronomy.ohio-state.edu

Nadège Lagarde University of Birmingham, Birmingham, UK nadege.lagarde@unige.ch

Sara Lucatello INAF Padova, Padova, Italy sara.lucatello@oapd.inaf.it

Paola Marigo Universita di Padova, Padova, Italy paola.marigo@unipd.it

Andrea Miglio University of Birmingham, Birmingham, UK miglioa@bison.ph.bham.ac.uk

Josefina Montalbán Université de Liège, Liège, Belgium J.Montalban@ulg.ac.be

Thierry Morel Université de Liège, Liège, Belgium morel@astro.ulg.ac.be

Arlette Noels Université de Liège, Liège, Belgium arlette.noels@ulg.ac.be

Bertrand Plez Université de Montpellier, Montpellier, France bertrand.plez@univ-montp2.fr

Ennio Poretti INAF Brera-Merate, Merate, Italy ennio.poretti@brera.inaf.it

Sofia Randich INAF Arcetri, Florence, Italy randich@arcetri.astro.it

Thaise Rodrigues INAF Padova, Padova, Italy thaise.rodrigues@oapd.inaf.it

Maurizio Salaris Liverpool John Moores University, Liverpool, UK ms@astro.livjm.ac.uk

Mathias Schultheis Nice Observatory, Nice, France mathias@obs-besancon.fr

Victor Silva Aguirre Aarhus University, Aarhus, Denmark victor@phys.au.dk

Dave Soderblom Space Telescope Science Institute, Baltimore, MD, USA drs@stsci.edu

Dennis Stello University of Sydney, Sydney, Australia stello@Physics.usyd.edu.au

Anders Thygesen Zentrum fur Astronomie, Heidelberg, Germany a.thygesen@lsw.uni-heidelberg.de

Marica Valentini Université de Liège, Liège, Belgium valentini@astro.ulg.ac.be

Simone Zaggia INAF Padova, Padova, Italy simone.zaggia@oapd.inaf.it

Gail Zasowski The Ohio State University, Columbus, OH, USA gail.zasowski@gmail.com

Part I
Introduction

Ages of Stars: Methods and Uncertainties

David R. Soderblom

Abstract Estimating ages for stars is difficult at best, but Galactic problems have their own requirements that go beyond those for other areas of astrophysics. As in other areas, asteroseismology is helping, and in this review I discuss some of the general problems encountered and some specific to large-scale studies of the Milky Way.

1 Why Care About Ages?

Much of what astronomers do in studying stars and our Galaxy explicitly or implicitly involves evolutionary changes: how things change with time, and the sequence of events. Yet time is not really a direct agent of change in stars, it is more a medium in which gradual changes occur. Because time is not a direct agent it leaves no direct indicators and we are left estimating age in mostly indirect—and so inexact—ways.

The problem is illustrated by considering the Sun. It is the only star for which we have a fundamental age, one for which all the physics is fully understood and all needed measurements can be made, and its age of $4{,}567 \pm 1 \pm 5$ Myr is both precise and exact. But the Sun itself tells us nothing of its age, and it is only from having Solar System material that we can analyze in the laboratory that such an exquisite result comes. For no other star can we do likewise.

Here is a scheme (from Soderblom 2010) for thinking about stellar ages, with five quality levels:

1. **Fundamental** age-dating methods, in which the physics is well understood and all the necessary quantities can be measured. The only fundamental age is that for the Sun just described.
2. **Semi-fundamental** methods that use well-understood physics, but which require some assumptions because not all the needed quantities are accessible to

D.R. Soderblom (✉)
Space Telescope Science Institute, Baltimore, MD, USA
e-mail: drs@stsci.edu

A. Miglio et al. (eds.), *Asteroseismology of Stellar Populations in the Milky Way*,
Astrophysics and Space Science Proceedings 39,
DOI 10.1007/978-3-319-10993-0_1

observation. These methods include nucleocosmochronology, for very old stars, and kinematic traceback, for young groups.
3. **Model-dependent** methods that, like most of stellar astrophysics, infer ages from detailed stellar models that are calibrated against the Sun. Model-dependent methods include fitting the loci of stars in clusters (especially the main sequence turn-off) and detecting the lithium depletion boundary (at the transition from stars to brown dwarfs for clusters and groups of stars), as well as isochrone placement and asteroseismology for individual objects.
4. **Empirical** methods that use an observable quantity such as rotation, activity, or lithium abundance that is seen to change with age but for which the physical mechanisms are not understood. Empirical methods are calibrated against model-dependent ages, generally by observing stars in open clusters. The paucity of open clusters older than $\sim 1/2$ Gyr makes calibrating empirical indicators problematic.
5. **Statistical** methods that rely on broad trends of quantities with age.

Before going further, I would like to narrow the discussion to methods relevant to Galactic problems as well as methods that produce useful results. First, in this context we are not interested in very young stars and so kinematic traceback, the lithium depletion boundary, and lithium depletion in general will be ignored. For a review about ages of young stars, see Soderblom et al. (2013). Second, nucleocosmochronology in principle is ideal for age-dating the very oldest stars in the Galaxy. It uses observations of isotopes of U and Th with long half-lives, but assumptions must be made about the starting abundances, generally done from other r-process elements. The results often differ by factors of two for the same star, and, in addition, the method needs excellent spectra of very high resolution to detect the weak U/Th features and so has been applied to only a handful of stars (Soderblom 2010). Third, there have been statistical studies of age-metallicity and age-velocity relations for the Galaxy, but they are at best very noisy relations that are hard to apply to individual objects, and in some cases their reality has been called into question. They will not be discussed further here.

2 Ages for Galactic Studies

There are both some special problems and potential advantages when it comes to estimating ages in order to understand the nature of our Galaxy. These naturally break down into two regimes based on the size scale being considered. In both cases one wishes to work with large samples of stars that can be selected with completeness or at least for which the biases are known. I will discuss small-scale samples (the solar neighborhood) as well as Galaxy-wide samples.

2.1 The Solar Neighborhood

Different studies use various concepts of "solar neighborhood" that depend on context. Here I will consider a radius of $\sim$ 100 pc. Within that distance, extinction and reddening are largely negligible; also there are only a very few clusters, and so field stars dominate. Solar-type stars (F, G, and K dwarfs) make an especially good population for studying this nearby portion of the Galaxy because they are reasonably bright and so identifiable within this sphere, and numerous enough to form a statistically useful sample. Also, the Sun has a main sequence lifetime of about 10 Gyr, and so G dwarfs are present from all epochs of star formation in the thin disk at least, and in the thick disk as well for late-G stars. Because they are similar to the Sun and have many narrow lines, G dwarfs yield abundances that are both more precise and more exact than for other stars. G dwarfs are amenable to age determinations in several ways. In particular, rotation and activity are known to decline with age, the problem being calibrating the relations, as described below.

The *Hipparcos* data make it easy to identify the G dwarfs within 50 pc, for instance, and there are about 3,000 stars from F8V to K2V, enough to make a useful statistical sample. Because *Hipparcos* was brightness limited, there are some biases in its sample: The sample favors binaries, and the completeness horizon diminishes in going to later spectral types, leading to smaller sample sizes.

2.2 The Galaxy as a Whole

If we want to delineate the structure of our Galaxy we need to use inherently luminous stars that occur everywhere and which can be seen at the far reaches, even when extincted. Red giants and stars on the asymptotic giant branch (AGB) fit that description well. In addition, for Galactic studies it is not necessary to always determine the ages of an entire sample, as one would like to do for, say, exoplanet hosts. Instead, Galactic work can be done in bulk with a finite failure rate as long as biases are known and can be controlled for. Finally, Galactic studies ideally need to determine stellar ages on an industrial scale, meaning 10,000 or more.

For these evolved, luminous stars, different age indicators are needed compared to the solar neighborhood sample. Rotation and activity are useless, as is isochrone placement because all the red giants pile up into a clump. But, as we will see, asteroseismology is very promising.

At intermediate distances (up to a few kpc), intermediate-mass stars can be helpful. Stars with main-sequence lifetimes of $\sim$2–4 Gyr (i.e., $\sim$1.5–2$M_{\odot}$) are promising because many are known and they evolve quickly enough to be placed on isochrones well.

3 Methods for Solar-Type Stars

The available methods of age-dating for solar-type stars are discussed in detail in Soderblom (2010) and here I will present only a brief synopsis with recent advances, particularly from asteroseismology.

3.1 Rotation and Activity

The trend of declining rotation with age for stars like the Sun has been known for some time (Skumanich 1972) and at least has a general scenario to explain it, if not a full physical model. In that scenario, it is the fact that the Sun carries energy through convection in its outer layers that leads to essentially all the aspects of the Sun that make it and similar stars "solar-like," and which make the Sun interesting. Convection and rotation—especially differential rotation—in the Sun's ionized outer layers interact to create a dynamo that regenerates a magnetic field. This field can grip an ionized stellar wind beyond the stellar surface and thereby transmit angular momentum to it, leading to spindown. Moreover, more rapid rotation produces a stronger magnetic field and thus more rapid spin down, leading to convergence in the rotation rates of a coeval sample that starts with a spread in initial angular momenta.

This convergence is seen, but it takes at least $\sim$ 500 Myr (i.e., the age of the Hyades) to occur at $\sim 1 M_{\odot}$ and longer for lower masses. Until that convergence occurs, each star has its own rotational history and the large scatter seen among young stars in clusters makes it impossible to get an age from rotation.

Past the point of convergence it is assumed that stars obey the $\tau^{-1/2}$ relation (τ = age) of Skumanich (1972), but, in fact, we have only the Sun as a well-defined anchor point and so the relation is poorly calibrated. Adding additional uncertainty, it is possible for a star's companion to add angular momentum late in its life if, say, a close-in giant planet comes close enough to a star to have tidal effects or to even be consumed by the star, adding the orbital angular momentum of the planet to the rotation of the star, causing significant spin-up. Thus it is possible for some old stars to masquerade as young stars without revealing their true nature.

The situation for activity is worse because activity is an observed manifestation of the magnetic field, which is an indirect consequence of rotation. In addition, activity varies to some degree on all time scales, from flares and faculae, to rotational modulation by spots, to long-term activity cycles. As with rotation, the inherent spread in activity among young stars is large. It is possible to construct a mean activity-age relation (Soderblom et al. 1991) that looks good, but averages can hide a lot of inherent noise.

Activity can be fairly easy to measure, requiring spectra with $R \sim$4,000 for the Ca II H and K lines, for instance, making it feasible to get data for many stars quickly. It is the interpretation of activity that is difficult and uncertain.

X-rays are another manifestation of activity, one with an especially high-contrast signature, but generally x-rays are only detected for the most active stars, which is to say those which are on the ZAMS or younger or which are in close binaries.

In summary, both rotation and activity are flawed as age indicators. The better of the two is rotation, but rotation versus age remains poorly calibrated for older stars, and there is no calibration at all for metal-poor stars. In addition, systematic effects can skew rotation rates, and it is not always possible to detect a rotation period for a star, even with very high quality photometry.

3.2 Isochrone Placement

Isochrones are loci of constant age computed from stellar models. Those models are fundamentally calibrated against the Sun, with further refinement from matching details of cluster H-R diagrams. Fitting isochrones to clusters to determine an age involves using a distribution of stars of many masses, even for sparse clusters or groups. Even then, fitting the turn-off region can be challenging because there may be only a few stars or the presence of binaries among them may be unappreciated.

One works with less information in placing individual stars in HRDs and so the uncertainties are greater. As an example, Jørgensen and Lindegren (2005) showed a synthetic study of isochrone placement for F stars. They took stars of a variety of masses and ages from about $1.2M_{\odot}$ on up, added realistic estimates of errors in luminosity and temperature, and then tested how well the original ages could be recovered. A significant problem in using isochrones is that they are not evenly spaced in the HRD, leading to biased results. Of the methods they tried, that using Bayesian techniques worked the best because that takes account of prior information about isochrone spacing. For fairly well-evolved stars above $1.2M_{\odot}$, the age errors were as small as 20 %, but were more typically 50 % for most stars. These are large for individual stars but could be acceptable for ensembles where averaging will reduce the uncertainty. Another limitation of the Bayesian method is that one ends up with a probability distribution function (PDF), not a specific value. In many cases the PDF is single-peaked, but there are instances when the PDFs have multiple peaks or give only upper- or lower limits, and, depending on how those are used they can distort or bias an average.

Isochrone placement remains the most favored technique for more massive stars ($> 1.5M_{\odot}$, say), where the relative errors are modest.

3.3 Asteroseismology

For individual stars, asteroseismology offers great promise as a way of determining precise ages, particularly for older stars. Asteroseismology is essentially like using isochrones, but with significantly better physical constraints. When

asteroseismology works, it works very well indeed, yielding ages as precise as 5 %. But for the method to work one must detect the oscillations in the first instance, and that requires special assets in almost all cases. Prior to CoRoT and *Kepler*, about half a dozen solar-type stars had asteroseismic ages, and each required coordinated observations at several observatories to avoid the problems caused by limited time sampling at just one facility (the diurnal side lobes in the power spectrum). CoRoT and *Kepler* have changed that, but only for stars in their specific fields.

In other words, we do not have a ready means to undertake asteroseismology for any star we'd like. Additionally, even with *Kepler* and its high-quality data one does not always detect the oscillations because the amplitudes are just too low. Many solar-type stars in the *Kepler* field were observed at the one-minute cadence for asteroseismic analysis, but those actually detected tend to be systematically more massive than the Sun and are evolved off the ZAMS. There are a few detections of oscillations at and below $1\,M_{\odot}$, but the number is very small.

Most asteroseismic analysis has been boutique, in the sense that models are calculated for individual stars, one at a time, a labor-intensive process. Galactic studies in particular will require ages at wholesale ($\sim 10^3$–10^4 stars) or even industrial scales ($> 10^5$). An attempt has been made to analyze *Kepler* data at the retail ($\sim$ 100 star) level (Chaplin et al. 2014), where a pipeline and scaling relations are used in place of individual tailoring. In that case age errors were 25–35 %, with a significant portion coming from inherent differences in different stellar models, even though these stars are all similar to the Sun.

4 Age-Dating Evolved Stars

Evolved stars are attractive for Galactic studies because they can be seen at great distances. They are also favored for determining fairly precise ages. Red giants exhibit solar-like oscillations that arise from the same mechanism as in the Sun, but the amplitudes are much larger and the periods longer. For example, the most luminous evolved stars on the asymptotic giant branch (AGB) have amplitudes up to $\sim$ 1 mmag.

For these stars, detection of the oscillations effectively indicates the mass, and from the mass one can get the age from the known main sequence lifetime. A large-scale survey at high photometric precision would be needed to detect the oscillations.

5 Prospects for Improvements

As noted, asteroseismology offers great promise in the area of stellar ages. When the oscillations can be detected, an analysis using models appropriate to the star can yield ages good to 5–10 % in favorable cases. This works especially well for older

stars, which is ideal since we lack old clusters to calibrate empirical age indicators against. In particular, stars in the *Kepler* field with detected oscillations may be very helpful, even if there are only a few of them. Oscillations should be easily detectable for evolved stars, at least with space-based data, and those are especially helpful for studying the Galaxy. The main limitation to seismology is simply being able to obtain data of the necessary quality for the star or stars that one would like.

The detected oscillations of solar-type stars are p (pressure) modes. Such stars also expected to have g (gravity) modes in their deep interiors. The g modes penetrate the stellar core, the one part of the star that is a true chronometer. So far all attempts to detect the Sun's g modes have failed, although some evolved stars in the *Kepler* data exhibit mixed modes because there are g-mode frequencies that are at or close to p-mode frequencies. In those cases the detected modes yield very precise ages. The ability to consistently detect g modes in stars would enable consistently precise ages.

Gaia won't get parallaxes for every star in our Galaxy, but it certainly should determine extremely accurate distances for all the clusters out to ~ 2 kpc, and there are many of those with a broad range of inherent properties such as metallicity. In so doing, the Gaia data essentially remove all distance ambiguity, and that greatly reduces uncertainty about extinction and reddening. These clusters will enable much more stringent tests of stellar models because of the range of composition available, which should at least range from [Fe/H] $= -1$ to $+0.4$. Also, by getting such good distances to clusters, Gaia may indirectly help us understand helium in stars much better than we do now.

Gaia will greatly reduce uncertainty in luminosity for individual stars out to at least $\sim$ 1 kpc, and that will improve ages from isochrone placement. However, errors in $T_{\rm eff}$ have been difficult to get below 50 K, and at that level the temperature error dominates the uncertainty in age. A good way is needed to measure $T_{\rm eff}$ more precisely and reliably.

References

Chaplin, W. J., Basu, S., Huber, D., et al. 2014, ApJS, 210, 1
Jørgensen, B. R. & Lindegren, L. 2005, A&A, 436, 127
Skumanich, A. 1972, ApJ, 171, 565
Soderblom, D. R. 2010, ARA&A, 48, 581
Soderblom, D. R., Duncan, D. K., & Johnson, D. R. H. 1991, ApJ, 375, 722
Soderblom, D. R., Hillenbrand, L. A., Jeffries, R. D., Mamajek, E. E., & Naylor, T. 2013, ArXiv e-prints

Solar-Like Oscillating Stars as Standard Clocks and Rulers for Galactic Studies

Andrea Miglio, Léo Girardi, Thaíse S. Rodrigues, Dennis Stello, and William J. Chaplin

Abstract The CoRoT and *Kepler* space missions have detected oscillations in hundreds of Sun-like stars and thousands of field red-giant stars. This has opened the door to a new era of stellar population studies in the Milky Way. We report on the current status and future prospects of harvesting space-based photometric data for ensemble asteroseismology, and highlight some of the challenges that need to be faced to use these stars as accurate clocks and rulers for Galactic studies.

1 Introduction

Prior to the advent of space-based photometric missions such as *Kepler* and CoRoT, age estimation of stars had to rely on constraints from their surface properties only. A severe limitation of such an approach applies in particular to objects in the red-giant phase: that stars of significantly different age and distance end up sharing very similar observed surface properties making it extremely hard to, for example, map and date giants belonging to the Galactic-disc population. That situation has now changed thanks to asteroseismology, with the detection of solar-like pulsations in hundreds of dwarfs and thousands of red giants observed by CoRoT and *Kepler*. The pulsation frequencies may be used to place tight constraints on the fundamental

A. Miglio (✉) • W.J. Chaplin
School of Physics and Astronomy, University of Birmingham, Birmingham, UK

Department of Physics and Astronomy, Stellar Astrophysics Centre (SAC), Aarhus University, Aarhus, Denmark
e-mail: a.miglio@bham.ac.uk

L. Girardi • T.S. Rodrigues
INAF—Osservatorio Astronomico di Padova, Vicolo dell'Osservatorio 5, Padova, Italy

D. Stello
Sydney Institute for Astronomy (SIfA), School of Physics, University of Sydney, Sydney, NSW, Australia

Department of Physics and Astronomy, Stellar Astrophysics Centre (SAC), Aarhus University, Aarhus, Denmark

A. Miglio et al. (eds.), *Asteroseismology of Stellar Populations in the Milky Way*,
Astrophysics and Space Science Proceedings 39,
DOI 10.1007/978-3-319-10993-0_2

stellar properties, including radius, mass, evolutionary state, internal rotation and age (see e.g. Chaplin and Miglio 2013 and references therein).

There are several important reasons why asteroseismic data, and in particular data on red giants, offer huge potential for populations studies. First, G and K giants are numerous. They are therefore substantial contributors by number to magnitude-limited surveys of stars, such as those conducted by CoRoT and *Kepler*. Moreover, the large intrinsic oscillation amplitudes and long oscillation periods mean that oscillations may be detected in faint targets observed in the "standard" long-cadence modes of operation of both CoRoT and *Kepler*. Second, with asteroseismic data in hand red giants may be used as accurate distance indicators probing regions out to about 10 kpc. As in the case of eclipsing binaries, the distance to each red giant may be estimated from the absolute luminosity, which is obtained from the asteroseismically determined radius and $T_{\rm eff}$. This differs from the approach adopted to exploit pulsational information from classical pulsators, notably Cepheid variables, where the observed pulsation frequency leads to an estimate of the mean density only and hence additional calibrations and assumptions are needed to yield an estimated distance.

Third, seismic data on red-giant-branch (RGB) stars in principle provide robust ages that probe a wide age range. Once a star has evolved to the RGB, its age is determined to a first approximation by the time spent in the core-hydrogen burning phase, which is predominantly a function of mass and metallicity. Hence, the estimated masses of red giants provide important constraints on age. The CoRoT and *Kepler* giants cover a mass range from $\simeq 0.9$ to $\simeq 3\,{\rm M}_{\odot}$, which in turn maps to an age range spanning ~ 0.3 to ~ 12 Gyr, i.e., the entire Galactic history.

Sun-like stars with detectable oscillations span a much more limited distance than the giants. When individual oscillation frequencies are available, however, the age determination of such stars can rely on the use of diagnostics specific to the conditions of the star's core, which can be used as proxies for the evolutionary state on the main sequence, and hence the absolute age (e.g. Christensen-Dalsgaard 1988; Roxburgh and Vorontsov 2003).

We are still in the infancy of using solar-like oscillators as probes of the Milky Way's properties, and the field is evolving so rapidly that any attempts at reviewing the status would be quickly outdated. In what follows we will therefore briefly summarise the asteroseismic data currently available, and which data will be available in the next decade, and flag some of the challenges that need to be faced in *ensemble asteroseismology*, i.e. the study of stellar populations including constraints from global, resonant oscillation modes.

2 Harvesting Data for Ensemble Seismology

The full exploitation of the available CoRoT and *Kepler* asteroseismic data is far from complete, both in terms of the extraction of seismic parameters and the characterisation of the observed stellar populations.

Only two CoRoT long-observational runs have been analysed so far (Hekker et al. 2009; Mosser et al. 2011; Miglio et al. 2013). Data collected in 15 additional runs, crucially exploring stellar populations at different galactocentric radii, are yet to be exploited. Figure 1 shows the number of stars targeted in CoRoT's observational campaigns in the colour-magnitude range expected to be populated by red giants with detectable oscillations. The analysis of these data is currently ongoing.

The full mining of the "nominal mission" *Kepler* data is also in its early stages. The scientific community is now just beginning to tackle the detailed fitting of individual oscillation modes. Multi-year data are now available on about one hundred solar-type stars and ∼20,000 red giants (Hekker et al. 2011; Stello et al. 2013).

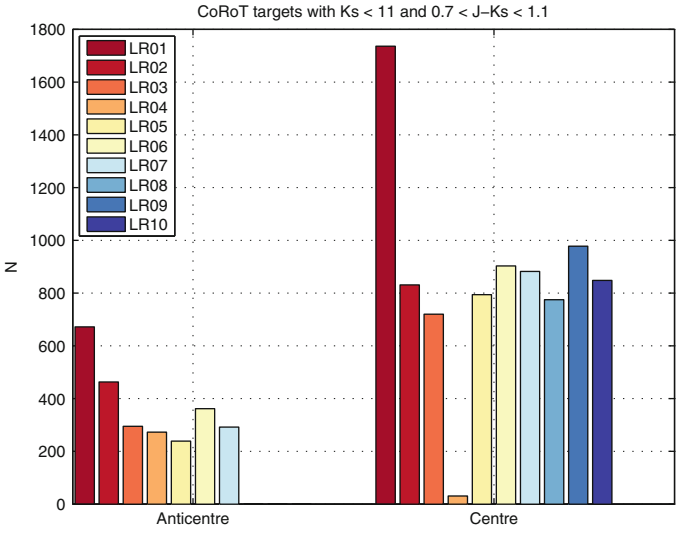

Fig. 1 Number of stars observed in CoRoT's exofields in the colour-magnitude range expected to be populated by red giants with detectable oscillations ($0.7 < J - K_s < 1.1, K_s < 11$). The analysis of the first two observational runs led to the detection of oscillations in about 1,600 (LRc01) and 400 (LRa01) stars, as reported in Hekker et al. (2009) and Mosser et al. (2010). The varying number of stars per field reflects different target selection functions used, the failure of two CCD modules, as well as the different stellar density in each field (Color figure online)

The outlook for the collection of new data in the near future also looks remarkably bright. In addition to CoRoT and *Kepler*, three more missions will supply asteroseismic data for large samples of stars: the re-purposed *Kepler* mission, K2 (Howell et al. 2014) and, in a few year's time, the space missions TESS[1] (Ricker 2014) and PLATO 2.0[2] (Rauer et al. 2013).

Although *Kepler* ceased normal operations in June 2013, we can now look forward to a new mission using the *Kepler* spacecraft and instrument. K2 has started performing a survey of stars in the ecliptic plane, with each pointing lasting around 80 days. The potential of K2 to study stellar populations is even greater than for CoRoT and *Kepler*, since regions of the sky near the ecliptic contain bright clusters and will also make it possible to map the vertical and radial structure of the Galaxy (see Fig. 2). The importance of this line of research was acknowledged by it being listed as a potential mission highlight by Howell et al. (2014). K2 was recently approved by the NASA senior review, and observations of ∼8,600 giants in the first full science campaign has already been made, and 5,000 more will be observed in Campaign 2. Future K2 observations may also provide constraints on giants belonging to the Galactic bulge (Campaign 9) and, crucially, in the globular cluster M4 which would serve as a much needed test for seismic scaling relations in the metal poor regime (Epstein et al. 2014) .

The all-sky mission TESS (Ricker 2014) will also significantly add to the harvest of bright Sun-like stars in the solar neighborhood, and is expected to be launched in 2017. Thanks to the early achievements with CoRoT and *Kepler*, Galactic archeology has now been included as one of the major scientific goals of ESA's medium-class mission PLATO 2.0 (see Rauer et al. 2013), which will supply seismic constraints for stars over a significantly larger fraction of the sky (and volume) compared to CoRoT, *Kepler*, and K2. An illustration of PLATO 2.0's observational strategy is presented in Fig. 3. By detecting solar-like oscillations in ∼85,000 nearby dwarfs and an even larger number of giants, PLATO 2.0 will provide a revolutionary complement to Gaia's view of the Milky Way. PLATO 2.0 is planned for launch by 2024.

[1] http://tess.gsfc.nasa.gov/.

[2] http://sci.esa.int/plato.

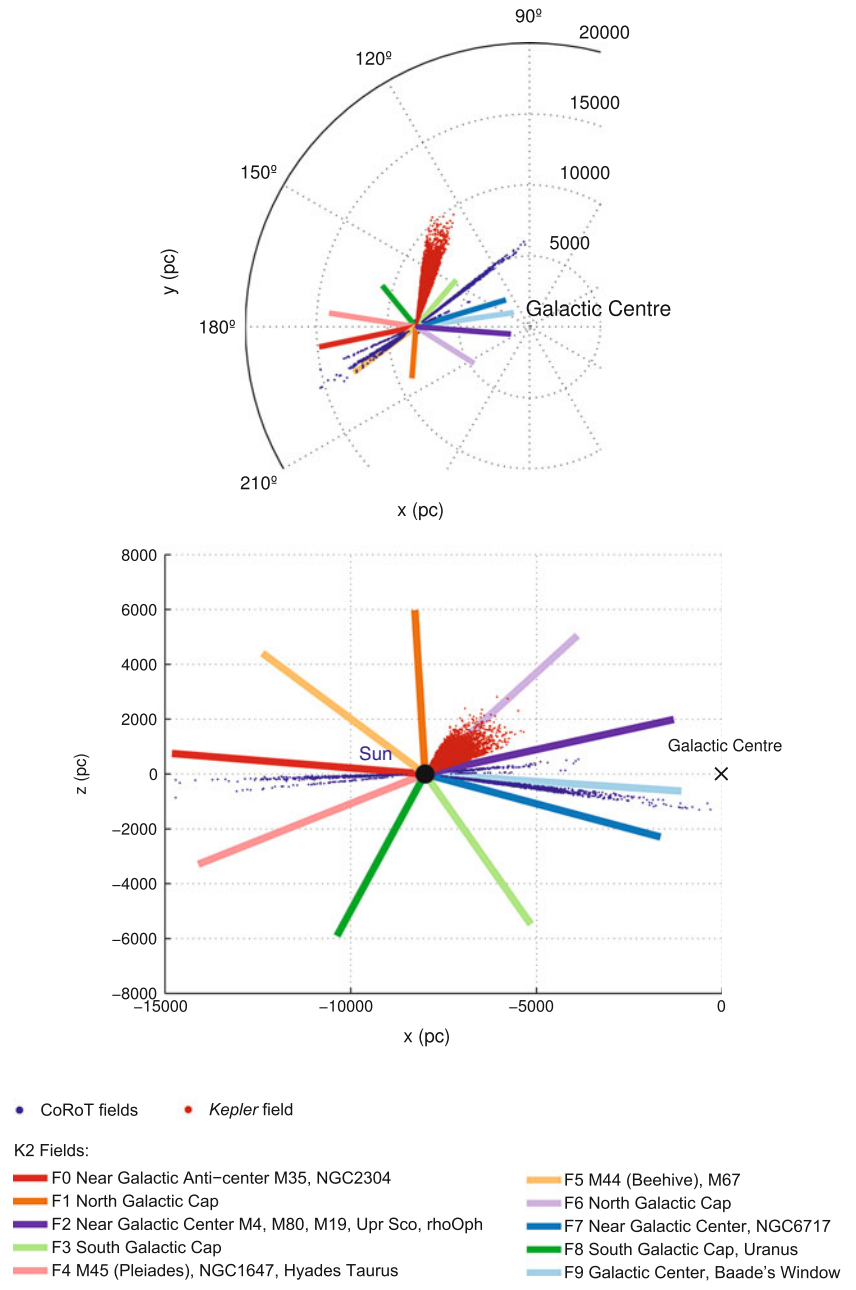

Fig. 2 Location in the Galaxy of stars with seismic constraints observed by CoRoT, *Kepler* and in the fields which will be monitored by K2

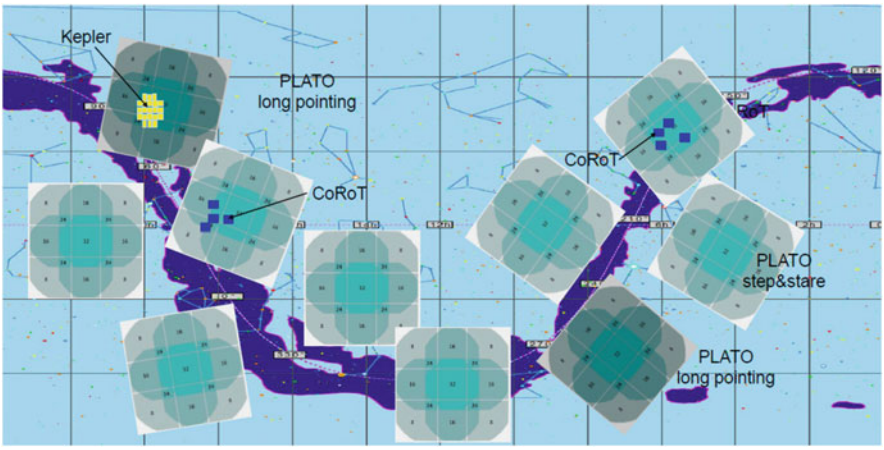

Fig. 3 Schematic comparison of PLATO 2.0, CoRoT and *Kepler*'s fields of view and observational strategy. With a combination of short (step-and-stare) and long duration pointings PLATO 2.0 will cover a large fraction of the sky. Note that the final locations of long and step-and-stare fields will be defined after mission selection and are drawn here for illustration only. Figure taken from http://www.oact.inaf.it/plato/PPLC/Science.html

3 From Precise to Accurate Clocks and Rulers

Seismic data analysis and interpretation techniques have undergone a rapid and considerable development in the last few years. However, they still suffer from limitations, e.g.:

- determination of individual oscillations mode parameters has been carried out for a limited set of Sun-like stars, and for only a handful of red giants;
- stellar mass and radius estimates in most cases are based on approximated scaling relations of average seismic properties ($\Delta\nu$ and $\nu_{\max}$), under-exploiting the information content of oscillation modes; and:
- systematic uncertainties on the inferred stellar properties due to limitations of current stellar models have not yet been quantified. This is crucial for age estimates, which are inherently model dependent.

Here, we mention some of the key sources of uncertainty on current estimates of stellar age and how, in some cases, we hope to make progress. We focus on evolved stars, and refer to Lebreton and Goupil (2014), and references therein, for the case of main-sequence stars.

The age of low-mass red-giant stars is largely determined by the time spent on the main sequence, hence by the mass of the red giant's progenitor. Knowledge of the star's metallicity is also key to determining the age, but we will assume in the

following that metallicities will be available thanks to spectroscopic constraints (see the contributions by Morel, Johnson, Epstein, Plez & Grevesse). With data on solar-like oscillations we can indeed estimate the mass of giants. What is challenging, however, is that if we aim at determining ages to 30 % or better, then we need to be able to the determine masses with an accuracy better than 10 %. Testing the accuracy of the asteroseismic mass scale to 10 % or better is very much "work in progress".

An example of possible systematic biases concerning the mass determination are departures from a simple scaling of $\Delta\nu$ with the square root of the stellar mean density (see e.g. White et al. 2011; Miglio et al. 2012, 2013; Belkacem et al. 2013). Suggested corrections to the $\Delta\nu$ scaling are likely to depend (to a level of few percent) on the stellar structure itself. Moreover, the average $\Delta\nu$ is known to be affected (to a level of $\sim$ 1 % in the Sun) by our inaccurate modelling of near-surface layers.

A way forward would be to determine the star's mean density by using the full set of observed acoustic modes, not just their average frequency spacing. This approach was carried out in at least two RGB stars (Huber et al. 2013; Lillo-Box et al. 2014), and led to determination of the stellar mean density which is $\sim$5–6 % higher than derived from assuming scaling relations, and with a much improved precision of $\sim$ 1.4 %.

While a relatively simple mass-age relation is expected for RGB stars, the situation for red-clump RC or early asymptotic-giant-branch (AGB) stars is of course different. If stars undergo a significant mass loss near the tip of the RGB, then the mass-age relation is not unique (for a given composition and input physics), since the mass observed at the RC or early-AGB stage may differ from the initial one. An extreme case is depicted in Fig. 4, where we compare the posterior

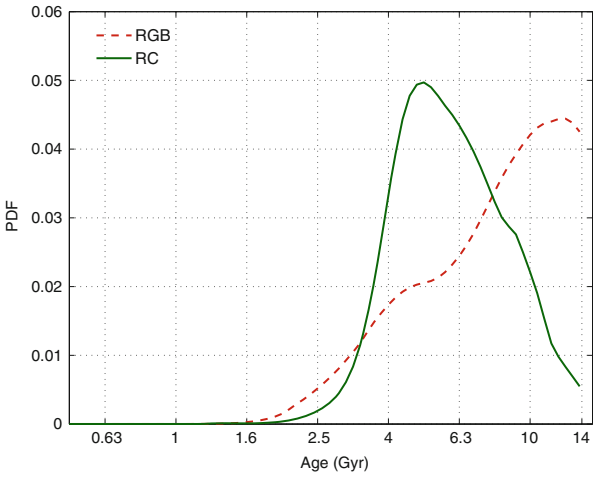

Fig. 4 Example of probability distribution function of age for a star with $M = 0.9\,M_\odot$ and $R = 10\,R_\odot$ which is assumed to be either in the red-giant-branch phase (*dashed line*) or in the core-He burning phase (*solid line*). Stellar evolutionary tracks used to determine the age assume that a significant mass loss occurs following Reimers' (Reimers 1975) prescription and a mass-loss efficiency parameter $\eta = 0.4$ (Color figure online)

probability density function of age for a synthetic star of 0.9 $M_\odot$ which we assume to be either on the RGB or in the RC. If significant mass loss occurs, the 0.9 $M_\odot$ RGB star would have to be significantly older than if it were on in the RC phase. In this context, the characterisation of populations of giants will benefit greatly from estimations of the period spacings of the observed gravity modes, which allows a clear distinction to be made between RGB and RC stars (Bedding et al. 2011), and early-AGB stars (Montalbán and Noels 2013). Knowledge of the efficiency of mass loss is however still needed to determine accurate ages of red/clump stars.

Other uncertainties on the input physics may affect main-sequence lifetimes, hence the age of red giants (see Noels and Bragaglia, this volume). As an example, consider the impact on RGB ages of uncertainties in predictions of the size of the central, fully-mixed region in main-sequence stars. We take the example of a model of mass 1.4 $M_\odot$. The difference between the main-sequence lifetime of a model with and without overshooting[3] from the core is of the order of 20 %. However, once the model reaches the giant phase, this difference is reduced to about 5 % (see Fig. 5). Low-mass models with a larger centrally mixed region experience a significantly shorter subgiant phase, the reason being that they end the main sequence with an isothermal helium core which is closer to the Schönberg-Chandrasekar limit (see Maeder 1975), hence partially offsetting the impact of a longer main-sequence lifetime. On the other hand, the effect of core overshooting on the age of RGB stars is more pronounced when the mass of the He core at the end of the main sequence is close to (or even larger than) the Schönberg-Chandrasekar limit (e.g., see the case of a 2.0 $M_\odot$ illustrated in Fig. 5). In that case, however, seismology may come to the rescue as at the beginning of the core-He burning phase the period spacing of gravity modes is a proxy for the mass of the helium core, and can potentially help to test models of extra mixing for stars in the so-called secondary clump (Montalbán et al. 2013).

Additional seismic diagnostics are still to be fully utilised and their dependence on stellar properties understood. Seismic signatures of sharp-structure variations can potentially lead to estimates of the envelope He abundance (see Broomhall et al. 2014). Promising indicators of global stellar properties include the small separation between radial and quadrupole modes (Montalbán et al. 2012) and the properties of mixed modes and coupling term which may lead to additional indirect constraints on the stellar mass (see e.g. Benomar et al. 2013).

[3]We assume an extension of the overshooting region equal to 0.2 H_p, where H_p is the pressure scale height at the boundary of the convective core, as defined by the Schwarzschild criterion.

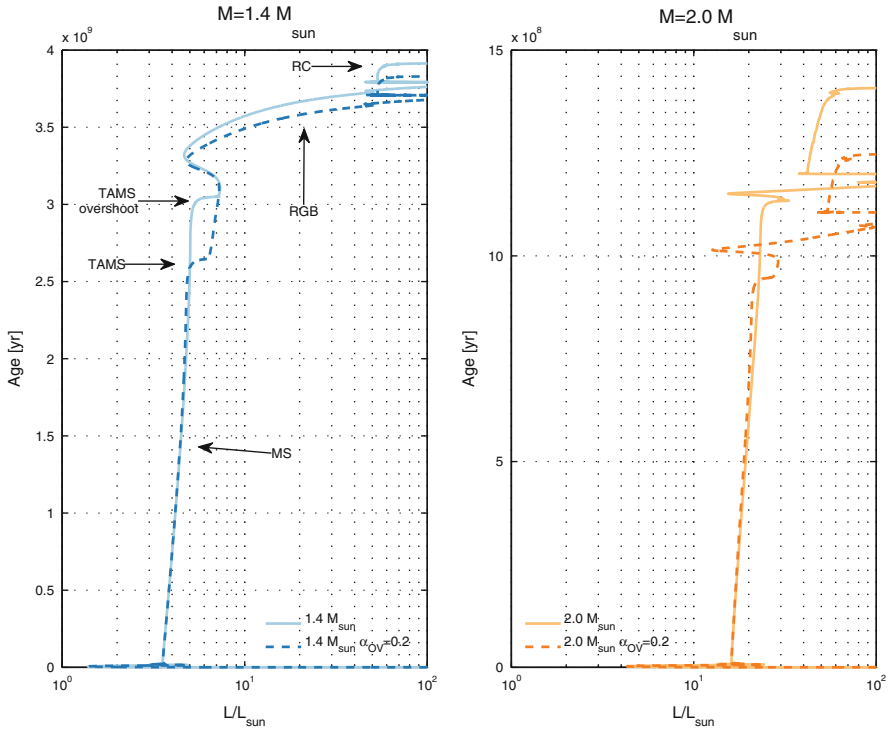

Fig. 5 *Left panel:* Age as a function of luminosity for a 1.4 $M_{\odot}$ stellar model computed with (*solid line*) and without (*dashed line*) extra mixing from the convective core during the main-sequence phase. Relevant evolutionary phases are marked on the plot: MS: main sequence, TAMS: terminal-age main sequence, RGB: red-giant branch, RC: red clump. *Right panel:* Same as *left panel* but for models of a 2 $M_{\odot}$ star (Color figure online)

An often overlooked point concerns the correlations between stellar properties derived by including seismic measurements, correlations which are yet to be quantified. As an example we show in Fig. 6 the strong correlation between radius (hence distance) and mass (hence age) as determined by considering average seismic quantities, effective temperature, and [Fe/H] as observables.

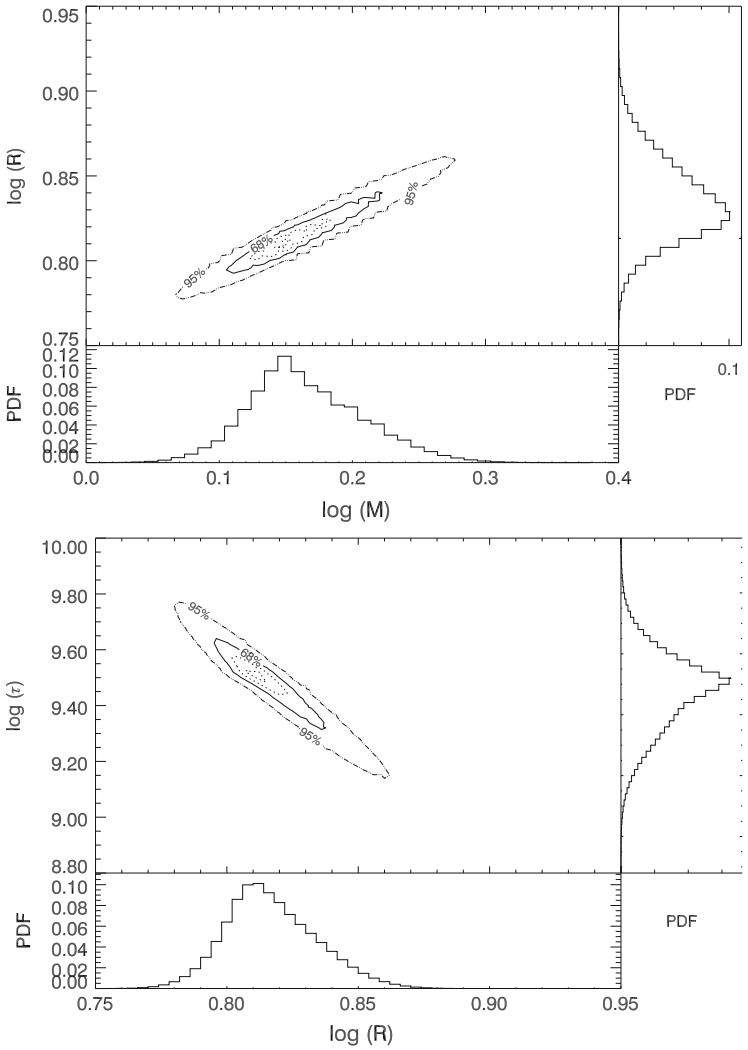

Fig. 6 Contour plots of joint and marginal probability density function of radius and mass (*upper panel*) as output of PARAM (Rodrigues et al. 2014). The *solid* and *dashed-dotted* contours represent 68 % and 95 % credible regions. The strong correlation between mass and radius is reflected in an anticorrelation between radius (or distance) and age (*lower panel*)

4 Summary

Thanks to K2, TESS, and PLATO 2.0 the future looks extremely bright in terms of collecting space-based photometric data for ensemble seismology, however, we are still faced with a number of challenges centred around the assessment of the accuracy by which the properties of stellar populations can be determined.

Robust predictions from stellar models are key to determining accurate stellar properties such as mass, radius, surface gravity and, crucially, age. A critical appraisal of how numerical and systematic uncertainties in model predictions impact the inferred stellar properties (in particular ages) is needed. In favourable cases (such as binary systems, clusters) stellar models will be tested against the seismic measurements and reduce (some of) the systematic uncertainties in the age determination related to, for example, near-core extra mixing during the main sequence, and mass loss on the red-giant branch. Given the additional constraints (stringent priors on age, chemical composition) stars in clusters (see the contributions by Salaris and Brogaard et al.) and binary systems (eclipsing and seismic, see e.g. Huber 2014; Miglio et al. 2014) represent the prime targets for testing models.

A significant step forward in ensemble seismology, as shown in this workshop, will be through an associative development of asteroseismic data analysis techniques, stellar modelling, spectroscopic anlyses and their combination to constrain and test chemodynamical models of the Milky Way.

References

Bedding, T. R., Mosser, B., Huber, D., et al. 2011, Nature, 471, 608
Belkacem, K., Samadi, R., Mosser, B., Goupil, M.-J., & Ludwig, H.-G. 2013, in Astronomical Society of the Pacific Conference Series, Vol. 479, Astronomical Society of the Pacific Conference Series, ed. H. Shibahashi & A. E. Lynas-Gray, 61
Benomar, O., Bedding, T. R., Mosser, B., et al. 2013, ApJ, 767, 158
Broomhall, A.-M., Miglio, A., Montalbán, J., et al. 2014, MNRAS, 440, 1828
Chaplin, W. J. & Miglio, A. 2013, ARA&A, 51, 353
Christensen-Dalsgaard, J. 1988, in IAU Symposium, Vol. 123, Advances in Helio- and Asteroseismology, ed. J. Christensen-Dalsgaard & S. Frandsen, 295
Epstein, C. R., Elsworth, Y. P., Johnson, J. A., et al. 2014, ApJ, 785, L28
Hekker, S., Gilliland, R. L., Elsworth, Y., et al. 2011, MNRAS, 414, 2594
Hekker, S., Kallinger, T., Baudin, F., et al. 2009, A&A, 506, 465
Howell, S. B., Sobeck, C., Haas, M., et al. 2014, PASP, 126, 398
Huber, D. 2014, ArXiv e-prints
Huber, D., Carter, J. A., Barbieri, M., et al. 2013, Science, 342, 331
Lebreton, Y. & Goupil, M.-J. 2014, ArXiv e-prints
Lillo-Box, J., Barrado, D., Moya, A., et al. 2014, A&A, 562, A109
Maeder, A. 1975, A&A, 43, 61
Miglio, A., Brogaard, K., Stello, D., et al. 2012, MNRAS, 419, 2077
Miglio, A., Chaplin, W. J., Farmer, R., et al. 2014, ApJ, 784, L3
Miglio, A., Chiappini, C., Morel, T., et al. 2013, in European Physical Journal Web of Conferences, Vol. 43, European Physical Journal Web of Conferences, 3004
Montalbán, J., Miglio, A., Noels, A., et al. 2012, in Red Giants as Probes of the Structure and Evolution of the Milky Way, ed. A. Miglio, J. Montalbán, A. Noels, A. Miglio, J. Montalbán, & A. Noels, ApSS Proceedings, 23
Montalbán, J., Miglio, A., Noels, A., et al. 2013, ApJ, 766, 118
Montalbán, J. & Noels, A. 2013, in European Physical Journal Web of Conferences, Vol. 43, European Physical Journal Web of Conferences, 3002
Mosser, B., Barban, C., Montalbán, J., et al. 2011, A&A, 532, A86
Mosser, B., Belkacem, K., Goupil, M.-J., et al. 2010, A&A, 517, A22

Rauer, H., Catala, C., Aerts, C., et al. 2013, ArXiv e-prints
Reimers, D. 1975, Mémoires of the Société Royale des Sciences de Liège, 8, 369
Ricker, G. R. 2014, Journal of the American Association of Variable Star Observers (JAAVSO), 42, 234
Rodrigues, T., Girardi, L., Miglio, A., et al. 2014, MNRAS, accepted
Roxburgh, I. W. & Vorontsov, S. V. 2003, A&A, 411, 215
Stello, D., Huber, D., Bedding, T. R., et al. 2013, ApJ, 765, L41
White, T. R., Bedding, T. R., Stello, D., et al. 2011, ApJ, 743, 161

Part II
Uncertainties on Models of Stellar Structure and Evolution: Testing Determinations of Stellar Properties in Well-Constrained Systems

Uncertainties in Stellar Evolution Models: Convective Overshoot

Alessandro Bressan, Léo Girardi, Paola Marigo, Philip Rosenfield, and Jing Tang

Abstract In spite of the great effort made in the last decades to improve our understanding of stellar evolution, significant uncertainties remain due to our poor knowledge of some complex physical processes that require an empirical calibration, such as the efficiency of the interior mixing related to convective overshoot. Here we review the impact of convective overshoot on the evolution of stars during the main Hydrogen and Helium burning phases.

1 Introduction

Thanks to the efforts of many different groups in the last decades, stellar evolution has now reached a high degree of accuracy and completeness. Indeed, it can now account for a variety of internal physical processes, follow the most advanced phases and deal with different chemical compositions, so that one could in principle reproduce any stellar environment disclosed by the continuously advancing observational facilities. At the same time observations themselves have become more and more detailed, even providing direct access to star interiors, like in the case of asteroseismology, thus posing a real challenge to theory. In spite of these efforts, some physical processes, because of their complexity, still suffer of large uncertainties. These processes are crucial when dealing with advanced evolutionary phases, e.g. the Red Giant Branch (RGB) and the Asymptotic Giant Branch (AGB), and even more for stellar populations that are not well represented in the solar

A. Bressan (✉) • J. Tang
SISSA, via Bonomea 265, 34136 Trieste, Italy
e-mail: sbressan@sissa.it; tang@sissa.it

L. Girardi
Osservatorio Astronomico di Padova, Vicolo dell'Osservatorio 5, 35122 Padova, Italy
e-mail: leo.girardi@oapd.inaf.it

P. Marigo • P. Rosenfield
Dipartimento di Fisica e Astronomia Galileo Galilei, Università di Padova,
Vicolo dell'Osservatorio 3, 35122 Padova, Italy
e-mail: paola.marigo@unipd.it; philip.rosenfield@unipd.it

A. Miglio et al. (eds.), *Asteroseismology of Stellar Populations in the Milky Way*,
Astrophysics and Space Science Proceedings 39,
DOI 10.1007/978-3-319-10993-0_3

vicinity or in our Galaxy. From the theoretical point of view there are several long lasting questions that still lack a definitive answer, such as the issue of convective energy transport and mixing and that of the efficiency of the mass-loss phenomenon. This review deals mainly with one of such questions, the effect of convective mixing during the main phases of stellar evolution. We will summarise the current theoretical situation with emphasis on those phases where the uncertainties become more critical.

We may expect that adding new dimensions to the HR diagram, such as those provided by asteroseismology, could allow the biggest improvements just where the uncertainties are the largest.

2 The New Release of Stellar Evolutionary Tracks with PARSEC

We begin with a brief review of the new code developed in Padova, PARSEC (*P*adova T*R*ieste *S*tellar *E*volution *C*ode), with which we obtained many of the results presented here. A detailed description can be found in Bressan et al. (2012) and a few more recent updates in Bressan et al. (2013). The equation of state (EOS) is computed with the FreeEOS code developed and updated over the years by A.W. Irwin.[1] Opacities in the high-temperature regime, $4.2 \leq \log(T/\mathrm{K}) \leq 8.7$, are obtained from the Opacity Project At Livermore (OPAL) team (Iglesias and Rogers 1996) while, in the low-temperature regime, $3.2 \leq \log(T/\mathrm{K}) \leq 4.1$, we use opacities generated with our ÆSOPUS[2] code (Marigo and Aringer 2009). Conductive opacities are included following Itoh et al. (2008). The nuclear reaction network consists of the p–p chains, the CNO tri-cycle, the Ne–Na and Mg–Al chains and the most important α-capture reactions, including the α-n reactions. The reaction rates and the corresponding Q-values are taken from the recommended rates in the JINA reaclib database (Cyburt et al. 2010). Microscopic diffusion, applied to all the elements considered in the code in the approximations that they are all fully ionized, is included following Salasnich (1999) with diffusion coefficients calculated following Thoul et al. (1994). The energy transport in the convective regions is described according to the mixing-length theory of Böhm-Vitense (1958). The mixing length parameter is fixed by means of the solar model calibration and turns out to be $\alpha_{\mathrm{MLT}} = 1.74$. A remarkable difference with respect to other solar calibrations concern the partition of metals for which we assume the abundances taken from Grevesse and Sauval (1998) but for the species recently revised by Caffau et al. (2011). According to this abundance compilation, the present-day Sun's metallicity is $Z_{\odot} = 0.01524$, intermediate between the most recent estimates, e.g. $Z_{\odot} = 0.0141$ of Lodders et al. (2009) or $Z_{\odot} = 0.0134$ of Asplund et al. (2009),

[1] http://freeeos.sourceforge.net/.

[2] http://stev.oapd.inaf.it/aesopus.

and the previous value of $Z_\odot = 0.017$ by Grevesse and Sauval (1998). We remind here that the assumption of a different metallicity for the Sun affects directly the calibration of the MLT parameter.

3 Convective Overshoot on the Main Sequence

Besides the choice of the microscopic physics, the evolution during and after the main sequence is affected by mixing processes related to the efficiency of convective core overshoot, atomic diffusion and rotation. In PARSEC we adopt a maximum overshooting efficiency $\Lambda_{\rm max} = 0.5$, i.e. a moderate amount of overshooting (Bertelli et al. 1994; Girardi et al. 2000), corresponding to about $0.25\,H_P$ of overshoot region *above* the unstable region as commonly adopted by other authors. In the transition region between stars with radiative cores and those with convective cores, say between $M_{\rm O1} \leq M \leq M_{\rm O2}$, we assume that the overshooting efficiency $\Lambda_{\rm c}$ increases linearly with mass from zero to the maximum value. We define $M_{\rm O1}$ as the minimum stellar mass for which a convective core is still present even after its central hydrogen has decreased by a significant amount ($X_{\rm c} \sim 0.2$) from the beginning of the main sequence. $M_{\rm O2}$ is set equal to $M_{\rm O1} + 0.3 M_\odot$. This choice is supported by the modelling of the open cluster M 67 (see Bressan et al. 2012), which indicates an overshooting efficiency $\Lambda_{\rm c} \simeq 0.5$ already at masses of M$\sim 1.3\,M_\odot$ for solar-metallicity stars; and by the SMC cluster NGC 419 (Girardi et al. 2009; Kamath et al. 2010), in which the turn-off probes masses between ~ 1.65 and $1.9\,M_\odot$. The run of the critical masses $M_{\rm O1}$ and $M_{\rm O2}$ as a function of the initial metallicity are shown in the left panel of Fig. 1. Constraints on these critical masses

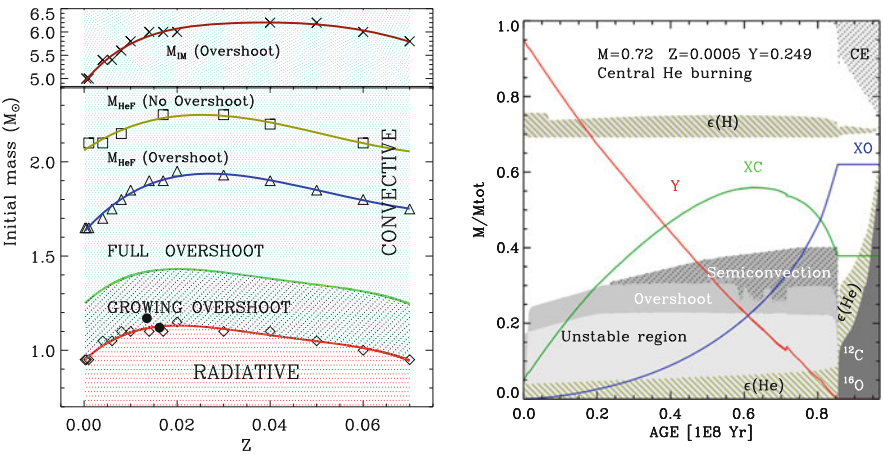

Fig. 1 *Left*: critical masses as a function of the metallicity. The *filled dots* represent the two models that best reproduce the asteroseismic data of Dushera (Silva Aguirre et al. 2013). *Right*: overshooting and semiconvective regions, during central He burning

are being set by asteroseismology. Indeed while earlier observations of α Cen A suggest negligible overshooting in solar-metallicity stars of mass $\sim 1.1\,M_{\odot}$ (de Meulenaer et al. 2010), recent studies of the nearby old low-mass star HD 203608, with $[Z/X] \simeq -0.5$, support the existence of sizable overshoot ($\alpha_{\rm ov} = 0.17$ corresponding to $\alpha_{\rm ov} \simeq 0.32$ in our formalism) at masses as low as $0.95\,M_{\odot}$, which is probably just slightly above the $M_{\rm O1}$ limit at the corresponding metallicity (Deheuvels et al. 2010). The full dots near $M_{\rm O1}$ at Z$\sim$0.015 represent the location of the two models that best reproduce the asteroseismic data of Dushera (Silva Aguirre et al. 2013), both requiring a sizeable overshoot ($\sim 0.2\,H_P$). Effects of core overshoot during the evolution on the main sequence, already thoroughly described in literature, are being used to obtain indirect calibrations of this process. Among them it is important to remind the difference between the threshold initial mass for undergoing helium flash between models with and without overshoot. The critical threshold as a function of the metallicity, M_{HeF}, decreases significantly with overshoot, as indicated in Fig. 1. The difference in mass between the two cases is significant and is certainly larger than the accuracy of the most recent determination of the mass with asteroseismic observations of evolved stars. Indeed, recent detailed studies of the evolutionary properties of He burning stars suggest to use the morphology of the red clump to trace stars with the mass around this critical transition (Girardi et al. 2013). Clearly, asteroseismology is opening a new window to constrain the mixing efficiency in the transition region from $M_{\rm O1}$ to $M_{\rm O2}$.

4 Overshoot and Mixing During the He Burning Phase

The presence of mixing beyond the unstable region in the core of He burning stars has been suspected since about fifty years.

Local Overshoot. As helium is converted into carbon in the convective core of He burning stars, the free-free opacity increases and so the radiative temperature gradient. This produces a discontinuity in the radiative temperature gradient just at the border of the convective core. It has been shown that this condition is unstable because the pollution with carbon rich material due to possible perturbations of any kind, renders the surrounding radiative layers irreversibly unstable to convection (Castellani et al. 1971). Thus, if these perturbations are allowed to occur by means of some artificial description of this kind of mixing, then the unstable region tend to grow during the evolution. This effect, known as *local* overshoot, increases the central He-burning lifetime almost proportionally to the growth of the core mass.

Semi-convection. In the more advanced stages, the star develops an intermediate zone, just above the convective core, which is marginally unstable to convection. This instability, known as semi-convection, gives rise to a smooth chemical profile maintaining the neutrality of the medium against convection. This mechanism is similar to the semi-convection that appears during hydrogen burning phase of massive stars though, in that case, it is due to the dependence of the electron scattering opacity on the hydrogen fraction (Schwarzschild and Härm 1958).

Notice that, in spite of the presence of a gradient in mean molecular weight, the Schwarzschild criterion should be preferred to the Ledoux one (Kato 1966; Spiegel 1969). Semi-convection contributes to the mixing in the central regions and gives rise to a further increase of the central helium exhausted core.

Breathing Pulses. Towards the end of central helium burning the star may undergo one or more breathing pulses of convection. This kind of instability is due to the luminosity feedback produced by the increase of the central He content that follows the growth of the mixed region when it enters a steep composition profile (Castellani et al. 1985). A further growth of the He exhausted core is produced by this mechanism which, in the HR diagram of intermediate mass stars, can be recognized by the presence of secondary blue loops toward central He exhaustion.

Non local overshoot. In presence of sizable *non local* overshoot, the discontinuity of the temperature gradient shifts well within the radiative stable regions where the radiative gradient is well below the adiabatic one. In this case the pollution of layers above the convective core does not destabilize the surrounding stable regions and local overshoot does not appear (Bressan et al. 1986). If one allows for large overshoot then also the semi-convective instability and even the breathing pulse phenomenon disappear. For the choice made in PARSEC, a sizable semi-convective region appears after the central He mass fraction falls below about 60 % (right panel of Fig. 1).

Overshoot (non local and/or local), semi-convection and breathing pulses may increase considerably the amount of fuel that the star can use during the central He-burning phase, increasing its lifetime. But the impact they have on the following phase, the Early Asymptotic Giant branch phase, is even larger. The star enters this phase with a larger he-exhausted core and the path toward the double shell phase may be shortened by a significant fraction. It has been soon recognized that the ratio between the observed number of stars in the E-AGB and in the HB branches of globular clusters, being proportional to the lifetime ratio of the corresponding evolutionary phases, may constitute a strong diagnostic for the efficiency of mixing during the helium burning phase (Buonanno et al. 1985). On the other hand, this simple diagnostic may be challenged by the presence of multiple populations because those with high helium content populate the HB but could escape the E-AGB phase. Nevertheless in some metal rich clusters there is no evidence of the latter evolutionary path and this diagnostic may still be used. For example, in the case of 47 Tuc we obtain from the ACS HST data (Sarajedini et al. 2007) $R2 = (n_{EAGB}/n_{HB}) = 0.14$–$0.15$. This value is in good agreement with the corresponding one predicted by PARSEC isochrones with $[\alpha/Fe] = 0.4$ and global metallicity $Z = 0.006$ and for a HB mass between $0.65\,M_{\odot}$ and $0.7\,M_{\odot}$.

5 Overshoot at the Bottom of the Convective Envelope

It has been argued that a moderate overshoot region (0.25–$1.0\,H_P$) below the base of the convective envelope may help to better reproduce the observed location of the RGB Bump in the red giant branch of low mass stars in globular clusters

and old open clusters (Alongi et al. 1991). The observed RGB bump in globular clusters is about 0.2 to 0.4 mag fainter than that predicted by models without envelope overshooting (Di Cecco et al. 2010) though, at the higher metallicities, this result depends on the adopted metallicity scale. Adopting an overshoot size of $\Lambda_e = 0.5\, H_P$, the RGB bump becomes typically ~ 0.3 mag fainter than in models with negligible envelope overshoot (Alongi et al. 1991), and in good agreement with observations. This value is in very good agreement with the overshoot size (not fully adiabatic however) at the base of the convective envelope in the Sun, that has been estimated to be $\Lambda_e \sim 0.4 - 0.6\, H_P$ using solar oscillations data (Christensen-Dalsgaard and et al. 2011).

Another interesting effect of the overshoot at the base of the convective envelope concerns the extension of the blue loops of intermediate mass and massive stars. During their central helium burning phases these stars may perform a characteristic excursion from the red to the blue side of the HR diagram, commonly referred to as the “blue loop". In nearby star-bursting dwarf galaxies this excursion give rise to two well resolved sequences of red helium burning (RHeB) and blue (BHeB) and stars (e.g., McQuinn et al. 2010), the latter being almost attached or even superimposed to the main sequence in the more metal poor galaxies. Indeed the blue loops become more pronounced at lower metallicities, but they may depend on several other factors. In particular it has been found that their extension decrease or they are even suppressed using either a lower $^{12}C(\alpha,\gamma)^{16}O$ reaction or a larger amount of core overshoot (Alongi et al. 1991; Godart et al. 2013). In spite of the strong evidence in favor of a significant amount of core overshoot (or an extended mixing beyond the formal convective core), models with convective core overshoot fail to reproduce the observed blue loops. To cure this problem Alongi et al. (1991) suggested to use a certain amount of overshoot from the convective envelope. They showed that by using an extra mixed region of at least 0.7 H_P below the formal Schwarzschild border of the envelope convection, they were able to obtain extended blue loops even with models computed with convective core overshoot.

It is possible to check the goodness of this assumptions by comparing the models with the colour magnitude diagrams of star-forming regions in nearby low metallicity galaxies. These regions, that contain a large number of intermediate mass and massive stars, are generally dominated by the latest star formation episodes for which one may assume a narrow range in metallicity or, often, even a single metallicity. We are analyzing this issue by comparing new evolutionary tracks with observed C-M diagram of selected nearby dwarf galaxies from the sample of Bianchi et al. (2012) as well as Dalcanton et al. (2009). We show in Fig. 2 how the HR diagram of intermediate/massive stars changes by increasing the amount of envelope overshoot. The simulations shown in Fig. 2 refers to a metal poor environment ($Z = 0.001$) and the amount of envelope overshoot is 0.7 H_P (left panel) the standard choice in PARSEC, 2 H_P (middle panel) and 4 H_P (right panel). A similar result is obtained for $Z = 0.002$. The comparisons with the observed CM diagrams of WLM, NGC 6822 and Sextans A, three dwarf galaxies with spectroscopic metallicities confined within the above range, indicate the need of an extra mixing of at least 2 H_P below the bottom of the convective envelope (Tang

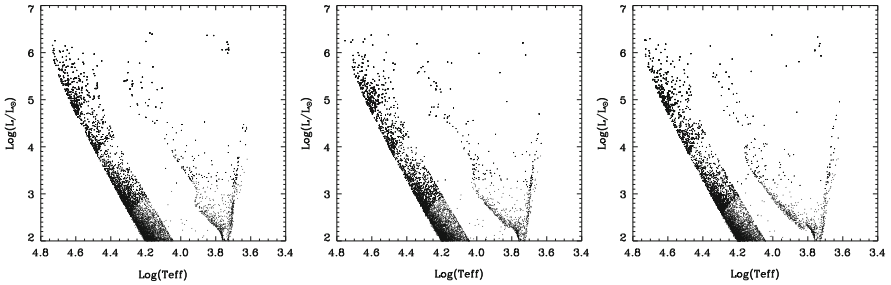

Fig. 2 Envelope overshoot and extension of blue loops in intermediate and massive stars at Z = 0.001. From *left* to *right* the simulations are made with EO = 0.7 H_P, 2 H_P and 4 H_P, respectively. For sake of clarity, different symbol sizes and total number of stars have been considered in the mass ranges M<4$M_\odot$, 4$M_\odot$ ≤M<10$M_\odot$, 10$M_\odot$ ≤M<20$M_\odot$ and M≥20$M_\odot$

et al. 2014). With the standard PARSEC choice (0.7 H_P), the C-M diagram of these galaxies could be reproduced only adopting a significantly lower metallicity, Z= 0.0005. Though large, the above value is not uncommon and similar values are used to enhance the efficiency of the carbon dredge-up during the thermally pulsing Asymptotic Giant Branch phase (Kamath et al. 2012).

Conclusions

Convective mixing plays a major role in stellar evolution, since it can modify the structure of the star in an irreversible way. Whether convection is accompanied by significant overshoot remains an unsolved problem. The existence of extra mixing is one of the most uncertain factors in stellar astrophysics affecting H-burning lifetimes and the lifetimes of advanced evolutionary phases (HB, E-AGB), luminosities and effective temperatures (Main Sequence termination, Clump stars, Blue He burning stars) and in particular cases also the surface chemistry. Classical tests with colour magnitude diagrams indicate the presence of this extra mixing outside the central convective region. Recent asteroseismic observations put even more robust constraints on this phenomenon, even if the nature of this mixing remains still unclear since it could also be due to the effects of rotational mixing. In some cases observations are even more challenging. In fact if one allows for a larger mixing above the convective core during the H-burning phase, the theoretical blue loops of intermediate and massive stars become less extended, at variance with observations, unless an even higher extra mixing is applied to the bottom of the convective envelopes. The size required to reproduce the observed blue loops in the CM diagrams of well studied star forming regions in nearby dwarf galaxies ($\geq$ 2 H_P), is significantly larger than that required to reproduce the RGB bump in globular clusters ($\sim$ 0.5 H_P).

References

Alongi, M., Bertelli, G., Bressan, A., & Chiosi, C. 1991, A&A , 244, 95
Asplund, M., Grevesse, N., Sauval, A. J., & Scott, P. 2009, ARA&A , 47, 481
Bertelli, G., Bressan, A., Chiosi, C., Fagotto, F., & Nasi, E. 1994, A&AS , 106, 275
Bianchi, L., Efremova, B., Hodge, P., & et al. 2012, AJ , 143, 74
Böhm-Vitense, E. 1958, ZA, 46, 108
Bressan, A., Bertelli, G., & Chiosi, C. 1986, Mem. Soc. Astron. Italiana, 57, 411
Bressan, A., Marigo, P., Girardi, L., & et al. 2012, MNRAS, 427, 127
Bressan, A., Marigo, P., Girardi, L., Nanni, A., & Rubele, S. 2013, in European Physical Journal Web of Conferences, Vol. 43, European Physical Journal Web of Conferences, 3001
Buonanno, R., Corsi, C. E., & Fusi Pecci, F. 1985, A&A , 145, 97
Caffau, E., Ludwig, H.-G., Steffen, M., & et al. 2011, Sol. Phys., 268, 255
Castellani, V., Chieffi, A., Tornambe, A., & Pulone, L. 1985, ApJ , 296, 204
Castellani, V., Giannone, P., & Renzini, A. 1971, Ap&SS , 10, 340
Christensen-Dalsgaard, J. & et al. 2011, MNRAS , 414, 1158
Cyburt, R. H., Amthor, A. M., Ferguson, R., & et al. 2010, ApJS , 189, 240
Dalcanton, J. J., Williams, B. F., Seth, A. C., & et al. 2009, ApJS , 183, 67
de Meulenaer, P., Carrier, F., Miglio, A., & et al. 2010, A&A , 523, A54
Deheuvels, S., Michel, E., Goupil, M. J., & et al. 2010, A&A , 514, A31
Di Cecco, A., Bono, G., Stetson, P. B., & et al. 2010, ApJ , 712, 527
Girardi, L., Bressan, A., Bertelli, G., & Chiosi, C. 2000, A&AS , 141, 371
Girardi, L., Marigo, P., Bressan, A., & Rosenfield, P. 2013, ApJ , 777, 142
Girardi, L., Rubele, S., & Kerber, L. 2009, MNRAS , 394, L74
Godart, M., Noels, A., & Scuflaire, R. 2013, in European Physical Journal Web of Conferences, Vol. 43, European Physical Journal Web of Conferences, 1008
Grevesse, N. & Sauval, A. J. 1998, Space Sci. Rev., 85, 161
Iglesias, C. A. & Rogers, F. J. 1996, ApJ , 464, 943
Itoh, N., Uchida, S., Sakamoto, Y., Kohyama, Y., & Nozawa, S. 2008, ApJ , 677, 495
Kamath, D., Karakas, A. I., & Wood, P. R. 2012, ApJ , 746, 20
Kamath, D., Wood, P. R., Soszyński, I., & Lebzelter, T. 2010, MNRAS , 408, 522
Kato, S. 1966, PASJ , 18, 374
Lodders, K., Palme, H., & Gail, H.-P. 2009, in Landolt-Börnstein - Group VI Astronomy and Astrophysics Numerical Data and Functional Relationships in Science and Technology Volume 4B: Solar System. Edited by J.E. Trümper, 2009, 4.4., ed. J. E. Trümper, 44
Marigo, P. & Aringer, B. 2009, A&A , 508, 1539
McQuinn, K. B. W., Skillman, E. D., Cannon, J. M., & et al. 2010, ApJ , 724, 49
Salasnich, B. 1999, PhD thesis, Univ. of Padova
Sarajedini, A., Bedin, L. R., Chaboyer, B., & et al. 2007, AJ , 133, 1658
Schwarzschild, M. & Härm, R. 1958, ApJ , 128, 348
Silva Aguirre, V., Basu, S., Brandão, I. M., & et al. 2013, ApJ , 769, 141
Spiegel, E. A. 1969, Comments on Astrophysics and Space Physics, 1, 57
Tang, J., Bressan, A., Rosenfield, P., et al. 2014, arXiv:1410.1745
Thoul, A. A., Bahcall, J. N., & Loeb, A. 1994, ApJ , 421, 828

Effects of Rotation on Stellar Evolution and Asteroseismology of Red Giants

Patrick Eggenberger

Abstract The impact of rotation on the properties of low-mass stars at different evolutionary stages is first described by discussing the properties of stellar models computed with shellular rotation. The observational constraints that are currently available to progress in our understanding of these dynamical processes are then presented, with a peculiar focus on asteroseismic measurements of red-giant stars.

1 Effects of Rotation on Stellar Properties

Rotation can have an important impact on stellar physics and evolution (Maeder 2009). These rotational effects are briefly discussed for different evolutionary phases of low-mass stars by comparing models computed with and without the inclusion of shellular rotation (Zahn 1992) with the Geneva stellar evolution code (Eggenberger et al. 2008). Two main kind of rotational effects can be distinguished: the direct effects on the stellar structure resulting from hydrostatic corrections due to the centrifugal force and the indirect effects due to rotational mixing.

1.1 Pre-main Sequence Evolution

During the pre-main sequence (PMS) evolution of a rotating solar-type star, only hydrostatic effects of rotation have a significant impact on the global stellar properties. As a result of the decrease of the effective gravity when rotation is taken into account, the evolutionary track in the HR diagram of a rotating PMS model is slightly shifted to lower effective temperatures and luminosities; it is then similar to the track of a non-rotating star computed with a slightly lower initial mass. This

P. Eggenberger (✉)
Observatoire de Genève, Université de Genève, 51 ch. des Maillettes, CH-1290 Sauverny, Switzerland
e-mail: patrick.eggenberger@unige.ch

A. Miglio et al. (eds.), *Asteroseismology of Stellar Populations in the Milky Way*,
Astrophysics and Space Science Proceedings 39,
DOI 10.1007/978-3-319-10993-0_4

shift observed in the HR diagram is directly related to the surface velocity of the model and is thus more pronounced for fast rotators.

Rotational mixing does not significantly influence the global stellar parameters during the PMS, but can change the surface abundances of light elements. Rotation is indeed found to increase the lithium depletion during the PMS by generating turbulence below the convective envelope through the shear instability. This decrease in the surface lithium abundance by rotational mixing is more directly related to the increase of differential rotation in the stellar interior than to the value of the rotational velocity at the stellar surface. The degree of differential rotation in the radiative zone of a PMS rotating model is sensitive to the duration of the disc-locking phase, during which the surface velocity of the model is simply assumed to remain constant. Consequently, stellar models computed with longer disc lifetimes exhibit lower surface lithium abundances on the zero-age main sequence (ZAMS) than models that experience a shorter disc-locking phase. Moreover, a model computed with a longer duration of the disc-locking phase also loses a larger amount of angular momentum and reaches the ZAMS with a lower surface rotational velocity. An interesting relation between the surface velocity and the lithium content on the ZAMS is then obtained, since stars with lower rotation rates on the ZAMS are predicted to be more depleted in lithium than stars that are fast rotators on the ZAMS (see Eggenberger et al. 2012a, for more details). Such a relation seems to be in good agreement with observations of lithium abundances and surface rotation rates in the Pleiades (e.g. Soderblom et al. 1993).

1.2 Main-Sequence Evolution

During the main-sequence (MS) evolution of a solar-type star, hydrostatic effects of rotation are only observed near the ZAMS, where rotating models are characterized by slightly lower luminosities and effective temperatures than non-rotating ones. Due to the magnetic braking undergone by solar-type stars, the surface rotational velocities of these models rapidly decrease during the MS and the impact of the centrifugal force on the global stellar parameters rapidly becomes negligeable. The effects of rotational mixing on the global stellar parameters become however more and more important during the evolution on the MS. Larger effective temperatures and luminosities are then found for rotating models compared to non-rotating ones. For models of solar-type stars characterized by a radiative core, this is mainly due to the fact that rotational mixing counterbalances atomic diffusion in the external layers of the star (Eggenberger et al. 2010b). This results in higher values of helium abundance at the surface of rotating models and hence to a decrease of the opacity in the external layers of the star, which explains the shift to the blue part of the HR diagram when rotational effects are taken into account. For more massive models with a convective core during the MS, the inclusion of rotational effects increases the size of the core and changes the chemical profiles in the radiative zone. This results in an increase of the luminosity and a widening of the MS for rotating

models compared to non-rotating ones (e.g. Eggenberger et al. 2010c). Rotational mixing also changes the properties in the central stellar layers by transporting fresh hydrogen fuel into the stellar core. This increases the value of the central abundance of hydrogen at a given age and leads to an enhancement of the main-sequence lifetime for rotating models compared to non-rotating ones.

The changes of the global stellar parameters and of the properties of the central layers induced by rotation have also an impact on the asteroseismic properties of solar-type stars (Eggenberger et al. 2010b). As a result of the decrease of the stellar radius when rotational effects are taken into account, the value of the mean large frequency separation at a given age is higher for rotating models than for non-rotating ones. Rotating models are also characterized by higher values of the mean small separation at a given age than non-rotating ones, because of the transport of hydrogen in the central layers by rotational mixing.

1.3 Post-main Sequence Evolution

Although red giants are generally characterized by low surface rotational velocities, the impact of rotation on these stars can be significant, because the evolution in the red giant phase is sensitive to the rotational history of the star and in particular to the changes of the stellar properties during the MS. For models massive enough to ignite helium burning in non-degenerate conditions, the increase of the luminosity when rotational effects are taken into account leads to a shift to higher luminosities of the location of the core helium-burning phase for rotating models compared to non-rotating ones. For low-mass red-giant models that undergo the helium flash, the situation is different, since the location of the core helium burning phase in the HR diagram is very similar for rotating and non-rotating models. For these stars, the inclusion of rotation has an impact on the location of the bump; at solar metallicity, rotating models exhibit a lower luminosity and a higher effective temperature at the bump than non-rotating ones (e.g. Charbonnel and Lagarde 2010; Eggenberger et al. 2012b).

2 Asteroseismic Studies of Red-Giant Stars

The brief description of the effects of rotation on the properties of low-mass stars presented above has been done in the context of shellular rotation. The outputs of these rotating models, and in particular the quantitative impact of rotational mixing, are sensitive to the prescriptions used for the modelling of meridional circulation and shear instabilities (Meynet et al. 2013). It is thus interesting to consider the observational constraints that are currently available to constrain these dynamical processes, with a peculiar focus on asteroseismic data.

The internal rotation profile of the Sun deduced from helioseismic measurements (Brown et al. 1989; Elsworth et al. 1995; Kosovichev et al. 1997; Couvidat et al. 2003; García et al. 2007) is a key observational constraint for rotating models. These observations show a nearly flat rotation profile, while solar models including only shellular rotation predict a rapidly rotating core (Pinsonneault et al. 1989; Chaboyer et al. 1995; Eggenberger et al. 2005; Turck-Chièze et al. 2010). This is a clear indication that another physical process is at work in the solar radiative interior. This still undetermined mechanism could be related to magnetic fields (e.g. Charbonneau and MacGregor 1993; Gough and McIntyre 1998; Eggenberger et al. 2005) or to angular momentum transport by internal gravity waves (e.g. Zahn et al. 1997; Talon et al. 2002; Charbonnel and Talon 2005; Mathis et al. 2013). The helioseismic results stimulated various attempts to detect and characterize solar-like oscillations for other stars than the Sun. Ground-based asteroseismic observations have enabled the detection of solar-like oscillations for a limited number of bright solar-type stars (see e.g. Bedding and Kjeldsen 2008) and for a few red giants (Frandsen et al. 2002; Barban et al. 2004; De Ridder et al. 2006). Thanks to the CoRoT (Baglin et al. 2006) and *Kepler* (Borucki et al. 2010) space missions, the observation and characterization of solar-like oscillations have now been obtained for a very large number of stars.

Concerning the rotational properties of stars, these seismic observations have led to the determination of rotational frequency splittings of mixed modes in red giants (Beck et al. 2012; Deheuvels et al. 2012; Mosser et al. 2012). By lifting the degeneracy in the azimuthal order of non-radial modes, rotation leads to $(2\ell + 1)$ frequency peaks in the power spectrum for each mode. Rotational splittings are then defined as the frequency separations between these peaks. These frequency spacings are related to the angular velocity and the properties of the modes in their propagation regions. Mixed modes are sensitive to the properties in stellar interiors and contain a different amount of pressure and gravity-mode influence. An oscillation mode dominated by its acoustic character will be more sensitive to the properties in the external layers of a red giant, while a gravity-dominated mode will be sensitive to the properties in the stellar core. Rotational splittings of mixed modes thus contain valuable information about internal rotation of red giants, which are of prime importance to better understand the dynamical physical processes at work in stellar interiors (see e.g. Eggenberger et al. 2012c; Marques et al. 2013; Goupil et al. 2013).

2.1 Mixed Modes in the Red Giant KIC 8366239

To illustrate in more details how the observation of rotational splittings of mixed modes in red giants can constrain the modelling of internal angular momentum transport, we first consider the case of the red giant KIC 8366239 observed by the *Kepler* spacecraft (Beck et al. 2012). The precise measurements of rotational splittings in KIC 8366239 show radial differential rotation in the stellar interior

with central layers rotating at least ten times faster than the envelope (see Beck et al. 2012, for more details).

By performing the modelling of this asteroseismic target, a model in the H-shell burning phase with a solar chemical composition and an initial mass of $1.5\,M_{\odot}$ is determined. This star is thus found to exhibit a convective core during its evolution on the main sequence. The theoretical rotational splittings corresponding to rotating models of KIC 8366239 are then computed and compared to the observed values. These rotating models predict an increase of the angular velocity in the stellar core, which seems at first sight to be in good agreement with the asteroseismic observations. However, the values of rotational splittings predicted by models including shellular rotation only are found to be much larger than the observed values, even in the case of models computed for very low initial velocities on the ZAMS (see Eggenberger et al. 2012c, for more details). This discrepancy is mainly due the large increase in the rotational velocity predicted in the core of rotating models. The internal rotation profile of models including shellular rotation is indeed found to be very steep during the red giant phase as a result of the central contraction occurring at the end of the main-sequence evolution (e.g. Palacios et al. 2006; Eggenberger et al. 2010c, 2012c; Marques et al. 2013). We then conclude that meridional circulation and shear instability alone produce an insufficient coupling to correctly reproduce the observed values of rotational splittings in KIC 8366239. This shows that an additional mechanism for the internal transport of angular momentun is at work during the post-main sequence evolution in order to obtain a predicted rotation profile during the red giant phase in agreement with asteroseismic data.

The observed values of rotational splittings for mixed modes in KIC 8366239 can be used to place constraints on the efficiency of this unknown additional mechanism for the internal transport of angular momentum. For this purpose, rotating models of the red giant KIC 8366239 are computed by adding a viscosity term corresponding to this unknown additional physical process in the equation describing the transport of angular momentum by the meridional circulation and the shear instability. In a first step, this viscosity is simply assumed to be constant. The rotation profiles predicted by models computed with different values for this additional viscosity are then confronted to asteroseismic data to determine the efficiency needed for this transport process to correctly reproduce the observed splittings. We then found that the ratio of rotational splittings for dipole gravity-dominated modes to those for modes dominated by their acoustic character strongly constrains the efficiency of this additional transport mechanism of angular momentum. In the case of the red giant KIC 8366239, a viscosity of $3 \times 10^4\,cm^2\,s^{-1}$ is determined for this unknown additional process (Eggenberger et al. 2012c). Interestingly, this value deduced from asteroseismic observations of a red giant is quite similar to the value required to correctly reproduce the spin-down of slowly rotating solar-type stars observed during the beginning of the evolution on the main sequence (Denissenkov et al. 2010). This may suggest that the same unknown transport mechanism of angular momentum is at work during the main-sequence and the post-main sequence evolution.

2.2 Mixed Modes in the Red Giant KIC 7341231

Rotational splittings have also been precisely characterized for 18 oscillation modes in the red giant KIC 7341231 observed during 1 year by the *Kepler* space mission (Deheuvels et al. 2012). These splittings have been used to perform an inversion of the rotation profile showing radial differential rotation with a rotation rate in the central stellar layers at least five times higher than in the envelope (see Deheuvels et al. (2012) for more details). This red giant star is characterized by a low metallicity ([Fe/H]≈ -1) and a low mass of about $0.84\,M_{\odot}$. Consequently, this star exhibits a radiative core during the main sequence. It is thus particularly interesting to compare the rotational properties of this target with the results describe above for KIC 8366239, which is a more massive star with a convective core during the main sequence.

Rotation profiles predicted by models of KIC 7341231 including a detailed treatment of shellular rotation have been compared to the internal rotation profile deduced form the asteroseimic measurements of KIC 7341231 (Ceillier et al. 2012, 2013). Such a comparison indicates that rotating models including shellular rotation only lead to internal rotation profiles that are too steep compared to the observed one. This shows that the efficiency of angular momentum transport through meridional circulation and shear instability is not sufficient to correctly reproduce the asteroseismic data obtained for a low-mass red giant like KIC 7341231. An additional mechanism for the internal transport of angular momentum is thus also needed in this case. The studies of KIC 8366239 and KIC 7341231 thus suggest that this unknown physical process is at work in the interiors of red giant stars exhibiting a convective core as well as a radiative core during the evolution on the main sequence. In the case of the low-mass star KIC 7341231, it is interesting to note that the efficiency of the internal transport of angular momentum during the main sequence has an important impact on the rotation profiles predicted during the red giant phase (see Ceillier et al. 2013, for more details). Tayar and Pinsonneault (2013) obtained similar results from limiting case scenarios of solid-body rotation or local conservation of angular momentum in radiative zones during the main-sequence and post-main-sequence evolution.

2.3 Rotational Splittings for a Large Sample of Red Giants

In addition to the detailed study of internal rotation profiles for a limited number of red giants, rotational frequency splittings have been obtained for a large sample of about 300 red-giant stars observed with the *Kepler* spacecraft (Mosser et al. 2012). This study shows that radial differential rotation is present for all red giants of the sample and provides an estimate of the mean core rotation period for red giant stars at different evolutionary stages. Interestingly, the mean core rotation period is found to be larger for red clump stars than for red-giant branch stars, suggesting

that an efficient mechanism for the internal transport of angular momentum is at work during the red-giant phase to explain the observed spin-down of the stellar core.

The comparison between these estimates of core rotation rates for red giants at different evolutionary stages and theoretical predictions of rotating models offers a particularly valuable mean to progress in the modelling of the different mechanisms responsible for the angular momentum transport in stellar interiors. A first comparison has been recently performed between the core rotation periods deduced from asteroseismic data for evolved secondary-clump stars and rotating models assuming solid-body rotation or local conservation of angular momentum in radiative zones (Tayar and Pinsonneault 2013). This study indicates that models computed by assuming solid-body rotation during the whole stellar evolution are able to correctly reproduce the observed core rotation rates of secondary-clump stars. By assuming solid-body rotation, these models are at odds with the observations of radial differential rotation in red giants, but they clearly underline the need of an efficient mechanism for angular momentum transport to correctly account for the asteroseismic data obtained for these stars.

Conclusion

We have first briefly described the impact of shellular rotation on the properties of low-mass stars at different evolutionary stages. Including rotational effects leads to changes of the global and asteroseismic properties of these stars. It will be particularly interesting to investigate in more details the impact of such changes on the global properties of stars in clusters (e.g. Girardi et al. 2011) and on population studies of red giants observed by current asteroseismic space missions (as done for instance by Miglio et al. 2009, using non-rotating models). The comparison between models computed with shellular rotation and asteroseismic measurements of red giants suggests that an additional mechanism for the internal transport of angular momentun is at work during the post-main sequence evolution. This still undetermined process could be related to the transport of angular momentum by internal gravity waves (e.g. Charbonnel and Talon 2005) or magnetic fields (e.g. Eggenberger et al. 2010a). This illustrates that we are still far from a satisfying description of the transport processes at work in stellar interiors and that asteroseismic measurements can help us progress in the modelling of these mechanisms.

Acknowledgements Part of this work was supported by the Swiss National Science Foundation.

References

Baglin, A., Auvergne, M., Boisnard, L., et al. 2006, in COSPAR Meeting, Vol. 36, 36th COSPAR Scientific Assembly, 3749
Barban, C., de Ridder, J., Mazumdar, A., et al. 2004, in ESA Special Publication, Vol. 559, SOHO 14 Helio- and Asteroseismology: Towards a Golden Future, ed. D. Danesy, 113
Beck, P. G., Montalban, J., Kallinger, T., et al. 2012, Nature, 481, 55
Bedding, T. R. & Kjeldsen, H. 2008, in Astronomical Society of the Pacific Conference Series, Vol. 384, 14th Cambridge Workshop on Cool Stars, Stellar Systems, and the Sun, ed. G. van Belle, 21
Borucki, W. J., Koch, D., Basri, G., et al. 2010, Science, 327, 977
Brown, T. M., Christensen-Dalsgaard, J., Dziembowski, W. A., et al. 1989, ApJ, 343, 526
Ceillier, T., Eggenberger, P., García, R. A., & Mathis, S. 2012, Astronomische Nachrichten, 333, 971
Ceillier, T., Eggenberger, P., García, R. A., & Mathis, S. 2013, A&A, 555, A54
Chaboyer, B., Demarque, P., & Pinsonneault, M. H. 1995, ApJ, 441, 865
Charbonneau, P. & MacGregor, K. B. 1993, ApJ, 417, 762
Charbonnel, C. & Lagarde, N. 2010, A&A, 522, A10
Charbonnel, C. & Talon, S. 2005, Science, 309, 2189
Couvidat, S., García, R. A., Turck-Chièze, S., et al. 2003, ApJ, 597, L77
De Ridder, J., Barban, C., Carrier, F., et al. 2006, A&A, 448, 689
Deheuvels, S., García, R. A., Chaplin, W. J., et al. 2012, ApJ, 756, 19
Denissenkov, P. A., Pinsonneault, M., Terndrup, D. M., & Newsham, G. 2010, ApJ, 716, 1269
Eggenberger, P., Haemmerlé, L., Meynet, G., & Maeder, A. 2012a, A&A, 539, A70
Eggenberger, P., Lagarde, N., & Charbonnel, C. 2012b, Impact of Rotational Mixing on the Global and Asteroseismic Properties of Red Giants, ed. A. Miglio, J. Montalbán, & A. Noels, 95
Eggenberger, P., Maeder, A., & Meynet, G. 2005, A&A, 440, L9
Eggenberger, P., Maeder, A., & Meynet, G. 2010a, A&A, 519, L2
Eggenberger, P., Meynet, G., Maeder, A., et al. 2008, Ap&SS, 316, 43
Eggenberger, P., Meynet, G., Maeder, A., et al. 2010b, A&A, 519, A116
Eggenberger, P., Miglio, A., Montalban, J., et al. 2010c, A&A, 509, A72
Eggenberger, P., Montalbán, J., & Miglio, A. 2012c, A&A, 544, L4
Elsworth, Y., Howe, R., Isaak, G. R., et al. 1995, Nature, 376, 669
Frandsen, S., Carrier, F., Aerts, C., et al. 2002, A&A, 394, L5
García, R. A., Turck-Chièze, S., Jiménez-Reyes, S. J., et al. 2007, Science, 316, 1591
Girardi, L., Eggenberger, P., & Miglio, A. 2011, MNRAS, 412, L103
Gough, D. O. & McIntyre, M. E. 1998, Nature, 394, 755
Goupil, M. J., Mosser, B., Marques, J. P., et al. 2013, A&A, 549, A75
Kosovichev, A. G., Schou, J., Scherrer, P. H., et al. 1997, Sol. Phys., 170, 43
Maeder, A. 2009, Physics, Formation and Evolution of Rotating Stars (Springer Berlin Heidelberg)
Marques, J. P., Goupil, M. J., Lebreton, Y., et al. 2013, A&A, 549, A74
Mathis, S., Decressin, T., Eggenberger, P., & Charbonnel, C. 2013, A&A, 558, A11
Meynet, G., Ekstrom, S., Maeder, A., et al. 2013, in Lecture Notes in Physics, Berlin Springer Verlag, Vol. 865, Lecture Notes in Physics, Berlin Springer Verlag, ed. M. Goupil, K. Belkacem, C. Neiner, F. Lignières, & J. J. Green, 3–642
Miglio, A., Montalbán, J., Baudin, F., et al. 2009, A&A, 503, L21
Mosser, B., Goupil, M. J., Belkacem, K., et al. 2012, A&A, 548, A10
Palacios, A., Charbonnel, C., Talon, S., & Siess, L. 2006, A&A, 453, 261
Pinsonneault, M. H., Kawaler, S. D., Sofia, S., & Demarque, P. 1989, ApJ, 338, 424
Soderblom, D. R., Jones, B. F., Balachandran, S., et al. 1993, AJ, 106, 1059

Talon, S., Kumar, P., & Zahn, J.-P. 2002, ApJ, 574, L175
Tayar, J. & Pinsonneault, M. H. 2013, ApJ, 775, L1
Turck-Chièze, S., Palacios, A., Marques, J. P., & Nghiem, P. A. P. 2010, ApJ, 715, 1539
Zahn, J.-P. 1992, A&A, 265, 115
Zahn, J.-P., Talon, S., & Matias, J. 1997, A&A, 322, 320

Open Clusters: Probes of Galaxy Evolution and Bench Tests of Stellar Models

Maurizio Salaris

Abstract Open clusters are the only example of single-age, single initial chemical composition populations in the Galaxy, and they play an important role in the study of the formation and evolution of the Galactic disk. In addition, they have been traditionally employed to test theoretical stellar evolution models. A brief review of constraints/tests of white dwarf models/progenitors, and rotating star models based on Galactic open clusters' observations is presented, introducing also recent contributions of asteroseismic analyses.

1 Introduction

Star clusters had traditionally played—and continue to play—a fundamental role as tools to both investigate the mechanisms of galaxy formation and evolution, and test theoretical stellar evolution models. For example, the timescale for the formation of the different Galactic populations can be investigated by means of stellar age dating. The most reliable stellar ages are obtained for the globular clusters in the halo, thick disk and bulge, and the open clusters (OCs) in the thin disk. In case of OCs, it is possible to employ techniques like gyrochronology or the lithium depletion boundary on young OCs, in addition to classical methods based on isochrone and colour-magnitude-diagrams (CMD).

Given the recent "downgrading" of individual globular clusters from SSPs to ensembles of almost coeval stellar populations with largely varying abundances of specific elements (C, N, O, Na, Mg, Al and He), OCs remain the only example of pure SSP in the Galaxy. There are about 1,500 known Galactic OCs, distributed at galactocentric distances (R_{GC}) between $\sim$5 and 20 kpc, and ages between a few Myr up to $\sim$10 Gyr. The old-age tail of this distribution is particularly important for Galaxy formation studies. In general, OCs are expected to be disrupted easily by encounters with massive clouds in the disk; however, the most massive OCs or

M. Salaris (✉)
Astrophysics Reaserch Institute, Liverpool John Moores University, IC2, Liverpool Science Park, 146 Brownlow Hill, Liverpool L3 5RF, UK
e-mail: M.Salaris@ljmu.ac.uk

A. Miglio et al. (eds.), *Asteroseismology of Stellar Populations in the Milky Way*, Astrophysics and Space Science Proceedings 39,
DOI 10.1007/978-3-319-10993-0_5

those with orbits that keep them far away from the Galactic plane for most of their lifetimes are expected to survive for longer periods of time. These old objects are therefore test particles—in analogy to the GCs—probing the earliest stages of the formation of the Galactic disk.

Besides the use of OCs to study the Galaxy, their CMDs provide a snapshot of magnitudes and colours of coeval and uniform initial composition stars of different masses at different evolutionary stages. CMD analyses plus star counts and spectroscopic studies along the various evolutionary sequences provide strong tests/constraints on stellar physics and evolutionary predictions.

The next sections will review briefly some OC-based constraints/tests of white dwarf models/progenitors, and rotating stellar models, introducing also the recent contributions of asteroseismic observations.

2 White Dwarfs

White dwarfs (WDs) are the last evolutionary phase of stars with initial mass smaller than about 10–11 $M_\odot$. The large majority of WDs, i.e. those with progenitor mass below 6–7 $M_\odot$ are made of an electron degenerate core of carbon and oxygen. More massive WDs have oxygen and neon cores. Given that most stars are or will become WDs, plus the existence of a relationship between their cooling time and luminosity, and their long timescales, WDs are attractive candidates to unveil the star formation history of the Galaxy. Due to their proximity compared to globular clusters, and their large range of ages, Galactic OCs are perfect systems to employ WDs as cosmochronometers, and study their properties.

2.1 Initial-Final Mass Relation

The initial-final mass relation (IFMR) for low- and intermediate-mass stars is an important input for many astrophysical problems. Given the initial main sequence mass of a formed star, the IFMR provides the expected mass during its final WD cooling stage, and is an estimate of the total mass lost by the star during its evolutionary history. A correct assessment of the IFMR is very important when predicting, for example, the chemical evolution history of stellar populations, or their mass-to-light ratio (defined as the ratio of the mass of evolving stars plus remnants—WDs, neutron stars and black holes—to the integrated luminosity of the population), and in general for any problem related to the origin and evolution of gas in stellar populations.

The IFMR depends on the competition between surface mass loss, growth of the CO core due to shell He-burning during the asymptotic giant branch phase, and the mixing episodes between envelope and intershell region, that limit the outward (in mass) movement of the He-burning shell. Due to our imperfect knowledge of mass

loss processes during the asymptotic giant branch and post asymptotic giant branch phases, and details of the mixing during the thermal pulses, we cannot predict accurately the mass of a WD produced by a progenitor with a given initial mass. Observational constraints are therefore absolutely necessary.

OCs have traditionally provided the observational data to determine semiempirically the IFMR, starting from Weidemann (2000). These determinations based on cluster WDs work as follows: after detection, spectroscopic estimates of the WD surface gravity g and T_{eff} are needed. For a fixed g-T_{eff} pair, interpolation within a grid of theoretical WD models covering a range of masses provides the final WD mass and the cooling age of the WD. Independent theoretical isochrone fits to the turn-off luminosity in the cluster CMD provide an estimate of the cluster age. The difference between cluster and WD cooling ages is equal to the lifetime of the WD progenitor from the main sequence until the start of the WD cooling (that is essentially the same as the lifetime at the end of central He-burning). Making use of mass-lifetime relationships from theoretical stellar evolution models (wihout including the short-lived asymptotic giant branch phase), the initial progenitor mass is derived.

An important issue here is the knowledge of the initial chemical composition of the cluster, given the strong dependence of the derived ages on the assumed metallicity of the models. The recent detailed analysis by Salaris et al. (2009) based on 10 OCs, have shown that the uncertainty in the final WD mass is dominated by observational errors, whilst the uncertainty in the initial mass has multiple reasons. On the one hand cluster chemical composition and isochrone details influence the cluster age and thus the progenitor mass; but also the uncertainty in the WD cooling age can sometimes be the dominant factor. None of the WDs employed in current IFMR determinations is close to the Chandrasekhar mass, not even the progeny of the more massive intermediate mass stars. Figure 1 displays the empirical IFMR determined by Salaris et al. (2009) employing BaSTI stellar isochrones with and without main sequence core overshooting from Pietrinferni et al. (2004). Overimposed are predicted relationships from BaSTI synthetic AGB models by Cordier et al. (2007), with and without main sequence convective core overshooting. Clearly, stellar models without convective overshooting during core hydrogen burning lead to internal inconsistencies in the semiempirical IFMR.

2.2 WD Ages

There are two main age indicators for stellar populations: the main sequence turn-off and the termination of the WD cooling sequence. Open clusters provide the ideal environment for the test/calibration of these two clocks. Although generally WD and turn-off ages are consistent within the error bars for the OCs where both indicators have been applied (von Hippel 2005), observations of the WD cooling sequence of the old open cluster NGC6791 has revealed a few surprises.

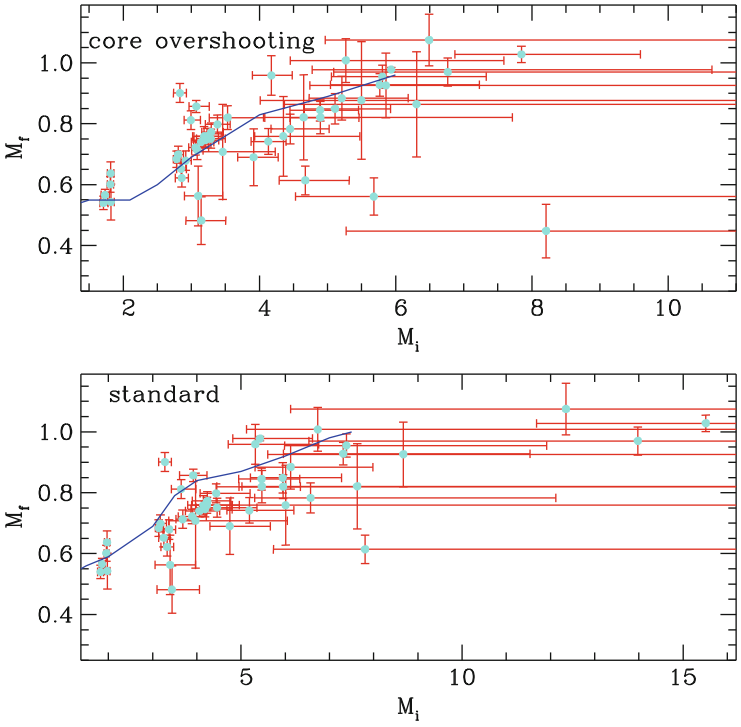

Fig. 1 Semiempirical IFMR determined with models with and without main sequence convective core overshooting, as labelled. The *solid lines* display theoretical IFMRs obtained from synthetic AGB models (see text for details)

A deep CMD by Bedin et al. (2008a) has provided a well populated WD luminosity function (LF) that reaches the end of the cluster cooling sequence. The LF, displayed in Fig. 2, displays a peak and sharp cut-off at low luminosities, caused by the finite age of the cluster (hence the finite WD cooling time), plus an unexpected secondary peak at higher luminosities, never observed in any other OC cooling sequence so far.

The cluster age derived from the magnitude of the cut-off of the LF appeared to be about ∼2 Gyr younger than the turn-off age, when calculated with standard WD cooling models. As shown conclusively by García-Berro et al. (2010) the inclusion of ^{22}Ne diffusion in the core, in the liquid phase—a physical process never included before in standard WD model calculations—slows down the cooling and can explain the discrepancy with the turn-off ages. The ^{22}Ne mass fraction in the core of NGC6791 WDs should be about 4 % by mass, essentially equal to the total mass fraction Z of this metal rich OC ([Fe/H]∼0.3–0.4). At the solar metallicities typical of the Galactic OCs, the amount of ^{22}Ne is not large enough to cause appreciable delays in the WD cooling, hence the lack of discrepancy between turn-off and WD

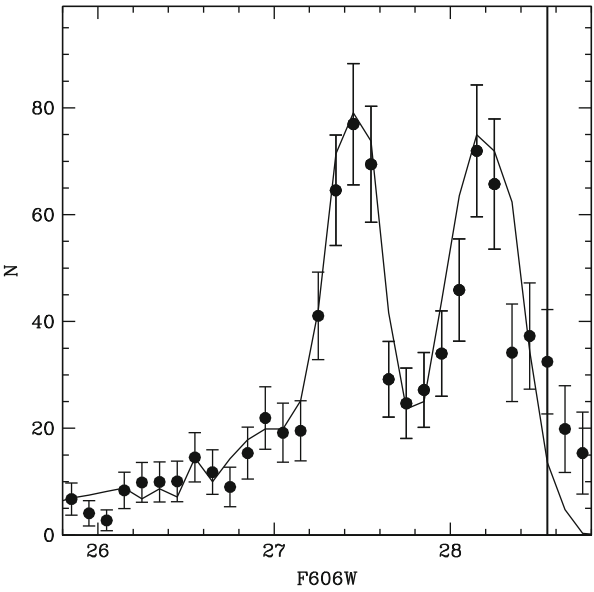

Fig. 2 WD luminosity function of NGC6791 (*filled circles*), and the best-match theoretical counterpart (*solid line*) with a ∼30 % fraction of WD + WD binaries (see text for details)

ages for other OCs. This result highlights very clearly the power of using OCs as tools to test and improve stellar evolution calculations.

The secondary peak at higher luminosities is more puzzling, and it could be produced by a population of unresolved binary white dwarfs. As shown by Bedin et al. (2008b) ∼30 % of unresolved WD + WD systems arising from a ∼50 % initial fraction of binary systems can reproduce both height and magnitude of the secondary peak (see Fig. 2). An alternative explanation put forward by Hansen (2005) is the presence of massive He-core WDs (mass essentially equal to the core mass at the He-flash along the RGB). This idea is supported by the fact that NGC 6791 contains a non-negligible number of blue He-burning stars that have very little mass in their envelopes, having lost nearly all of the envelope during their red giant branch evolution. This explanation requires a certain fine-tuning of the initial-final mass relation for these He-core objects, and an overall very large amount of mass lost along the red giant branch.

3 Rotation

In the regime of solar-like stars, it is long known that stellar rotation periods increase approximately as the square root of age, due mainly to mass and angular momentum loss in a magnetized wind, see e.g., Skumanich (1972). Theoretical predictions of the rotational evolution of stars are however difficult, because the theory of angular momentum evolution in stars is very complex, for one has to understand not only

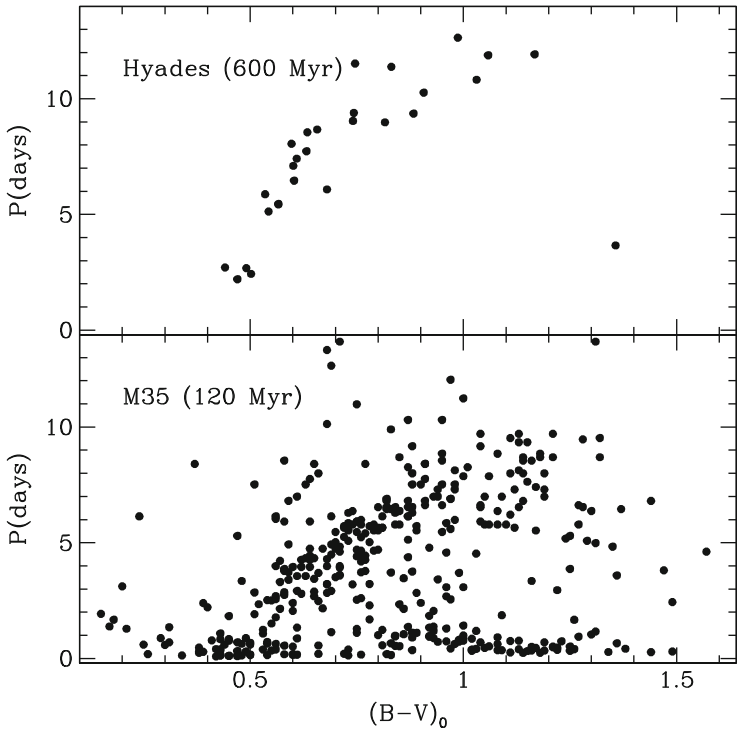

Fig. 3 Colour-P diagram for a sample of main sequence stars in the Hyades and M35 OCs (see text for details)

the initial distribution of angular momentum, but also its transport in stellar interiors and wind losses.

Observations of the evolution of rotational periods in nearby OCs provide important clues about how to use the evolution of rotational properties as a clock for low mass main sequence field stars, whose ages would be extremely difficult if not impossible to measure from their position in CMDs. These empirical results, in turn, can be used to calibrate the rotational evolution of stellar models.

Figure 3 shows measurements of Period (P) against colour ($B - V$) of samples of main sequence stars (in the range between $\sim$0.6 and $\sim$1.4 $M_\odot$) in the $\sim$600 Myr old Hyades, and in the $\sim$120 Myr old M35 OCs. It is easy to appreciate the large period spread of P values at fixed colour in M35, with two well defined sequences. One sequence of fast rotators with period P <1 day, independent of colour—denoted as sequence C in Barnes (2007)—or convective sequence, in the assumption that these objects lack large scale dynamos and are inefficient at slowing down their rotation; a diagonal sequence of faster rotating/warmer stars and slower rotating/cooler stars (sequence I, or interface, given the theoretical expectation that these stars are producing their magnetic flux near the convective-radiative interface). A comparison of the two clusters suggests that by the age of the Hyades almost all

stars along sequence C have moved onto sequence I. The stars populating the gap between these two sequences in the younger cluster are interpreted as objects in transition from the C to the I sequence. The colour-P diagrams also suggest that the dependence of P on colour along the I sequence is the same in both clusters, hence the value of the rotation period P along this sequence can be expressed as:

$$P = \mathrm{f}(B-V)\ \mathrm{g(t)} \tag{1}$$

with $\mathrm{f}(B-V) = a\ [(B-V)_0 - c]^b$ and $\mathrm{g(t)} = \mathrm{t}^n$, as proposed by Barnes (2007). The recent determinations of the coefficients a, b, c, n by Meibom et al. (2009) provide $a = 0.770 \pm 0.014$, $b = 0.553 \pm 0.052$, $c = 0.472 \pm 0.027$, based on the I sequence in M35. The exponent n is determined by ensuring that the colour dependence gives the solar rotation period at the solar age, that gives $n = 0.519 \pm 0.007$. Age determinations based on this so-called "gyrochronology" rely on fitting the I sequence rotational isochrone determined by Eq. (3) with age as a free parameter, to individual field stars—or clusters, where one can determine the position of the I sequence even in the presence of fast rotators—in the colour-period diagram. This calibration is based on OCs younger than 1 Gyr, with a time dependence covering ages up to ∼5 Gyr, based just on the Sun. Very recently Meibom et al. (2011) have used photometry from the *Kepler* mission, and ground based spectroscopy to determine the colour-P diagram of the ∼1 Gyr old OC NGC 6811, that shows clearly the I sequence. This improves the calibration of gyrochronology by extending the age baseline of the reference clusters.

These results are not only important for gyrochronology, but can be used also to constrain the rotational evolution of cool stars during the main sequence phase. Let's remember that rotation plays a crucial role in stellar structure and its evolution, for it influences the evolutionary tracks in the CMD through transport processes which induce rotational mixing of chemical species and the redistribution of angular momentum. In turn, stellar evolution affects the rotational properties.

Additional information on the rotational properties of the deep interior would also help to better understand the effect of rotation on stellar evolution, and recently rotational splittings of dipole mixed modes were measured by Mosser et al. (2012) in about 300 red giants observed during more than 2 years with *Kepler*. The measured splittings provide an estimate of the mean core rotation period, and reveal that along the the red giant branch the period increases more slowly than expected in case of homologous spinning down at constant total angular momentum. Angular momentum is transferred from the core to the envelope, but a strong differential rotation profile takes place during the red giant branch ascent. Rotation periods are larger for red clump stars compared to red giant branch objects, implying a transfer of angular momentum between the rapidly rotating core and the slowly rotating envelope, however the mechanism responsible for the redistribution of angular momentum spins down the mean core rotation with a time scale too long for reaching a solid body rotation.

Acknowledgements I wish to thank the organizers for their kind invitation and the organization of the workshop in such an enchanting place.

References

Barnes, S. A. 2007, ApJ, 669, 1167
Bedin, L. R., King, I. R., Anderson, J., et al. 2008a, ApJ, 678, 1279
Bedin, L. R., Salaris, M., Piotto, G., et al. 2008b, ApJ, 679, L29
Cordier, D., Pietrinferni, A., Cassisi, S., & Salaris, M. 2007, AJ, 133, 468
García-Berro, E., Torres, S., Althaus, L. G., et al. 2010, Nature, 465, 194
Hansen, B. M. S. 2005, ApJ, 635, 522
Meibom, S., Barnes, S. A., Latham, D. W., et al. 2011, ApJ, 733, L9
Meibom, S., Mathieu, R. D., & Stassun, K. G. 2009, ApJ, 695, 679
Mosser, B., Goupil, M. J., Belkacem, K., et al. 2012, A&A, 548, A10
Pietrinferni, A., Cassisi, S., Salaris, M., & Castelli, F. 2004, ApJ, 612, 168
Salaris, M., Serenelli, A., Weiss, A., & Miller Bertolami, M. 2009, ApJ, 692, 1013
Skumanich, A. 1972, ApJ, 171, 565
von Hippel, T. 2005, ApJ, 622, 565
Weidemann, V. 2000, A&A, 363, 647

Exploiting the Open Clusters in the *Kepler* and CoRoT Fields

Karsten Brogaard, Eric Sandquist, Jens Jessen-Hansen, Frank Grundahl, and Søren Frandsen

Abstract The open clusters in the *Kepler* and CoRoT fields potentially provide tight constraints for tests of stellar models and observational methods because they allow a combination of complementary methods. We are in the process of identifying and measuring parameters for detached eclipsing binaries (dEBs) in the open clusters in the *Kepler* and CoRoT fields. We make use of measurements of dEBs in the clusters to test the accuracy of asteroseismic scaling relations for mass. We are able to provide strong indications that the asteroseismic scaling relations overestimate the stellar mass, but we are not yet able to distinguish between different proposed corrections from the literature. We argue how our ongoing measurements of more dEBs in more clusters, complemented by dEBs in the field, should be able to break the degeneracy. We also briefly describe how we can identify cluster stars that have evolved through non-standard evolution by making use of ensemble asteroseismology.

1 Introduction

Open star clusters are often observed to exploit the advantages of the additional information that comes from observing an ensemble of stars with identical ages and similar metallicities. The open clusters in the *Kepler* and CoRoT fields extend the prospects for such an approach because they make the identification of detached eclipsing binary stars much easier and allow us to combine classical observational methods with asteroseismology of giant stars. We are in the process of identifying and measuring parameters for dEBs in the open clusters in the *Kepler* (NGC6791, NGC6811, NGC6819, and NGC6866) and CoRoT (NGC6633) fields.

K. Brogaard (✉) • J. Jessen-Hansen • S. Frandsen • F. Grundahl
Department of Physics and Astronomy, Stellar Astrophysics Centre, Aarhus University, Ny Munkegade 120, 8000 Aarhus C, Denmark
e-mail: kfb@phys.au.dk; jensjh@phys.au.dk; srf@phys.au.dk; fgj@phys.au.dk

E. Sandquist
Department of Astronomy, San Diego State University, San Diego, CA 92182, USA
e-mail: erics@mintaka.sdsu.edu

A. Miglio et al. (eds.), *Asteroseismology of Stellar Populations in the Milky Way*,
Astrophysics and Space Science Proceedings 39,
DOI 10.1007/978-3-319-10993-0_6

Our long term goal is to test and improve stellar models and gain detailed insights into stellar evolution in the clusters by making use of measurements of multiple dEBs in combination with asteroseismology of single giant stars. In this contribution we use the measurements of dEBs in the clusters to test the accuracy of the asteroseismic scaling relations for mass.

2 Tests of Asteroseismic Scaling Relations

The asteroseismic scaling relations for mass and radius,

$$\frac{M}{\mathrm{M}_\odot} \simeq \left(\frac{\nu_{\max}}{\nu_{\max,\odot}}\right)^3 \left(\frac{\Delta\nu}{\Delta\nu_\odot}\right)^{-4} \left(\frac{T_{\rm eff}}{T_{\rm eff,\odot}}\right)^{3/2},$$
$$\frac{R}{\mathrm{R}_\odot} \simeq \left(\frac{\nu_{\max}}{\nu_{\max,\odot}}\right) \left(\frac{\Delta\nu}{\Delta\nu_\odot}\right)^{-2} \left(\frac{T_{\rm eff}}{T_{\rm eff,\odot}}\right)^{1/2}, \quad (1)$$

(e.g. see Miglio et al. 2012) provide a relatively easy way of measuring the mass and radius of a star showing solar-like oscillations using a light curve from *Kepler* or CoRoT. However, these relations are only approximate and their accuracy is not known in great detail. Moreover, several corrections have been suggested in the literature. Some are based on observations and/or model predictions (Miglio et al. 2012; White et al. 2011), while others try to deal with systematics arising due to not fulfilling assumptions in the derivation of the scaling relations (Mosser et al. 2013). The accuracy and precision of the scaling relations and their suggested corrections needs verification.

We wish to employ our measurements of eclipsing binaries in the open clusters for such tests. First rough comparisons of masses between the methods were already done for NCG6791 (Brogaard et al. 2012) and NGC6819 (Sandquist et al. 2013). Those results, shown in Table 1, indicate that masses from the asteroseismic scaling relations are slightly overestimated.

Here we do a more detailed comparison for NGC6819 and then elaborate on how including the additional clusters will provide improved insights.

Table 1 Mean mass of giant stars in clusters from different methods

Cluster	Asteroseismic $< M_{\rm RGB}/M_\odot >$	Asteroseismic $< M_{\rm RGB}/M_\odot >$	$< M_{\rm RGB}/M_\odot >$ from eclipsing binaries
NGC 6791	1.22 ± 0.01[a]	1.23 ± 0.02[b]	1.15 ± 0.02[c]
NGC 6819	1.68 ± 0.03[a]	1.61 ± 0.04[b]	1.55 ± 0.06[d]

[a]Based on asteroseismic grid-modelling measurements by Basu et al. (2011)
[b]Based on asteroseismic scaling relation measurements by Miglio et al. (2012)
[c]Based on measurements of eclipsing binaries by Brogaard et al. (2012)
[d]Based on measurements of eclipsing binaries by Jeffries et al. (2013) and Sandquist et al. (2013)

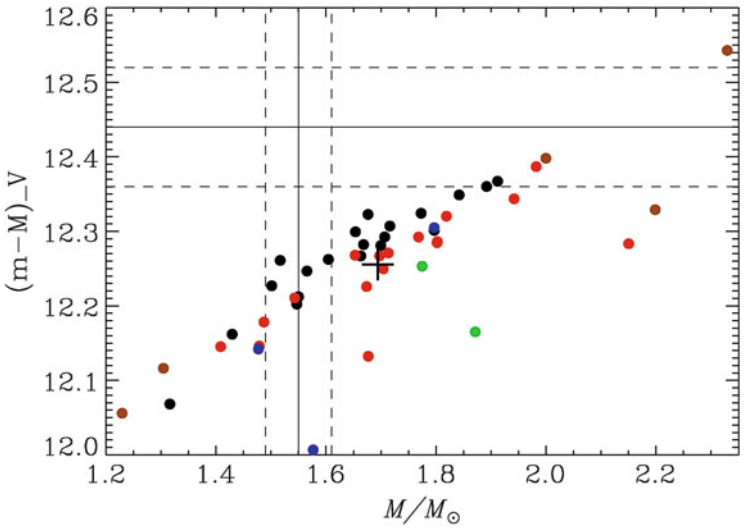

Fig. 1 Measurements of mass and distance modulus for giant stars in NGC6819. The *solid lines* indicate the values inferred from the eclipsing binaries, and the *dashed lines* the corresponding values $\pm 1-\sigma$ uncertainty. *Solid dots* are values for individual giant stars using the asteroseismic scaling relations in the form of Miglio et al. (2012). *Black dots* are RGB stars. *Brown dots* are cool RGB stars with $(V-K_s)$ colour ≥ 3.1, which are close to or above the validity level of the colour-$T_{\rm eff}$ relations of Ramírez and Meléndez (2005). *Red dots* are red clump stars determined from asteroseismology, while *blue dots* are RC stars determined from the CMD for cases where asteroseismology could not determine the evolutionary phase. *Green dots* are over-massive RGB stars in binary systems (Corsaro et al. 2012). The plus sign marks the mean asteroseismic values, excluding over-massive stars, see Sect. 3 (Color figure online)

Table 2 NGC6819 parameters determined from eclipsing binary members

Parameter	Value
$(m-M)_V$	12.44 ± 0.08[a]
$M_{\rm RGB}/M_\odot$	1.55 ± 0.06[b]

[a]Recalculated using radii, spectroscopic $T_{\rm eff}$s and photometric data for the eclipsing binaries from Jeffries et al. (2013) and Sandquist et al. (2013) with bolometric corrections from Casagrande and VandenBerg (2014)
[b]From range of numbers in Sandquist et al. (2013)

In order to get a more detailed view of the situation we show, in Fig. 1, the measurements in a plot of mass versus apparent distance modulus. The solid lines indicate the measurement of the mass of a star on the red giant branch (RGB) and the cluster distance modulus from the eclipsing binary measurements of Sandquist et al. (2013) and Jeffries et al. (2013), slightly adjusted as in Table 2, due to our use of bolometric corrections from Casagrande and VandenBerg (2014). Each circle marks the asteroseismic measurement of mass and distance modulus for a giant star in the cluster, recalculated *exactly* as in Miglio et al. (2012), e.g. using the scaling relations in the form of Eq. (1), with $T_{\rm eff}$ values calculated using $V-K_s$ colours

and the colour-$T_{\rm eff}$ relations of Ramírez and Meléndez (2005) and bolometric corrections from Flower (1996). The asteroseismic measurements are from Corsaro et al. (2012).

The plus sign marks the ensemble mean, which is too high compared to the binary measurements. Notice how the asteroseismic measurements fall more or less along a tilted line. This is the consequence of the way the random uncertainties in $T_{\rm eff}$ and the seismic parameters affect the position of a star in this diagram; all uncertainties shift the star along approximately the same line. Therefore, there appears to be no way of reaching agreement with the binary result, as the mean asteroseismic values can only shift approximately along the line already defined by the asteroseismic measurements. However, as we shall see, this is an artifact arising due to the use of colour-temperature relations and bolometric corrections from different sources, which underlines the importance of using self-consistent calibrations.

Figure 2 shows the situation when all measurements are made using the bolometric corrections and colour-temperature calibrations of Casagrande and VandenBerg (2014) based on MARCS models. We assumed $E(B-V) = 0.15$ and $E(V-Ks)/E(B-V) = 2.72$ since this results in $T_{\rm eff}$ for the red clump stars in agreement with spectroscopic measurements (Bragaglia et al. 2001). This shifts the asteroseismic measurements such that there is an overlap region with the binary results. However, to shift the mean asteroseismic mass close to the binary result, a correction to the scaling relations was still needed. We have therefore also applied

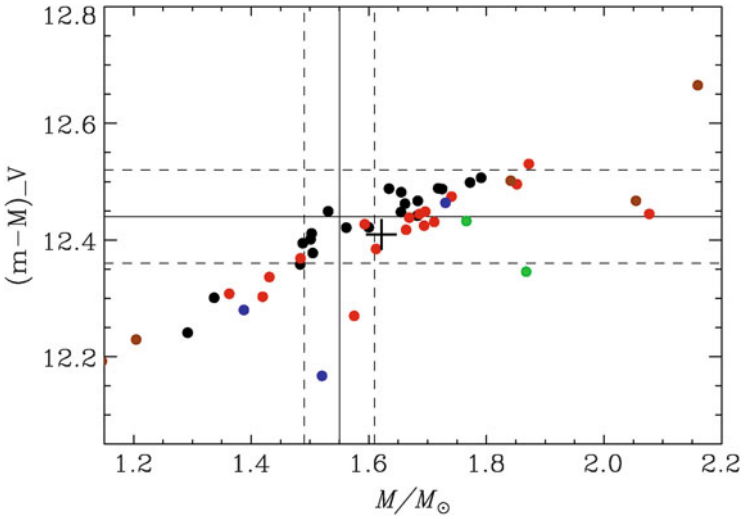

Fig. 2 As Fig. 1 but using bolometric corrections and colour-temperature relations from Casagrande and VandenBerg (2014) and the correction to the scaling relations from White et al. (2011). We use a modified version of their suggested correction, since it is clear from their Fig. 5 that the form of their correction breaks down below ∼4,700 K. Below that value we keep the correction constant. The relative correction between RGB and RC stars determined by Miglio et al. (2012) is still applied to the RC stars

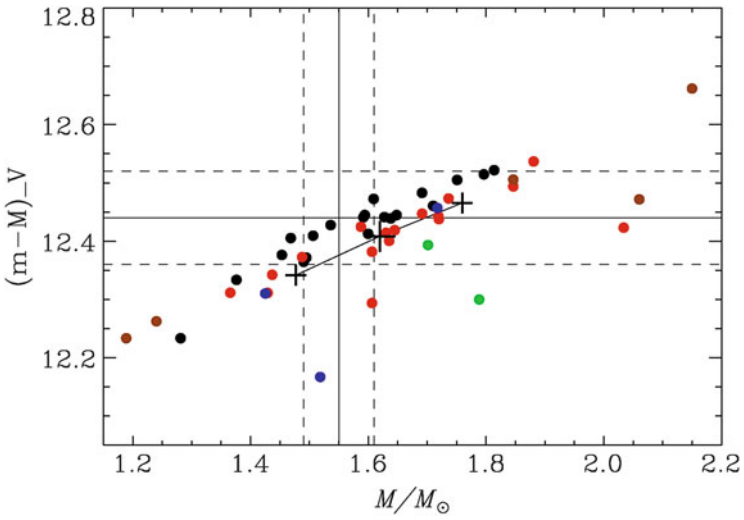

Fig. 3 As Fig. 1 but using bolometric corrections and colour-temperature relations from Casagrande and VandenBerg (2014) and the correction to the scaling relations from Mosser et al. (2013). The relative correction between RGB and RC stars determined by Miglio et al. (2012) is still applied to the RC stars

the correction to the scaling relations suggested by White et al. (2011) in Fig. 2. That way, we can obtain a reasonable agreement! However, as shown in Fig. 3, a similar agreement can be obtained by using instead the correction suggested by Mosser et al. (2013). In principle, the correct correction might be expected to decrease the scatter among the measured masses and distance moduli, but unfortunately the different corrections are too similar and random uncertainties too large to allow such a test (the small plus signs attached to the mean value in Fig. 3 shows the effect on the cluster mean when $\nu_{\max}$ is changed by $\pm 1 - \sigma$ for all stars). Thus, we are left in a situation where indications are that the asteroseismic scaling relations overestimate masses of giant stars, but we cannot distinguish between different suggested corrections, because they both work equally well, at least in this situation.

The correction suggested by White et al. (2011) depends on $T_{\rm eff}$ and similar corrections have been calculated by Miglio et al. (2013), where they also extend to the helium-burning red clump phase of evolution, showing a different correction to red clump stars compared to stars in the red giant branch phase (see the details in Fig. 5 of White et al. 2011 and Fig. 2 of Miglio et al. 2013). Note especially that for the case of the open cluster NGC6811, where the giants are younger and hotter, the correction predicted by Miglio et al. (2013) becomes small while for the red clump stars of the even younger clusters NGC6866 and NGC6633 this correction becomes large, but in the opposite direction! On the other hand, the correction suggested by Mosser et al. (2013) does not depend on $T_{\rm eff}$. Therefore, by extending our investigation to other clusters of different ages, and therefore different masses and $T_{\rm eff}$'s for the giant stars, it should be possible to find a suitable form of

a correction. We are already in the process of identifying, observing and analysing detached eclipsing systems and oscillating giant stars in the open clusters NGC6791, NGC6811, NGC6866, and NGC6633.

There are, however, some additional difficulties in this procedure. One issue we have noticed is that the $T_{\rm eff}$ of the red clump stars measured spectroscopically for NGC6819 (Bragaglia et al. 2001) and NGC6811 (Molenda-Żakowicz and et al. 2014) are higher than the corresponding $T_{\rm eff}$ calculated by Miglio et al. (2013) for the corresponding asteroseismic masses. As shown in the contribution by A. Miglio in this volume, different models predict different $T_{\rm eff}$ for the giant stars. This introduces an additional challenge when wanting to apply a correction to the asteroseismic scaling relations based on model $T_{\rm eff}$'s.

It is also not currently known whether a correction that depends directly on the metallicity should be made (to either $\Delta\nu$ or $\nu_{\rm max}$, or perhaps both?). Unfortunately, there are no metal-poor clusters in the sample of open cluster in the *Kepler* and CoRoT fields, so no such tests can presently be done. In order to check for possible metallicity effects, we are instead working on potentially metal-poor detached eclipsing binaries in the *Kepler* field which contain a giant star showing solar-like oscillations. We will analyse these along the lines of Frandsen et al. (2013) and compare directly to the asteroseismic signal of the giant component of the binary. Our sample contains three systems that have [Fe/H] ≈ -0.4 according to the *Kepler* input catalogue.

3 Identification of Stars That Evolved Through Non-standard Evolution

The red giant phase of evolution is so short-lived that the difference in mass among the giants in a cluster is much smaller than our asteroseismic measurement uncertainty. Therefore, it makes sense to use the ensemble mean mass as the most precise measure of the mass of an RGB stars in a cluster. However, if there are giants in the sample that did not evolve as a single star, they are likely to have a different mass and should be excluded when calculating a mean mass from the ensemble.

An asteroseismic study by Corsaro et al. (2012) has already identified such stars in NGC6819 by investigating the period spacing of dipole modes caused by gravity modes in the oscillation spectra, $\Delta P_{\rm obs}$. By comparing their Fig. 8 diagram of $\Delta\nu$ versus $\Delta P_{\rm obs}$ to the corresponding diagram in Fig. 4 of Stello et al. (2013) calculated using models, one sees that for red clump stars, the differences in $\Delta\nu$ are caused by a combination of differences in mass *and* evolution. Returning to Fig. 3 we find a red clump star with a mass of 2.05 $M_{\odot}$. It turns out that this star, KIC5023953, sits in the expected location for normal red clump stars of NGC6819 in Fig. 8 of Corsaro et al. (2012), despite our evidence of a larger mass. But since the red clump sequence in that diagram is also affected by evolution during the helium-burning phase, the star is consistent with being an over-massive star well into the helium-

burning phase. The fact that the star is a binary (Stello et al. 2011; Hole et al. 2009) supports this interpretation, since the higher mass could have originated from mass-transfer. This example shows that it is wise to combine information from several diagrams before drawing definitive conclusions about specific stars. Any star not lying along the scatter line of the majority of stars in a diagram like Fig. 3 should be investigated for signs of non-standard evolution.

Conclusions
We have shown indications that the asteroseismic scaling relations for solar-like oscillators [Eq. (1)] will overestimate the mass of a star unless some kind of correction is applied. At present we are unable to distinguish between different corrections suggested in the literature, since they work equally well. An ongoing expanded investigation employing eclipsing binaries in more open clusters and in the field will allow more firm conclusions to be made.

Acknowledgements K. Brogaard acknowledges funding from the Villum Foundation.

Funding for the Stellar Astrophysics Centre is provided by The Danish National Research Foundation (Grant agreement no.: DNRF106). The research is supported by the ASTERISK project (ASTERoseismic Investigations with SONG and Kepler) funded by the European Research Council (Grant agreement no.: 267864).

References

Basu, S., Grundahl, F., Stello, D., et al. 2011, ApJ, 729, L10
Bragaglia, A., Carretta, E., Gratton, R. G., et al. 2001, AJ, 121, 327
Brogaard, K., VandenBerg, D. A., Bruntt, H., et al. 2012, A&A, 543, A106
Casagrande & VandenBerg 2014, MNRAS, 444, 392
Corsaro, E., Stello, D., Huber, D., et al. 2012, ApJ, 757, 190
Flower, P. J. 1996, ApJ, 469, 355
Frandsen, S., Lehmann, H., Hekker, S., et al. 2013, A&A, 556, A138
Hole, K. T., Geller, A. M., Mathieu, R. D., et al. 2009, AJ, 138, 159
Jeffries, Jr., M. W., Sandquist, E. L., Mathieu, R. D., et al. 2013, AJ, 146, 58
Miglio, A., Brogaard, K., Stello, D., et al. 2012, MNRAS, 419, 2077
Miglio, A., Chiappini, C., Morel, T., et al. 2013, in European Physical Journal Web of Conferences, Vol. 43, European Physical Journal Web of Conferences, 3004
Molenda-Żakowicz et al. 2014, MNRAS, accepted (arXiv:1409.5132)
Mosser, B., Michel, E., Belkacem, K., et al. 2013, A&A, 550, A126
Ramírez, I. & Meléndez, J. 2005, ApJ, 626, 465
Sandquist, E. L., Mathieu, R. D., Brogaard, K., et al. 2013, ApJ, 762, 58
Stello, D., Huber, D., Bedding, T. R., et al. 2013, ApJ, 765, L41
Stello, D., Meibom, S., Gilliland, R. L., et al. 2011, ApJ, 739, 13
White, T. R., Bedding, T. R., Stello, D., et al. 2011, ApJ, 743, 161

Part III
Photospheric Constraints and Reports on Ongoing Spectroscopic Surveys (e.g. GESS, APOGEE, GALAH)

Photometric Stellar Parameters for Asteroseismology and Galactic Studies

Luca Casagrande

Abstract Asteroseismology has the capability of delivering stellar properties which would otherwise be inaccessible, such as radii, masses and thus ages of stars. When coupling this information with classical determinations of stellar parameters, such as metallicities, effective temperatures and angular diameters, powerful new diagnostics for both stellar and Galactic studies can be obtained. I review how different photometric systems and filters carry important information on classical stellar parameters, the accuracy at which these parameters can be derived, and summarize some of the calibrations available in the literature for late-type stars. Recent efforts in combining classical and asteroseismic parameters are discussed, and the uniqueness of their intertwine is highlighted.

1 Introduction

Late-type stars (broadly FGKM) are long-lived objects and can be regarded as snapshots of the stellar populations that are formed at different times and places over the history of our Galaxy. The fundamental properties of a sizeable number of these stars in the Milky Way enable us to directly access different phases of its formation and evolution, and for obvious reasons, stars in the vicinity of the Sun have been preferred targets to this purpose, both in photometric and spectroscopic investigations (e.g., Gliese 1957; Wallerstein 1962; Twarog 1980; Strömgren 1987; Edvardsson et al. 1993; Nordström et al. 2004; Reddy et al. 2006; Casagrande et al. 2011; Bensby et al. 2013). Properties of stars in the solar neighbourhood, in particular ages and metallicities, are still the main constraint for Galactic chemo(dynamical) models and provide important clues to understand some of the main processes at play in galaxy formation and evolution (e.g., Matteucci and Francois 1989; Portinari et al. 1998; Chiappini et al. 2001; Schönrich and Binney 2009; Minchev et al. 2013; Bird et al. 2013).

L. Casagrande (✉)
Research School of Astronomy & Astrophysics, Mount Stromlo Observatory,
The Australian National University, Canberra, ACT 2611, Australia
e-mail: luca.casagrande@anu.edu.au

A. Miglio et al. (eds.), *Asteroseismology of Stellar Populations in the Milky Way*,
Astrophysics and Space Science Proceedings 39,
DOI 10.1007/978-3-319-10993-0_7

A common feature of all past and current stellar surveys is that, while it is relatively straightforward to derive some sort of information on the chemical composition of the targets observed (and in many cases even detailed abundances), that is not the case when it comes to stellar masses, radii, distances and, in particular, ages. Even when accurate astrometric distances are available to allow comparison of stars with isochrones (assuming other parameters involved in this comparison—such as effective temperatures and metallicities—are also well determined), the derived ages are still highly uncertain, and statistical techniques are required to avoid biases. Furthermore, isochrone dating is meaningful only for stars in restricted regions of the HR diagram (e.g., Soderblom 2010, for a review).

By measuring oscillation frequencies in stars, asteroseismology allows us to measure fundamental physical quantities, masses and radii *in primis*, which otherwise would be inaccessible in single field stars, and which can be used to obtain information on stellar distances and ages (e.g., Chaplin and Miglio 2013, for a review). In particular, global oscillation frequencies (see Sect. 3) not only are the easiest ones to detect and analyze, but are also able to provide the aforementioned parameters for a large number of stars with an accuracy that is generally much better than achievable by isochrone fitting in the traditional sense.

Thanks to space-borne missions such as CoRoT (Baglin and Fridlund 2006) and *Kepler* (Gilliland et al. 2010), global oscillation frequencies are now robustly detected in few hundreds main-sequence and subgiant, and several thousands giant stars (e.g., De Ridder et al. 2009; Stello et al. 2013). Asteroseismology is thus emerging as a new tool for studying stellar populations, and initial investigations in this direction have already been done (Chaplin et al. 2011; Miglio et al. 2013b). However, until now asteroseismic studies of stellar populations had only coarse information on classical stellar parameters such as effective temperatures ($T_{\rm eff}$) and metallicities ([Fe/H]). Coupling classical parameters with seismic information, not only improves the seismic masses and ages obtained for stars (Lebreton and Montalbán 2009; Chaplin et al. 2014), but it also allows to address other important questions, both in stellar (e.g., Deheuvels et al. 2012; Silva Aguirre et al. 2013) and Galactic (e.g., Casagrande et al. 2014b) evolution.

To fully harvest the potential that asteroseismology brings to studies in these areas, classical stellar parameters are thus vital. Both photometry and spectroscopy are able to deliver these parameters, each of these techniques having its own pros and cons (see e.g., Bessell 2005; Asplund 2005, for reviews). At the risk of being over-simplistic, one can say that a stellar spectrum encodes a lot of information on stellar parameters (for the sake of this review $T_{\rm eff}$, [Fe/H] and $\log g$), but these are usually strongly coupled to each other. Realistic model atmospheres, the input atomic and molecular physics, the line formation modelling and last but not the least the resolution and the signal-to-noise of the observations are all crucial to decipher the spectral fingerprints. On the contrary, photometric indices do (part of) the analysis for us, although more often than not with lower precision than spectroscopy, and they crucially depend on how a given magnitude is translated into a physical flux (i.e. on the photometric standardization and absolute calibration) and/or on the availability of realistic photometric calibrations linking a colour

index (or a combination of those) to a given stellar parameter (which indeed could have been derived from spectroscopy, or better whenever possible via fundamental measurements). Interstellar extinction can seriously limit the power of photometric techniques for objects located outside of the local bubble, unless detailed reddening maps are used to correct for it (e.g., Zasowski 2012; Schlafly et al. 2013; Lallement et al. 2014).

Concerning $T_{\rm eff}$, photometric techniques are usually superior to spectroscopy (modulo reddening), while the latter can provide exquisite detailed abundances impossible for photometry, as well as radial velocities (important for kinematic studies). On the other hand, using modern CCD cameras, (wide) field imaging is very efficient even compared to multi-fiber spectroscopy and can go several magnitudes fainter. Field imaging also has the advantage that minimal pre-selection is made on targets, thus greatly simplifying the selection function for the purpose of population and Galactic studies: all stars that fall in a given brightness regime are essentially observed. It is thus obvious that photometry and spectroscopy, rather than being in competition with each other, are complementary. Without further entering the merit of one or another technique, it suffices to say that in the following of this review I shall concentrate exclusively on stellar parameters derived from photometry.

2 Photometric Stellar Parameters

Photometric systems and filters carry information on various fundamental stellar properties and also when studying more complex systems, integrated magnitudes and colours of stars can be used to infer the properties of the underlying stellar populations. To this purpose, filter systems are designed to sort out regions in the stellar spectra where variations of the atmospheric parameters leave their characteristic traces with enough prominence to be detected in photometric data. Starting from the influential papers by Johnson (1966) and Strömgren (1966) describing the basis of broad- and intermediate-band photometry, a large number of systems exists nowadays, and more are coming into place with the advent of extensive photometric surveys (e.g., Bessell 2005, for a review).

Broad-band colours are most of the times tightly correlated with the stellar effective temperature, although metallicity, and to a minor extent surface gravity ($\log g$) also play a role, especially towards the near ultraviolet and the Balmer discontinuity (e.g., Eggen et al. 1962; Ridgway et al. 1980; Bell and Gustafsson 1989; Alonso et al. 1996; Casagrande et al. 2010b). On the other hand, intermediate- or narrow-band photometry centred on specific spectral feature(s) can have a much higher sensitivity to a given stellar parameter (e.g., Strömgren 1966; Wing 1967; McClure and van den Bergh 1968; Golay 1972; Mould and Siegel 1982; Worthey et al. 1994). While broad-band photometry can be easily used to map and study sizeable stellar populations and/or large fraction of the sky also at faint luminosities (e.g., Stetson et al. 1998; Bedin et al. 2004; Ivezić et al. 2007; Saito et al. 2012),

intermediate- and narrow-band photometry are more limited in this respect, although still very informative (e.g., Mould and Bessell 1982; Bonnell and Bell 1982; Yong et al. 2008; Árnadóttir et al. 2010).

In principle, determining stellar parameters from photometric data is a basic task, yet empirical calibrations are often limited to certain spectral types and/or involve substantial observational work. In recent years, considerable efforts have been invested in newly deriving empirical calibrations linking photometric indices to effective temperatures (e.g., Casagrande et al. 2006, 2008; González Hernández & Bonifacio 2009; Casagrande et al. 2010b, 2012; Pinsonneault et al. 2012). The latter have often been derived in a semi-fundamental way via the InfraRed Flux Method (IRFM), which nowadays can be easily implemented on stars, thanks to large photometric infrared surveys such as 2MASS or WISE (Cutri et al. 2003; Cutri and et al. 2012). Particular attention is now being paid to the absolute zero-point of the $T_{\rm eff}$ scale, using both solar twins (e.g., Casagrande et al. 2010b; Datson et al. 2012) and interferometry (e.g., Huber et al. 2012). Up until now, the major obstacle in making full use of interferometric measurements was the limited brightness regime sampled by those, essentially limited to relatively nearby and bright stars (the easiest targets to spatially resolve), which are saturated in most of the modern photometric surveys (2MASS in particular). This dichotomy has prevented from safely extending well calibrated relations to the faint stars targeted in large spectroscopic and photometric surveys. This obstacle has now been alleviated with dedicated near infrared photometric observations of interferometric targets (Casagrande et al. 2014a). It is also worth mentioning the increasing spatial resolution of interferometers, thanks to optical beam combiners (Ireland et al. 2008) and repeated, careful observations which are pushing the limit for reliable angular diameters down to about 0.5 mas (e.g., Huber et al. 2012; White et al. 2013). This finally allows to target fainter stars having good 2MASS photometry, and directly test a number of effective temperature scales. Caution, however, must be used when indirectly testing a $T_{\rm eff}$ scale via colour relations, as well as when assessing the reliability of interferometric measurements, especially at sub-milliarcsec level. As shown in Casagrande et al. (2014a), when using certain colour relations, rather different effective temperature scales can be compatible with a given subset of interferometric data. A more conclusive comparison is obtained when deriving $T_{\rm eff}$ in a more robust way such as via the IRFM, which, after a critical evaluation of the systematics involved, is able to deliver 1 % accuracy (or better) in effective temperatures and angular diameters.

The importance of securing the zero-point of the $T_{\rm eff}$ scale is far from being a technicality. In fact, a systematic shift of 100 K in effective temperatures implies a shift of about 0.1 dex on spectroscopically derived metallicities. This, e.g., has implications in determining the peak of the metallicity distribution function in the solar neighbourhood, with a number of consequences for Galactic chemical evolution models as well as for interpreting the Sun in a Galactic context (Casagrande et al. 2011). A sound setting of the $T_{\rm eff}$ scale is crucial also for other reasons, e.g., in comparison with theoretical stellar models (VandenBerg et al. 2014; Casagrande and VandenBerg 2014) or to derive absolute abundances (Meléndez et al. 2010a).

The use of solar twins is also helpful to accurately set the zero-points of the [Fe/H] scale (e.g., Meléndez et al. 2010b; Datson et al. 2012; Porto de Mello et al. 2013). Excellent photometric metallicities can be derived from intermediate-band colours such as the Geneva, the DDO and the Strömgren system. The latter is probably the most popular one (also thanks to the observational efforts of Olsen and collaborators, and a shallow all-sky survey such as the Geneva-Copenhagen Survey), with a number of [Fe/H] calibrations existing in the literature, both for dwarfs (Olsen 1984; Schuster and Nissen 1989; Haywood 2002; Nordström et al. 2004; Twarog et al. 2007; Casagrande et al. 2011) and giants (Faria et al. 2007; Calamida et al. 2007; Grebel and Richtler 1992; Hilker 2000; Casagrande et al. 2014b). These calibrations are built upon samples of stars with measured spectroscopic [Fe/H]: Casagrande et al. (2011) put efforts in deriving a photometric metallicity scale built upon spectroscopic measurements having $T_{\rm eff}$ consistent with the absolutely calibrated scale of Casagrande et al. (2010b). As a result of these works, the peak of the metallicity distribution function in the solar neighbourhood has shifted around the solar value. The super solar regime of most photometric metallicity calibrations is still partly unexplored (in particular for giants), while on the metal-poor side Strömgren indices lose any sensitivity to [Fe/H] below about -2 dex in the rather featureless spectra of hot subdwarfs (Casagrande et al. 2011). However, this does not seem to be the case for cool metal-poor red giants (Adén et al. 2011; Casagrande et al. 2014b).

While the low sensitivity of broad-band colours to [Fe/H] and $\log g$ makes them ideal for the sake of deriving $T_{\rm eff}$, it also implies that these broad-band filters are less than optimal for obtaining photometric metallicities (see e.g., Árnadóttir et al. 2010, for the performances of a number of Strömgren and broad-band metallicity calibrations). A few broad-band metallicity calibrations are available, in particular for the Sloan system (Ivezić et al. 2008), and they strongly rely on having measurements in the ultraviolet/blue (around 3,500 Å).

The Strömgren system is also able to deliver $\log g$ in late-type stars by measuring the Balmer discontinuity. More than providing a precise measurement, it essentially allows to discriminate between dwarf and giant stars, which for some investigations it is already a very valuable information (e.g., Árnadóttir et al. 2010). However, for the sake of asteroseismology, a photometric or spectroscopic determination of $\log g$ in late-type stars is of little importance, since exceedingly precise surface gravities can be derived using seismic masses and radii, as I discuss further below.

3 Seismic Stellar Parameters

Late-type stars span a vastly different range of gravities and luminosities on the HR diagram and thus have very different internal structures. As a result, they probe a plethora of distances, and have been preferential targets of past and current Galactic surveys. Be it a dwarf or a giant, their cold surface temperatures are the realm of interesting atomic and molecular physics shaping the emergent spectra. The

determination of their physical properties based on the emerging flux (appropriately filtered by the transmission functions of the photometric systems in use) has been the subject of the previous Section. This temperature regime is dominated by convection, which is then the main driver underlying the fundamental oscillation modes we are now able to detect with asteroseismology ("bloody F stars" excluded from now on).

Stellar oscillations driven by surface convection are visible in the power spectrum of time series photometry as a series of Lorentzian-shaped peaks whose peak height has an approximately Gaussian shape (Chaplin and Miglio 2013). Two quantities can be readily extracted from this oscillation pattern, without the need for individual frequency determinations (e.g., Ulrich 1986; Brown et al. 1991): the large frequency separation $\Delta\nu$ (the average separation between peaks of the same spherical angular degree l and consecutive radial order n), and the frequency of maximum amplitude $\nu_{\rm max}$ (located in correspondence of the Gaussian peak). These two frequencies are tightly correlated to the stellar mass, radius and $T_{\rm eff}$ via the so called scaling relations (e.g., Hekker et al. 2009; Stello et al. 2009; Miglio et al. 2009). Provided we have a measurement of $T_{\rm eff}$ (see previous Section), it thus follows that the global oscillation frequencies $\Delta\nu$ and $\nu_{\rm max}$ are able to provide the stellar mass and radius. This is known as the direct method. Another approach is to use stellar models and search for the best solution (using different flavours of frequentist, bayesian, MCMC, etc... inference) to a number of observed properties, among which (but not exclusively) $\Delta\nu$, $\nu_{\rm max}$ and $T_{\rm eff}$: this is known as the grid-based method (e.g., Silva Aguirre et al. 2012; Chaplin et al. 2014).

Understandably, a good deal of effort is currently invested to test the accuracy of the scaling relations and derived stellar properties, or whether scaling relations have any dependence on other parameters such as e.g., metallicity (e.g., White et al. 2011). Radii derived from scaling relations have been shown to be accurate to better than about 5 % in dwarfs and subgiants (e.g., Huber et al. 2012; Silva Aguirre et al. 2012; White et al. 2013), while masses are better than 10 % (at least around solar metallicity, but see Epstein et al. 2014 for the metal poor regime), but are also less tested (see e.g., Miglio et al. 2013a, for a summary). Thus, while awaiting for further tests, for the asteroseismic scaling relations we can adopt the motto "Se non è vero, è ben trovato!".[1]

4 A Match Made in Heaven

From the discussion in the previous Section, it is obvious that combining global oscillation frequencies to classical stellar parameters discloses us very elusive stellar properties, such as radii and masses, which would be otherwise impossible to measure in single field stars. Also, photometric angular diameters and seismic radii

[1] Even if it is not true, it is well conceived.

can be used to derive distances with a quality comparable to that provided by the *Hipparcos* satellite (Silva Aguirre et al. 2012). With this information (masses in particular) we are thus in the position to derive stellar ages in a more sophisticated fashion than via classical isochrone fitting. Using the grid-based method, Chaplin et al. (2014) have derived seismic ages for more than 500 main-sequence and sub-giant stars using only $\Delta\nu$, $\nu_{\rm max}$ and photometric $T_{\rm eff}$. The median uncertainty in the parameters derived by Chaplin et al. (2014) is $\lesssim$ 0.02 dex in $\log g$, 4.4 % in radius and $\sim$ 11 % in mass. This implies ages with a median uncertainty of 34 %; for comparison, this uncertainty is about the best it can be achieved for field main-sequence and sub-giant stars in the absence of seismology, when high-quality parallaxes, $T_{\rm eff}$ and [Fe/H] are available (e.g., Nordström et al. 2004; Casagrande et al. 2011). The above uncertainties in mass and radius reduce by almost a factor of two when [Fe/H] measurements are available, while the median age uncertainty decreases to 25 %, with 80 % of the stars having ages determined to better than 30 % (while again, for comparison, in a non-seismic studies such as Nordström et al. (2004); Casagrande et al. (2011) only about 50 % of stars have ages determined to better than 30 %).

Similar investigations are now carried out using red giant stars, in particular thanks to the APOGEE (Mészáros et al. 2013) and SAGA (Casagrande et al. 2014b) surveys, which based on spectroscopy and photometry respectively, aim at exploiting the full potential of asteroseismology by providing classical stellar parameters. Preliminary investigations (Casagrande et al. 2014b) indicate that uncertainties similar to those derived by Chaplin et al. (2014) apply also for giants, although ages have been still largely unexplored.

There might still be tears in heaven when it comes to fit global oscillation frequencies for the purpose of determining the helium mass fraction Y in (mildly) metal-poor stars (Bonaca et al. 2012). This reminds very closely the issue with fitting another global stellar property in Casagrande et al. (2007), namely the stellar model $T_{\rm eff}$ scale. Both Bonaca et al. (2012) and Casagrande et al. (2007) could avoid the problem of having unrealistically low values of Y by changing convection prescriptions (namely, the mixing-length value with metallicity). Model boundary conditions (indeed linked to the global oscillation frequencies) and/or opacities could also be among the culprits in the helium problem (Portinari et al. 2010; Casagrande et al. 2010a). This is an interesting possibility, considering the role played by opacities in the current tension on the solar chemical composition (e.g., Asplund et al. 2009; Villante et al. 2013).

Conclusions and Future Perspectives

The combination of classical and seismic parameters enables the enthralling possibility of addressing outstanding questions in Galactic astronomy. In particular, using red giants it is possible to probe distances spanning several kpc across the Galaxy, with a median uncertainty of just a few percent

(continued)

(Miglio et al. 2013b; Casagrande et al. 2014b). This makes red giants optimal probes for studies of Galactic structure (e.g., Miglio 2012). In particular, having metallicity information will become increasingly important; not just to improve the precision of seismic parameters as I discussed in the previous Section, but also to allow the study of metallicity and age gradients, as well as the age-metallicity relation in (part of) the Galaxy. Also, when individual abundances will be available from spectroscopy, these will provide stunning new insights/constraints into the chemical enrichment history for these elements.

Until now, deriving reliable ages for red giant stars has been the major limitation, since isochrones with vastly different ages can fit equally well observational constraints such as effective temperatures, metallicities and surface gravities within their errors. However, once a star has evolved on the red giant phase, its age is determined to good approximation by the time spent in the hydrogen burning phase, and this is predominantly a function of mass (e.g., Miglio 2012). Thus, asteroseismology has the potential of delivering ages where other methods are striving or have failed. Investigations are currently going on to assess whether, and how reliably seismic ages for red giants can be obtained, in particular when seismology also provides the distinction between stars climbing the red giant branch and those in the clump phase (Stello et al. 2013), as well as to estimate the effect of mass-loss on age determination for stars in the clump phase.

It is also worth to mention that while global oscillation frequencies are enough for population studies, beautiful investigations in stellar structure and evolution are made possible by the use of individual frequencies, or a combination of these (e.g., Deheuvels et al. 2012; Silva Aguirre et al. 2013). In contrast to global oscillation frequencies, it has been shown that at least for main sequence stars, the use of individual frequencies can yield an accuracy of just a few percent in both mass and radius, and 10 % in age (Silva Aguirre et al. 2013). The exploitation of individual frequencies is more demanding, both observationally and theoretically, but rewarding. For future population studies (at least on the main sequence) it is conceivable to develop an "age ladder": first, achieve the highest possible precision on a number of benchmark stars for which individual frequencies are available (Appourchaux et al. 2012), and then use the parameters so derived as benchmark for stars with only global oscillation frequencies. As last step, asteroseismic ages can then be used to benchmark against classical isochrone fitting. In this context, future asteroseismic missions such as K2 and TESS hold promises in making possible—among other things—to derive seismic parameters (and ages) for all stars in the Geneva-Copenhagen survey (Nordström et al. 2004; Casagrande et al. 2011), a gold standard for Galactic models.

Acknowledgements This review has benefited immensely from collaborations and discussions with a number of outstanding scientists. In particular V. Silva Aguirre for the seismic part, and the other members of the SAGA Survey team. A. Miglio and the other organizers of the Sexten conference "Asteroseismology of stellar populations in the Milky Way" are also kindly acknowledged for inviting to attend a spectacular meeting.

References

Adén, D., Eriksson, K., Feltzing, S., et al. 2011, A&A, 525, A153+
Alonso, A., Arribas, S., & Martinez-Roger, C. 1996, A&A, 313, 873
Appourchaux, T., Chaplin, W. J., García, R. A., et al. 2012, A&A, 543, A54
Árnadóttir, A. S., Feltzing, S., & Lundström, I. 2010, A&A, 521, A40+
Asplund, M. 2005, ARA&A, 43, 481
Asplund, M., Grevesse, N., Sauval, A. J., & Scott, P. 2009, ARA&A, 47, 481
Baglin, A. & Fridlund, M. 2006, in ESA Special Publication, Vol. 1306, ESA Special Publication, ed. M. Fridlund, A. Baglin, J. Lochard, & L. Conroy, 11
Bedin, L. R., Piotto, G., Anderson, J., et al. 2004, ApJ, 605, L125
Bell, R. A. & Gustafsson, B. 1989, MNRAS, 236, 653
Bensby, T., Feltzing, S., & Oey, M. S. 2013, ArXiv e-prints
Bessell, M. S. 2005, ARA&A, 43, 293
Bird, J. C., Kazantzidis, S., Weinberg, D. H., et al. 2013, ApJ, 773, 43
Bonaca, A., Tanner, J. D., Basu, S., et al. 2012, ApJ, 755, L12
Bonnell, J. & Bell, R. A. 1982, MNRAS, 201, 253
Brown, T. M., Gilliland, R. L., Noyes, R. W., & Ramsey, L. W. 1991, ApJ, 368, 599
Calamida, A., Bono, G., Stetson, P. B., et al. 2007, ApJ, 670, 400
Casagrande, L., Flynn, C., & Bessell, M. 2008, MNRAS, 389, 585
Casagrande, L., Flynn, C., Portinari, L., Girardi, L., & Jimenez, R. 2007, MNRAS, 382, 1516
Casagrande, L., Portinari, L., & Flynn, C. 2006, MNRAS, 373, 13
Casagrande, L., Portinari, L., & Flynn, C. 2010a, in IAU Symposium, Vol. 268, IAU Symposium, ed. C. Charbonnel, M. Tosi, F. Primas, & C. Chiappini, 129–134
Casagrande, L., Portinari, L., Glass, I. S., et al. 2014a, MNRAS, 439, 2060
Casagrande, L., Ramírez, I., Meléndez, J., & Asplund, M. 2012, ApJ, 761, 16
Casagrande, L., Ramírez, I., Meléndez, J., Bessell, M., & Asplund, M. 2010b, A&A, 512, A54+
Casagrande, L., Schönrich, R., Asplund, M., et al. 2011, A&A, 530, A138
Casagrande, L., Silva Aguirre, V., Stello, D., et al. 2014b, ApJ, 787, 110
Casagrande, L., & VandenBerg, D.A., 2014, MNRAS, 444, 392
Chaplin, W. J., Basu, S., Huber, D., et al. 2014, ApJS, 210, 1
Chaplin, W. J., Kjeldsen, H., Christensen-Dalsgaard, J., et al. 2011, Science, 332, 213
Chaplin, W. J. & Miglio, A. 2013, ARA&A, 51, 353
Chiappini, C., Matteucci, F., & Romano, D. 2001, ApJ, 554, 1044
Cutri, R. M. & et al. 2012, VizieR Online Data Catalog, 2311, 0
Cutri, R. M., Skrutskie, M. F., van Dyk, S., et al. 2003, 2MASS All Sky Catalog of point sources. (The IRSA 2MASS All-Sky Point Source Catalog, NASA/IPAC Infrared Science Archive. http://irsa.ipac.caltech.edu/applications/Gator/)
Datson, J., Flynn, C., & Portinari, L. 2012, MNRAS, 426, 484
De Ridder, J., Barban, C., Baudin, F., et al. 2009, Nature, 459, 398
Deheuvels, S., García, R. A., Chaplin, W. J., et al. 2012, ApJ, 756, 19
Edvardsson, B., Andersen, J., Gustafsson, B., et al. 1993, A&A, 275, 101
Eggen, O. J., Lynden-Bell, D., & Sandage, A. R. 1962, ApJ, 136, 748
Epstein, C. R., Elsworth, Y. P., Johnson, J. A., et al. 2014, ApJ, 785, L28
Faria, D., Feltzing, S., Lundström, I., et al. 2007, A&A, 465, 357

Gilliland, R. L., Brown, T. M., Christensen-Dalsgaard, J., et al. 2010, PASP, 122, 131
Gliese, W. 1957, Astron. Rechen-Institut, Heidelberg, 89 Seiten, 8, 1
Golay, M. 1972, Vistas in Astronomy, 14, 13
González Hernández, J. I. & Bonifacio, P. 2009, A&A, 497, 497
Grebel, E. K. & Richtler, T. 1992, A&A, 253, 359
Haywood, M. 2002, MNRAS, 337, 151
Hekker, S., Kallinger, T., Baudin, F., et al. 2009, A&A, 506, 465
Hilker, M. 2000, A&A, 355, 994
Huber, D., Ireland, M. J., Bedding, T. R., et al. 2012, ApJ, 760, 32
Ireland, M. J., Mérand, A., ten Brummelaar, T. A., et al. 2008, in Society of Photo-Optical Instrumentation Engineers (SPIE) Conference Series, Vol. 7013, Society of Photo-Optical Instrumentation Engineers (SPIE) Conference Series
Ivezić, Ž., Sesar, B., Jurić, M., et al. 2008, ApJ, 684, 287
Ivezić, Ž., Smith, J. A., Miknaitis, G., et al. 2007, AJ, 134, 973
Johnson, H. L. 1966, ARA&A, 4, 193
Lallement, R., Vergely, J.-L., Valette, B., et al. 2014, A&A, 561, A91
Lebreton, Y. & Montalbán, J. 2009, in IAU Symposium, Vol. 258, IAU Symposium, ed. E. E. Mamajek, D. R. Soderblom, & R. F. G. Wyse, 419–430
Matteucci, F. & Francois, P. 1989, MNRAS, 239, 885
McClure, R. D. & van den Bergh, S. 1968, AJ, 73, 313
Meléndez, J., Casagrande, L., Ramírez, I., Asplund, M., & Schuster, W. J. 2010a, A&A, 515, L3+
Meléndez, J., Schuster, W. J., Silva, J. S., et al. 2010b, A&A, 522, A98+
Mészáros, S., Holtzman, J., García Pérez, A. E., et al. 2013, AJ, 146, 133
Miglio, A. 2012, Asteroseismology of Red Giants as a Tool for Studying Stellar Populations: First Steps, ed. A. Miglio, J. Montalbán, & A. Noels, 11
Miglio, A., Chiappini, C., Morel, T., et al. 2013a, in European Physical Journal Web of Conferences, Vol. 43, European Physical Journal Web of Conferences, 3004
Miglio, A., Chiappini, C., Morel, T., et al. 2013b, MNRAS, 429, 423
Miglio, A., Montalbán, J., Baudin, F., et al. 2009, A&A, 503, L21
Minchev, I., Chiappini, C., & Martig, M. 2013, A&A, 558, A9
Mould, J. R. & Bessell, M. S. 1982, ApJ, 262, 142
Mould, J. R. & Siegel, M. J. 1982, PASP, 94, 223
Nordström, B., Mayor, M., Andersen, J., et al. 2004, A&A, 418, 989
Olsen, E. H. 1984, A&AS, 57, 443
Pinsonneault, M. H., An, D., Molenda-Żakowicz, J., et al. 2012, ApJS, 199, 30
Portinari, L., Casagrande, L., & Flynn, C. 2010, MNRAS, 406, 1570
Portinari, L., Chiosi, C., & Bressan, A. 1998, A&A, 334, 505
Porto de Mello, G. F., da Silva, R., da Silva, L., & de Nader, R. V. 2013, ArXiv e-prints
Reddy, B. E., Lambert, D. L., & Allende Prieto, C. 2006, MNRAS, 367, 1329
Ridgway, S. T., Joyce, R. R., White, N. M., & Wing, R. F. 1980, ApJ, 235, 126
Saito, R. K., Minniti, D., Dias, B., et al. 2012, A&A, 544, A147
Schlafly, E., Green, G., & Finkbeiner, D. P. 2013, in American Astronomical Society Meeting Abstracts, Vol. 221, American Astronomical Society Meeting Abstracts, 145.06
Schönrich, R. & Binney, J. 2009, MNRAS, 396, 203
Schuster, W. J. & Nissen, P. E. 1989, A&A, 221, 65
Silva Aguirre, V., Basu, S., Brandão, I. M., et al. 2013, ApJ, 769, 141
Silva Aguirre, V., Casagrande, L., Basu, S., et al. 2012, ApJ, 757, 99
Soderblom, D. R. 2010, ARA&A, 48, 581
Stello, D., Chaplin, W. J., Basu, S., Elsworth, Y., & Bedding, T. R. 2009, Monthly Notices of the Royal Astronomical Society: Letters, 400, L80
Stello, D., Huber, D., Bedding, T. R., et al. 2013, ApJ, 765, L41
Stetson, P. B., Hesser, J. E., & Smecker-Hane, T. A. 1998, PASP, 110, 533
Strömgren, B. 1966, ARA&A, 4, 433

Strömgren, B. 1987, in NATO ASIC Proc. 207: The Galaxy, ed. G. Gilmore & B. Carswell, 229–246
Twarog, B. A. 1980, ApJ, 242, 242
Twarog, B. A., Vargas, L. C., & Anthony-Twarog, B. J. 2007, AJ, 134, 1777
Ulrich, R. K. 1986, ApJ, 306, L37
VandenBerg, D. A., Casagrande, L., & Stetson, P. B. 2010, AJ, 140, 1020
Villante, F. L., Serenelli, A. M., Delahaye, F., & Pinsonneault, M. H. 2013, ArXiv e-prints
Wallerstein, G. 1962, ApJS, 6, 407
White, T. R., Bedding, T. R., Stello, D., et al. 2011, ApJ, 743, 161
White, T. R., Huber, D., Maestro, V., et al. 2013, MNRAS, 433, 1262
Wing, R. F. 1967, PhD thesis, UNIVERSITY OF CALIFORNIA, BERKELEY.
Worthey, G., Faber, S. M., Gonzalez, J. J., & Burstein, D. 1994, ApJS, 94, 687
Yong, D., Grundahl, F., Johnson, J. A., & Asplund, M. 2008, ApJ, 684, 1159
Zasowski, G. 2012, PhD thesis, University of Virginia

Spectroscopic Constraints for Low-Mass Asteroseismic Targets

Thierry Morel

Abstract A full exploitation of the observations provided by the CoRoT and *Kepler* missions depends on our ability to complement these data with accurate effective temperatures and chemical abundances. We review in this contribution the major efforts that have been undertaken to characterise late-type, seismic targets based on spectra gathered as part of the ground-based, follow-up campaigns. A specific feature of the spectroscopic studies of these stars is that the gravity can be advantageously fixed to the more accurate value derived from the pulsation spectrum. We will describe the impact that such an approach has on the estimation of $T_{\rm eff}$ and [Fe/H]. The relevance of red-giant seismic targets for studies of internal mixing processes and stellar populations in our Galaxy will also be briefly discussed.

1 Introduction

The great potential of asteroseismology to address some unresolved issues in stellar physics and even, as was discussed during this meeting, to study the stellar populations making up our Galaxy cannot be overstated. Yet these expectations cannot be completely met if some fundamental quantities that are not encoded in seismic data are not accurately known (e.g., Creevey et al. 2012). For this reason, by providing the effective temperature and chemical composition (but also other important information such as the $v \sin i$ or the binary status), a traditional field such as stellar spectroscopy will still play an important role in the future for the study of seismic targets. Conversely, asteroseismology can provide the fundamental quantities (e.g., mass, age, evolutionary status in the case of red giants) that are needed to best interpret the abundance data. These two fields are therefore closely connected and can greatly benefit from each other.

T. Morel (✉)
Institut d'Astrophysique et de Géophysique, Université de Liège, Allée du 6 Août, Bât. B5c, 4000 Liège, Belgium
e-mail: morel@astro.ulg.ac.be

A. Miglio et al. (eds.), *Asteroseismology of Stellar Populations in the Milky Way*,
Astrophysics and Space Science Proceedings 39,
DOI 10.1007/978-3-319-10993-0_8

The large discrepancies between the $\log g$ and [Fe/H] values derived from spectroscopy and those in the *Kepler* Input Catalog (Bruntt et al. 2012; Thygesen et al. 2012) illustrate the clear superiority of spectroscopic techniques over photometric ones for the estimation of these two parameters. Determining accurate temperatures from photometric indices is also challenging in the presence of a significant (and patchy) reddening (e.g., for some CoRoT fields that lie close to the Galactic plane).

2 The Samples Discussed

Numerous spectroscopic analyses of individual seismic targets have been conducted during the last few years (e.g., Mathur et al. 2013; Morel et al. 2013). However, we will restrict ourselves here to discussing the results of studies dealing with a sizeable number of stars observed by either the CoRoT or *Kepler* space missions.

The CoRoT satellite operated either through the seismology (observations of a small number of bright stars in the context of seismic studies) or the exoplanet (observations of numerous faint stars to detect planetary transits) channel. The parameters of a large number of stars in the CoRoT exofields and in various evolutionary stages have been determined using an automated pipeline by Gazzano et al. (2010), while a more comprehensive analysis of 19 red giants in the seismology fields has been presented by Morel et al. (2014).[1] In the latter case, a standard analysis is employed that imposes excitation and ionisation equilibrium of iron based on the equivalent widths of a set of Fe I and Fe II lines.

On the other hand, a study of dwarfs and giants in the *Kepler* field has been performed by Bruntt et al. (2012) and Thygesen et al. (2012), respectively (the latter study superseding that of Bruntt et al. 2011). In both cases, the analysis relied on the spectral-synthesis software package `VWA` (see, e.g., Bruntt et al. 2002).

Table 1 gives for all the studies mentioned above the uncertainties associated to the determination of the parameters. Based on the (sometimes rather scanty) information provided in the papers, it may be concluded that these figures are claimed to be representative of the *accuracy* of the results. Although the measurements are also affected by a number of issues (e.g., calibration, angular diameter corrections, reddening), the satisfactory agreement with the less model-dependent estimates provided by interferometry for stars at near-solar metallicities (e.g., Bruntt et al. 2010; Huber et al. 2012; Morel et al. 2014) suggests that the values quoted in Table 1 for $T_{\rm eff}$ are reasonable in this metallicity regime (however, this may not be true for metal-poor stars where non-LTE and 3D effects become important; Lind et al. 2012; Dobrovolskas et al. 2013). Much more extensive and stringent tests can be expected in the future thanks to the advent of new long-baseline interferometric facilities.

[1] Note that the sample of Morel et al. (2014) discussed in the following contains a few stars which were eventually not observed by the satellite, as well as a number of benchmark stars used for validation purposes.

Table 1 Typical 1-σ uncertainty of the parameter determination for the seismic targets

Type of stars	Magnitude range	Type of data	$\sigma_{T_{eff}}$	$\sigma_{\log g}$	$\sigma_{[Fe/H]}$	Reference
Stars in CoRoT exofields	$12 < r' < 16$	Medium resolution[a]	140	0.27	0.19	1
Giants in CoRoT seismofields	$6 < V < 9$	High resolution	85	0.20	0.10	2
			60	0.07	0.08	2
Dwarfs in *Kepler* field	$7 < V_T < 10.5$	High resolution	70	0.08	...	3
			60	0.03	0.06	3
Giants in *Kepler* field	$7 < V < 12$	High resolution	80	0.20	0.15	4

When available, the second row gives for a given study the uncertainties in case the gravity is fixed to the seismic value (see Sect. 3). References: (1) Gazzano et al. (2010); (2)Morel et al. (2014); (3) Bruntt et al. (2012); (4) Thygesen et al. (2012).[a] Also small wavelength coverage (∼200 Å)

A comparison for a subset of *Kepler* targets between the parameters obtained by Bruntt et al. (2012) and Thygesen et al. (2012), and those derived by two other methods has recently been presented by Molenda-Żakowicz et al. (2013). For the reader interested in the differences arising from the use of different spectroscopic methods, see, e.g., Gillon and Magain (2006) and Creevey et al. (2012). The impact of the neglect of non-LTE effects on the parameters inferred from excitation and ionisation balance of iron is discussed by, e.g., Lind et al. (2012) and Bensby et al. (2014).

3 Adopting the Seismic Gravity in Spectroscopic Analyses

As has been exhaustively discussed in the recent literature, $\log g$ can be estimated in various ways from seismic observables: either from a detailed modelling of the oscillation spectrum or from scaling relations/grid-based methods that make use of $\Delta\nu$ (the average large frequency separation) and ν_{max} (the frequency corresponding to maximum oscillation power). A number of empirical tests (e.g., Chaplin and Miglio 2013, and references therein) indicate that such estimates are significantly more accurate than those derived from spectroscopic methods (typically 0.05 vs. 0.15–0.20 dex). There is therefore an advantage in fixing the gravity to the seismic value in spectroscopic analyses, as is indeed now routinely done (e.g., Huber et al. 2013).[2] We will first discuss in the following the quantitative impact of adopting the seismic gravity on the determination of $T_{\rm eff}$ and [Fe/H], and then turn our attention to the issue of the best metallicity to adopt when such a hybrid approach is employed.

[2]The possibility of using an independent and more accurate gravity value is also shared by stars with planetary transits (e.g., Torres et al. 2012).

3.1 Impact on the Determination of the Other Parameters

For the *Kepler* targets, there is a good level of agreement in a statistical sense between the spectroscopic and seismic gravities, with no evidence for global systematic offsets: $\langle \log g \text{ (spectroscopy)} - \log g \text{ (seismology)} \rangle = +0.08 \pm 0.07$ for dwarfs (Bruntt et al. 2012) and –0.05±0.30 dex for giants (Thygesen et al. 2012), respectively. However, large differences can be found on a star-to-star basis (up to 0.7 dex). As shown by Morel et al. (2011), even larger discrepancies are evident for the red giants studied by Gazzano et al. (2010) (see also discussion by Valentini et al. 2013 who independently re-analysed these data and found a more satisfactory agreement, especially for spectra with a low signal-to-noise ratio). On the other hand, the values are identical within the errors for all the giants analysed by Morel et al. (2014).

The effect of fixing the gravity to the seismic value on the $T_{\rm eff}$ and [Fe/H] determinations is illustrated in Fig. 1. A change in $\log g$ of 0.1 dex typically leads for giants in the CoRoT seismology fields to variations in $T_{\rm eff}$ of 15 K and in [Fe/H] of 0.04 dex. The good agreement between the two sets of $\log g$ values only implies relatively small adjustments for $T_{\rm eff}$ and the abundances (generally below 50 K

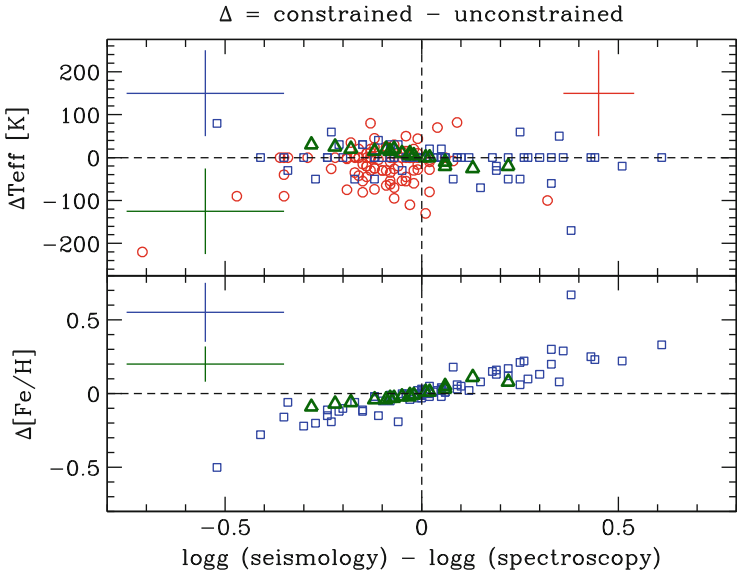

Fig. 1 Effect on the $T_{\rm eff}$ and [Fe/H] determinations of using either the seismic or the spectroscopic gravity. The (un)constrained results are for the $\log g$ (not) fixed to the seismic value. *Red circles*: *Kepler* dwarfs (Bruntt et al. 2012), *blue squares*: *Kepler* giants (Thygesen et al. 2012), *green triangles*: red giants in CoRoT seismofields (Morel et al. 2014). Note that the metallicities obtained using the spectroscopic gravities are not available for the *Kepler* dwarfs (Bruntt et al. 2012). The extreme outlier KIC 4070746 is not included in this figure (see discussion in Thygesen et al. 2012) (Color figure online)

and 0.1 dex). A similar sensitivity of [Fe/H] against changes in $\log g$ is obtained for *Kepler* giants. However, variations in the adopted $\log g$ are in this case not accompanied in a coherent way by $T_{\rm eff}$ changes. It is in particular not completely clear how $\log g$ changes amounting to up to 0.6 dex can lead to exactly identical $T_{\rm eff}$ values. There is also a lack of correlation between the $\log g$ and $T_{\rm eff}$ changes for *Kepler* dwarfs. On the other hand, Huber et al. (2013) found for exoplanet host candidates (mostly solar-like) that a change in $\log g$ of 0.1 dex typically leads to variations of 50 K and 0.03 dex for $T_{\rm eff}$ and [Fe/H], respectively. It is important to note that the figures quoted above for dwarfs and giants cannot be generalised and depend on the exact procedures that are implemented to derive the parameters (see Torres et al. 2012).

3.2 The Ambiguity Surrounding the Best Metallicity Value

The surface gravity is usually determined from spectroscopic data by requiring that ionisation balance of iron is fulfilled. In many cases, this condition will no longer be satisfied once the seismic gravity is adopted (Bruntt et al. 2012; Thygesen et al. 2012). As a result, the mean abundances derived from the Fe I and Fe II lines will differ, and there will therefore be an ambiguity as to which iron abundance should be preferred. As an illustration, using the seismic constraints, Bruntt et al. (2012) obtained [Fe I/H]$= -0.02$, but [Fe II/H]$= +0.32$ for KIC 3424541. The metallicity is an essential ingredient of any seismic modelling, and adopting one value or the other will clearly lead to substantially different estimates for the fundamental stellar parameters, such as the age, for instance.

The Fe II lines are known in solar-like dwarfs to be less affected than the Fe I lines by both non-LTE and granulation effects (e.g., Asplund et al. 2000). The mean Fe II-based abundance hence appears to be a better proxy of the stellar metallicity when using a 1D, LTE analysis. However, the choice is not as straightforward for red giants. Although the departures from LTE are also much less severe for the Fe II lines, these features are affected by a number of caveats: (1) they are usually only a few, difficult to measure, and potentially more affected by blends; (2) they are very sensitive to errors in $T_{\rm eff}$ (varying it by 50 K while keeping the gravity fixed typically changes the Fe I abundances by only 0.01–0.02 dex, but the Fe II ones by 0.06 dex); (3) they may suffer more than the Fe I lines at near-solar metallicity from the neglect of granulation effects (Collet et al. 2007; Kučinskas et al. 2013; see also Fig. 15 of Dobrovolskas et al. 2013). In view of the uncertainties plaguing both the Fe I and Fe II abundances, it is unclear whether the Fe II-based abundances should be deemed as (systematically) more reliable for evolved objects.

4 A Step Beyond the Determination of the Basic Parameters: The Detailed Chemical Composition

The detailed abundance pattern can be obtained for stars observed with high-resolution spectrographs. Figure 2 shows some abundance ratios with respect to iron as a function of [Fe/H] for the samples of Bruntt et al. (2012), Thygesen et al. (2012), and Morel et al. (2014). Because of the chemical evolution of the Galaxy, it is well established that—depending on their nucleosynthesis—each element displays a distinct behaviour as a function of the iron content. For instance, the abundance ratio of the α elements (e.g., Ca) increases when [Fe/H] decreases, whereas the iron-peak elements (e.g., Ni) closely follow Fe. An enhancement with respect to solar of some important species such as oxygen should be taken into account when modelling low-metallicity asteroseismic targets. Some elements behave qualitatively as expected in Fig. 2 (e.g., Si and Ni), but the expected trends at low metallicities are not seen in

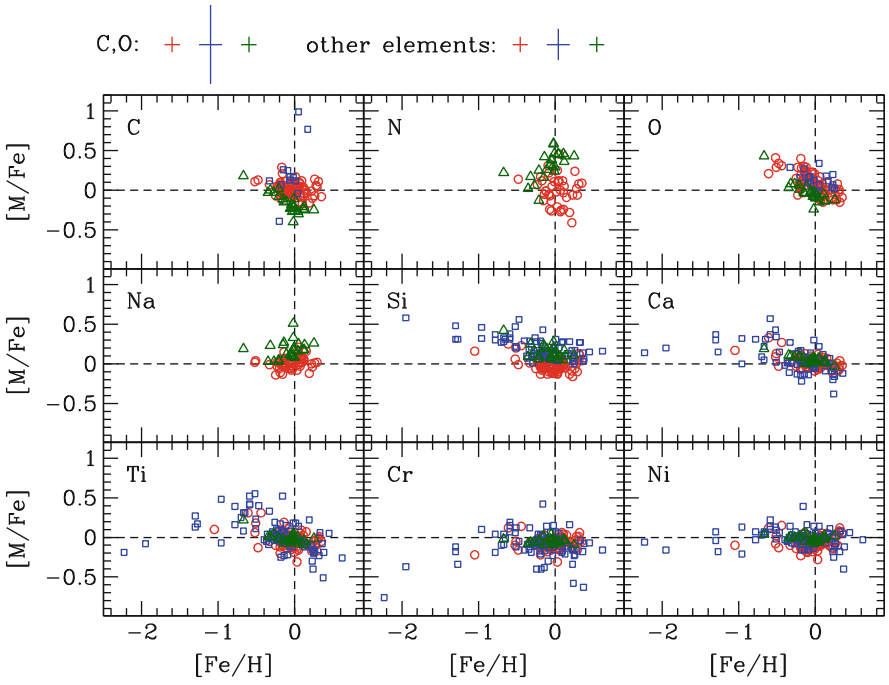

Fig. 2 Abundance ratios with respect to iron as a function of [Fe/H] for stars in the *Kepler* and CoRoT fields. The results have been obtained using a 1D, LTE analysis and (except for the CoRoT stars) the seismic gravities. Same symbols as in Fig. 1. For the *Kepler* stars, [Fe/H] is based on the Fe II lines and the abundances of the other elements on the neutral species. Following Bruntt et al. (2012), we only consider mean abundances for *Kepler* dwarfs with $v \sin i$ below 25 km s^{-1} and computed based on at least five lines of each element (except for nitrogen and oxygen: two and three lines, respectively)

some cases (e.g., Ti and Cr) and the patterns generally much noisier than found in the literature for disc stars in the solar neighbourhood (e.g., Bensby et al. 2014). This can at least be partly attributed to the limitations of (semi)automated pipelines applied to data of lower quality. The fainter *Kepler* targets have often only been observed with 1m- or 2m-class telescopes (Bruntt et al. 2012; Thygesen et al. 2012; Molenda-Żakowicz et al. 2013).

The data shown in Fig. 2 are heterogeneous and any study-to-study difference in the global patterns may be misinterpreted as being of physical origin whereas it merely reflects systematic effects. However, the carbon depletion and nitrogen excess of the CoRoT giants compared to *Kepler* dwarfs may be expected because of mixing (see, e.g., Luck and Heiter 2007, in the case of C). More robust conclusions could have been drawn for carbon by comparing the data for *Kepler* dwarfs and giants (thanks to the similarity of the analyses carried out by Bruntt et al. 2012 and Thygesen et al. 2012), but the results for giants are affected by large uncertainties.

The extent of mixing experienced by red giants results from the combined action of different physical processes (convective and rotational mixing, as well as arguably thermohaline instabilities) whose relative efficiency is a complex function of their evolutionary status, mass, metallicity, and rotational history (e.g., Charbonnel and Lagarde 2010). Fortunately, several key indicators with a different sensitivity to each of these processes can be measured in the optical wavelength domain (Li, CNO, Na, and $^{12}C/^{13}C$) and used to constrain theoretical models. As can be seen in Fig. 3, the occurrence of internal mixing phenomena is betrayed in CoRoT red giants by the existence of well-defined trends between the surface abundances of some species (for a discussion of these results, see Morel et al. 2014).

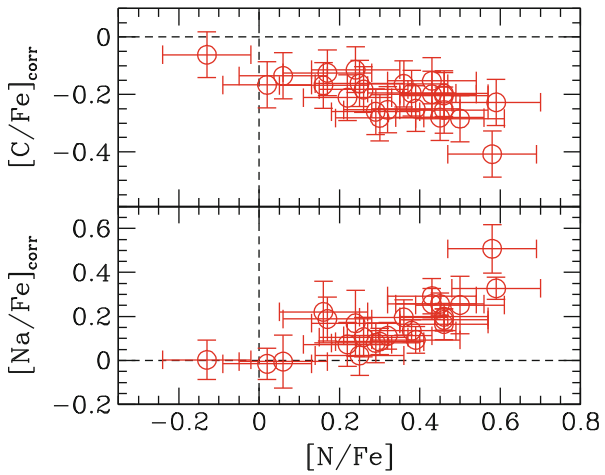

Fig. 3 *Top* and *bottom panels*: [C/Fe] and [Na/Fe] as a function of [N/Fe] for the red giants in the CoRoT seismology fields. The C and Na data have been corrected for the effects of the chemical evolution of the Galaxy (for details, see Morel et al. 2014). The results have been obtained using the spectroscopic gravities (Color figure online)

It is important to note that such abundance studies applied to asteroseismic targets may lead to a leap forward in our understanding of transport phenomena in evolved, low- and intermediate-mass stars because of the availability of an accurate mass estimate and, in some cases, a knowledge of the evolutionary status.

5 Some Perspectives

A detailed spectroscopic analysis has been carried out so far for only a tiny fraction of all the stars observed by CoRoT and *Kepler*. Much more is expected (or may be achievable) in the near future. We briefly mention below two of the most promising avenues of research.

Seismic targets are currently used as benchmark stars in various ongoing or soon-to-be-started large-scale surveys, such as APOGEE (Mészáros et al. 2013), Gaia-ESO (Gilmore et al. 2012), or GALAH (Freeman 2012). The combination of the spectroscopic data with the asteroseismic ones for the radii, masses, ages, and distances will be of great relevance for investigating the properties of the stellar populations constituting our Galaxy (see, e.g., Chiappini 2012; Miglio et al. 2013). The *Gaia* satellite will dramatically contribute to this harvest by providing kinematic information of unprecedented quality.

The various evolutionary sequences of red-giant stars can be distinguished from asteroseismic diagnostics (e.g., Stello et al. 2013; Montalbán et al. 2013). This opens up the possibility of mapping out the evolution of the mixing indicators during the shell-hydrogen and core-helium burning phases for a very large number of stars with accurate masses (see the tentative results for carbon of Luck and Heiter 2007). Knowing the fundamental parameters (e.g., mass, age) of dwarfs and having the possibility of probing their internal structure also make them particularly suitable for investigating the destruction of lithium during the early stages of stellar evolution.

Acknowledgements I acknowledge financial support from Belspo for contract PRODEX GAIA-DPAC. I am very grateful to the Fonds National de la Recherche Scientifique (FNRS) and Annie Baglin for providing the financial resources that made my attendance possible.

References

Asplund, M., Nordlund, Å., Trampedach, R., & Stein, R. F. 2000, A&A, 359, 743
Bensby, T., Feltzing, S., & Oey, M. S. 2014, A&A, 562, A71
Bruntt, H., Basu, S., Smalley, B., et al. 2012, MNRAS, 423, 122
Bruntt, H., Bedding, T. R., Quirion, P.-O., et al. 2010, MNRAS, 405, 1907
Bruntt, H., Catala, C., Garrido, R., et al. 2002, A&A, 389, 345
Bruntt, H., Frandsen, S., & Thygesen, A. O. 2011, A&A, 528, A121
Chaplin, W. J. & Miglio, A. 2013, ARA&A, 51, 353
Charbonnel, C. & Lagarde, N. 2010, A&A, 522, A10

Chiappini, C. 2012, Red Giant Stars: Probing the Milky Way Chemical Enrichment, ed. A. Miglio, J. Montalbán, & A. Noels, 147
Collet, R., Asplund, M., & Trampedach, R. 2007, A&A, 469, 687
Creevey, O. L., Doğan, G., Frasca, A., et al. 2012, A&A, 537, A111
Dobrovolskas, V., Kučinskas, A., Steffen, M., et al. 2013, A&A, 559, A102
Freeman, K. C. 2012, in Astronomical Society of the Pacific Conference Series, Vol. 458, Galactic Archaeology: Near-Field Cosmology and the Formation of the Milky Way, ed. W. Aoki, M. Ishigaki, T. Suda, T. Tsujimoto, & N. Arimoto, 393
Gazzano, J.-C., de Laverny, P., Deleuil, M., et al. 2010, A&A, 523, A91
Gillon, M. & Magain, P. 2006, A&A, 448, 341
Gilmore, G., Randich, S., Asplund, M., et al. 2012, The Messenger, 147, 25
Huber, D., Chaplin, W. J., Christensen-Dalsgaard, J., et al. 2013, ApJ, 767, 127
Huber, D., Ireland, M. J., Bedding, T. R., et al. 2012, ApJ, 760, 32
Kučinskas, A., Steffen, M., Ludwig, H.-G., et al. 2013, A&A, 549, A14
Lind, K., Bergemann, M., & Asplund, M. 2012, MNRAS, 427, 50
Luck, R. E. & Heiter, U. 2007, AJ, 133, 2464
Mathur, S., Bruntt, H., Catala, C., et al. 2013, A&A, 549, A12
Mészáros, S., Holtzman, J., García Pérez, A. E., et al. 2013, AJ, 146, 133
Miglio, A., Chiappini, C., Morel, T., et al. 2013, MNRAS, 429, 423
Molenda-Żakowicz, J., Sousa, S. G., Frasca, A., et al. 2013, MNRAS, 434, 1422
Montalbán, J., Miglio, A., Noels, A., et al. 2013, ApJ, 766, 118
Morel, T., Miglio, A., Lagarde, N., et al. 2014, A&A, 564, A119
Morel, T., Miglio, A., & Valentini, M. 2011, Journal of Physics Conference Series, 328, 012010
Morel, T., Rainer, M., Poretti, E., Barban, C., & Boumier, P. 2013, A&A, 552, A42
Stello, D., Huber, D., Bedding, T. R., et al. 2013, ApJ, 765, L41
Thygesen, A. O., Frandsen, S., Bruntt, H., et al. 2012, A&A, 543, A160
Torres, G., Fischer, D. A., Sozzetti, A., et al. 2012, ApJ, 757, 161
Valentini, M., Morel, T., Miglio, A., Fossati, L., & Munari, U. 2013, in European Physical Journal Web of Conferences, Vol. 43, European Physical Journal Web of Conferences, 3006

Preliminary Evaluation of the *Kepler* Input Catalog Extinction Model Using Stellar Temperatures

Gail Zasowski, Deokkeun An, and Marc Pinsonneault

Abstract The *Kepler* Input Catalog (KIC) provides reddening estimates for its stars, based on the assumption of a simple exponential dusty screen. This project focuses on evaluating and improving these reddening estimates for the KIC's giant stars, for which extinction is a much more significant concern than for the nearby dwarf stars. We aim to improve the calibration (and thus consistency) amongst various photometric and spectroscopic temperatures of stars in the *Kepler* field by removing systematics due to incorrect extinction assumptions. The revised extinction estimates may then be used to derive improved stellar and planetary properties. We plan to eventually use the large number of KIC stars as probes into the structure and properties of the Galactic ISM.

1 Introduction

The dusty interstellar medium (ISM) of the Milky Way (MW) permeates the entire galaxy, with non-zero reddening observed even at the Galactic poles. Even though the effects of extinction at infrared (IR) wavelengths are smaller than those at optical wavelengths, both optical and near-IR images of the MW demonstrate that interstellar dust is strongly concentrated in the midplane but not exclusively confined there. And the *Kepler* field, lying 5°–20° off the midplane, is hardly free of its effects. One of the major problems with unaccounted-for extinction

G. Zasowski (✉)
The Ohio State University, Columbus, OH 43210, USA
Johns Hopkins University, Baltimore, MD 21218, USA
e-mail: gail.zasowski@gmail.com

D. An
Ewha Womans University, Seoul, South Korea
e-mail: deokkeun.an@gmail.com

M. Pinsonneault
The Ohio State University, Columbus, OH 21218, USA
e-mail: pinsonneault.1@osu.edu

A. Miglio et al. (eds.), *Asteroseismology of Stellar Populations in the Milky Way*,
Astrophysics and Space Science Proceedings 39,
DOI 10.1007/978-3-319-10993-0_9

is that it changes properties inferred from photometry (e.g., luminosity, distance, temperature) in a *systematic* way—stars always look cooler and fainter, never the other way around.

Of course, much effort has been made to address this issue, leading to a large number of extinction maps and models derived using a variety of methods and ISM tracers. To name just a few examples, Drimmel et al. (2003) and Drimmel and Spergel (2001) have built an analytic model of the MW's ISM, complete with a smooth disk and superimposed dusty spiral arms. The commonly adopted all-sky reddening maps by Schlegel et al. (1998) use primarily the dust emission at 100 μm to trace extinction, along with some assumptions about the dust homogeneity that make the maps tricky to apply within 20° or so of the midplane. Marshall et al. (2006) compared NIR color-magnitude diagrams to those predicted by the Besançon MW stellar populations model and published extinction maps spanning the MW's midplane. Very recently, Gonzalez et al. (2012) published maps of the Galactic bulge, using red clump stars from the VVV to trace extinction on arcmin scales.

In comparison, the *Kepler* Input Catalog (KIC) assumed the extinction model of a smooth, vertically-exponential dust disk, with a scaleheight H of 150 pc and an extinction density κ_0 normalized to 1 mag of V-band extinction per kpc at $b = 0°$:

$$E(B-V)_{\rm KIC} = 0.367\kappa_0 \int_0^d e^{-\frac{s}{H}\sin b} {\rm d}s, \tag{1}$$

(adapted from Brown et al. 2011). Thus the reddening can be parameterized as a function of distance d and latitude b alone, with typical values for the KIC stars of $E(B-V) \sim 0.05$–0.18 mag. However, the KIC stellar parameters were derived simultaneously along with the reddening, meaning that the final $E(B-V)$ values are implicitly tied to all of the parameters, including the effective temperature ($T_{\rm eff}$) and the metallicity. These correlations mean that the catalog reddening values have strong implications for other properties of interest further down the pipeline, such as planetary radii or the stellar distances derived using the KIC parameters in other methods, which are important for any Galactic structure work or study of metallicity or age gradients (to name but a few possibilities).

2 Comparison of Photometric and Spectroscopic Temperatures

In the top left panel of Fig. 1, we show the comparison between two photometric temperature methods: the original KIC $T_{\rm eff}$ values and those derived from SDSS *griz* colors by Pinsonneault et al. (2012). An offset of ∼100–200 K demonstrates that adopting the KIC reddening values, along with internally consistent color-$T_{\rm eff}$ relations, would give rise to systematically hotter temperatures. The bottom panel of Fig. 1 shows that the *griz* temperatures (corrected for giant stars) are far more consistent with those derived with the InfraRed Flux Method (IRFM; Casagrande

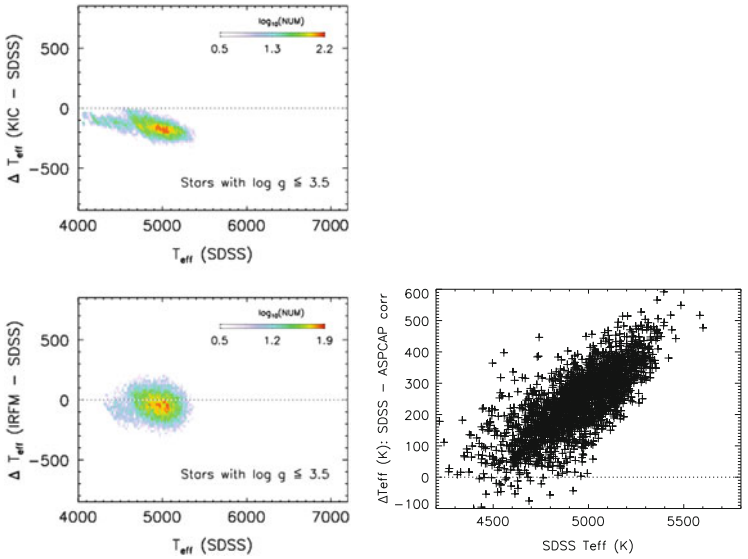

Fig. 1 *Left:* Comparison between the SDSS *griz* $T_{\rm eff}$ values and (*top*) the KIC $T_{\rm eff}$ and (*bottom*) IRFM $T_{\rm eff}$ for giant stars. (Fig. 18 of ref Pinsonneault et al. 2013). *Right:* Difference between the SDSS *griz* $T_{\rm eff}$ values and those from APOGEE/ASPCAP, as a function of SDSS $T_{\rm eff}$, for the ∼2,000 giants in the APOKASC sample

et al. 2010), which arguably represent a more fundamental measurement of effective temperature as it is defined.

At least two studies have targeted *Kepler* stars for spectroscopic followup and evaluation of the KIC stellar parameters. Thygesen et al. (2012) and Molenda-Żakowicz et al. (2013) observed a total of ∼200 stars, and both found an offset of up to a couple hundred K (which was strongly $T_{\rm eff}$-dependent in Thygesen et al. 2012).

A much larger spectroscopic comparison sample is provided by the APOKASC program, a collaboration between APOGEE, a high-resolution, H-band spectroscopic survey of MW red giant stars (Majewski 2012), and KASC, the core working group of *Kepler* asteroseismic science. The APOKASC team is combining asteroseismic and spectroscopic measurements and their respective derived parameters for $\sim 10^4$ stars (see Sect. 8.3 of Zasowski et al. 2013). The APOKASC catalog at the time of this proceeding contains ∼2,000 giant stars, an increase of nearly an order of magnitude over the previous sample. Figure 1 also shows the comparison between the photometric *griz* $T_{\rm eff}$ and the spectroscopic APOGEE $T_{\rm eff}$, where the latter have been "corrected" to a temperature scale calibrated to a number of well-studied star clusters. Despite this correction, a strongly temperature-dependent offset is clearly present, in addition to a ± 100 K scatter. Possible reasons for the persistent discrepancy include systematic offsets in the APOGEE pipeline and/or potential errors in the theoretical corrections applied to the dwarf-derived *griz*-$T_{\rm eff}$ relations to make them suitable for giants.

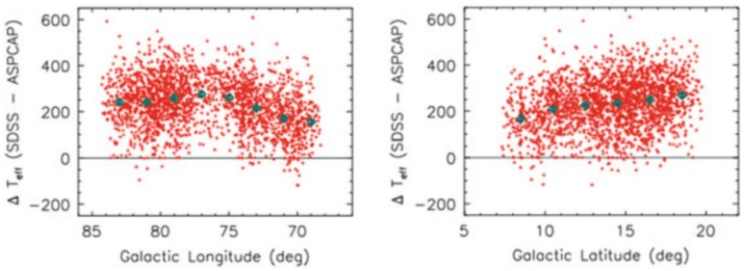

Fig. 2 Difference in *griz* $T_{\rm eff}$ and APOGEE/ASPCAP $T_{\rm eff}$ as a function of (*left*) Galactic longitude and (*right*) Galactic latitude, assuming the original KIC reddening (Color figure online)

2.1 Impact of Extinction?

Figure 2 shows the difference between the *griz* temperatures (which assume a reddening value) and the APOGEE temperatures (which do not), as functions of Galactic longitude (left) and latitude (right). There is no monotonic trend with longitude, though there are hints of coherent structure, but there is a systematic trend with latitude. As any observed $T_{\rm eff}$ offsets should be independent of spatial position, the behavior seen here suggests a problem with the extinction model, which is smooth in longitude but dependent on latitude. In order to test the form and scale of the KIC extinction model, we require a large number of KIC stellar extinction estimates that do not depend on any global Galactic model (which would unavoidably include its own assumptions about the underlying dust structure).

3 Revision of the KIC Extinctions

3.1 RJCE Extinctions

For independent extinction estimates, we turn to the Rayleigh–Jeans Color Excess method (RJCE; Majewski et al. 2011), which provides stellar foreground extinction estimates based on the star's near- and mid-IR photometry. Like other color excess methods, the basis of RJCE is the assumption that all stars in a given sample have a common intrinsic color, such that any observed excess in that color may be attributed to line-of-sight reddening. Where RJCE improves upon earlier color excess approaches is in the combination of NIR + MIR photometry, which sample the Rayleigh–Jeans (RJ) tail of a star's spectral energy distribution (SED). The slope of the RJ tail is almost entirely independent of stellar temperature or metallicity, which means that colors comprising filters measuring this part of the SED are truly homogeneous across a very large fraction of the MW's stellar populations. In contrast, color excess methods relying on more temperature-dependent optical or

NIR-only colors must know a priori, or assume, the spectral type of the stars under consideration. See Majewski et al. (2011) for an expanded description and example applications of the RJCE approach.

Most relevant for the current analysis is that the RJCE extinction values are free from assumptions about the spatial distribution of the MW's dust content and thus provide a good comparison to the KIC values, which are strongly dependent on the KIC's assumed dust disk model. Also relevant are some caveats on RJCE's applicability. Due to [Fe/H]-dependent spectral features, very metal-poor stars ([Fe/H] < -1.5) appear to have intrinsic colors deviating from those assumed in RJCE, such that their extinction values are systematically overestimated. Fortunately, such stars are relatively rare in the *Kepler* field. The uncertainties in the RJCE extinction values arise from the photometric uncertainties as well as uncertainty in the adopted extinction law; typical values for the KIC sample are $\sigma(A[K_s]) < 0.05$ mag.

3.2 Extinction Map Comparison

For this initial assessment of the KIC extinction, we used stars meeting the following criteria: $A(K_s)_{\rm RJCE} \geq 0$, $\sigma(A[K_s])_{\rm RJCE} \leq 0.05$, 2MASS nearest neighbor distance (*prox*) of $\geq 10''$, $4{,}000 \leq (T_{\rm eff})_{\rm KIC} \leq 5{,}000$ K, and $(\log g)_{\rm KIC} \leq 3.7$. These requirements produced a sample of $\sim 13,500$ red giant stars with well-measured RJCE extinction values.

This sample includes stars as faint as $H \sim 15$, while the spectroscopic APOKASC sample is limited to stars with $H \leq 11$. Because we want to ensure that any corrections calculated are applicable to the stars being corrected, we performed the analysis below both with and without an $H \leq 11$ limit on the sample. We found that this limit actually had little-to-no impact on the outcome, which is a result of the fact that stars in our sample with $H \leq 11$ have a very similar extinction distribution (in RJCE and the KIC) as those with $11 < H < 15$. Since the fainter giants comprise more distant stars, as well as intrinsically fainter ones, this result may be somewhat surprising, given the assumption of a strongly distance-dependent extinction distribution. What this suggests is that a foreground extinction screen model may be appropriate for this particular sample (certainly not generally applicable to MW stellar populations!), which provides further justification for the approach adopted below (in which we do not apply the $H \leq 11$ limit). Of course, the KIC extinction values *are* distance dependent, and there is a slightly larger discrepancy between the $E(B-V)$ distributions of the $H \leq 11$ and $11 < H < 15$ subsamples than between the RJCE reddening distributions of the same subsamples, but the discrepancy is still not large enough to significantly affect the outcome below.

We created two extinction maps spanning the entire *Kepler* field, taking as the value of each $0.4° \times 0.2°$ pixel the median KIC $E(B-V)$ or RJCE $A(K_s)$ extinction

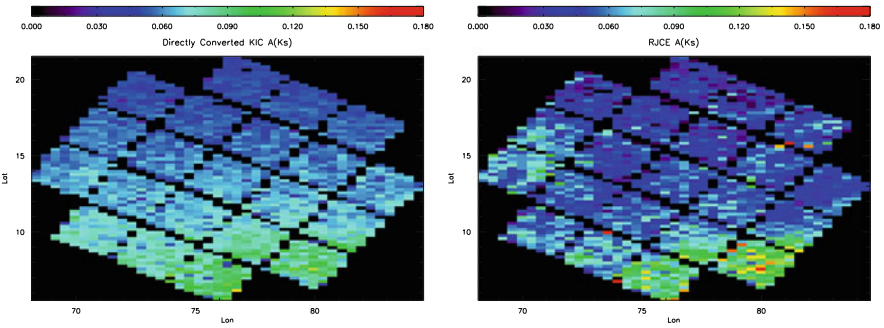

Fig. 3 *Left:* Median map of KIC $A(K_s)$ values, assuming $A(K_s) = 0.388 \times E(B-V)$. *Right:* Median map of RJCE $A(K_s)$ values (Color figure online)

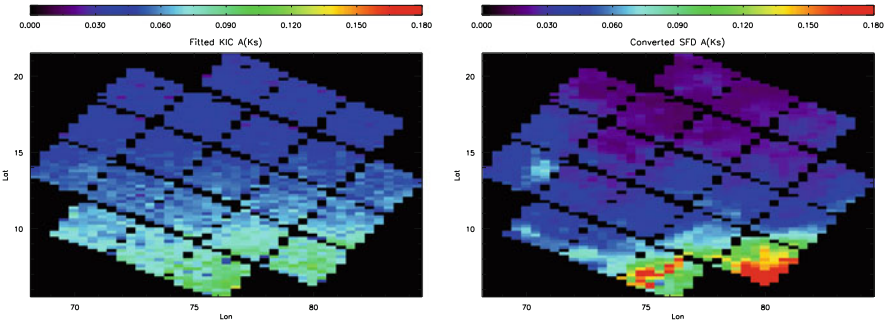

Fig. 4 *Left:* Median map of revised KIC $A(K_s)$ values. *Right:* Median map of Schlegel et al. (1998) $A(K_s)$ values

of the stars in that pixel (Fig. 3, where we have converted the KIC $E(B-V)$ to $A(K_s)$ for comparison purposes). This pixel size was chosen to ensure $\geq$10 stars per bin, and the asymmetry reflects the fact that in both maps, the variations in b have a shorter scale than those in l. We chose to parameterize this first "correction" with a zero-point offset, an extinction-dependent scale factor, and a b-dependent scale factor.

3.3 Results

The fitting of the KIC map to the RJCE one yields: $E(B-V) = E(B-V)_{\rm KIC} \times (1.29 - 1.75 \sin b) + 0.02$. The median extinction map using these fitted KIC reddening values is shown in the left panel of Fig. 4. The impact of this correction scaling is to reduce the effective scaleheight of the KIC model's dust layer, whose original value was even noted in Brown et al. (2011) to be larger than the literature suggested, and to bring the reddening values more in line with those calculated

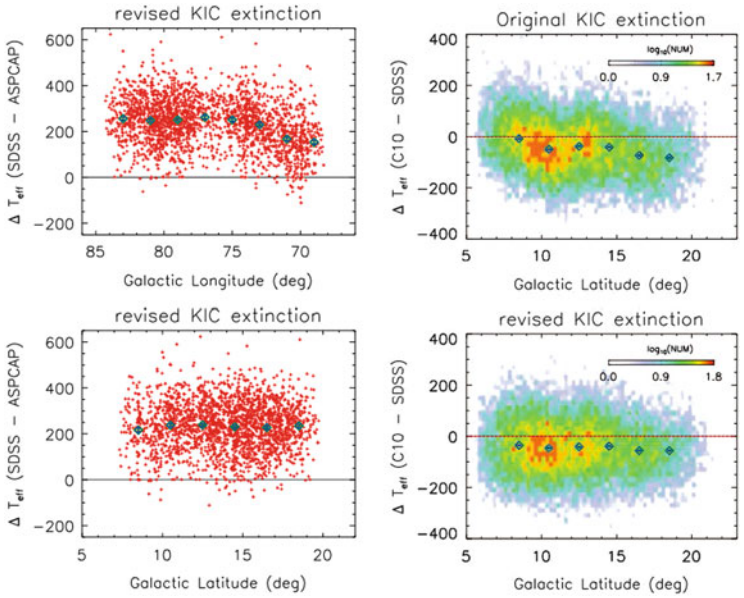

Fig. 5 *Left:* Difference in $T_{\rm eff}$ from SDSS colors and from APOGEE/ASPCAP as functions of (*top*) Galactic longitude and (*bottom*) Galactic latitude, using the revised KIC reddening. Compare to Fig. 2. *Right:* Difference in $T_{\rm eff}$ calculated with the IRFM method (Casagrande et al. 2010) and with SDSS *griz* colors, assuming (*top*) the original KIC reddening and (*bottom*) the revised KIC reddening

from the independent RJCE method (i.e., compare Fig. 3 [right] with Fig. 4 [left]). As a further sanity check, we compare the revised KIC map with the Schlegel et al. (1998) dust map (Fig. 4, right), and we see much better agreement with the revised map than with the original KIC one, in terms of latitude dependence.

In the left column of Fig. 5, we show that the revised map clearly mitigates the spatial dependencies of the offsets between the photometric *griz* temperatures and the spectroscopic APOGEE ones. In the top panel, the longitude structure is reduced (but not eliminated, suggesting further improvement can be made; Sect. 4), and in the bottom panel, the latitude dependence has disappeared entirely. Note that there is still a ∼200 K offset—the revised reddening map has not solved the entire problem, but it does remove that particular systematic contribution to the behavior.

The reddening revisions even appear to reduce some systematics in the comparison of photometric temperatures. The right-hand column of Fig. 5 shows the difference between the IRFM and the *griz* $T_{\rm eff}$ values as a function of b, using the original KIC $E(B-V)$ (top) and the revised $E(B-V)$ (bottom). Both of these methods use extinction estimates but to different degrees. Thus, an offset trend with b is visible (though weaker than in the comparison to spectroscopic $T_{\rm eff}$) but disappears with the revised reddening, most noticeably at higher b.

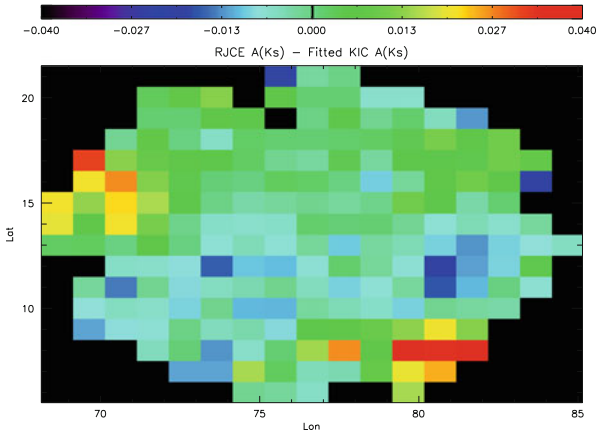

Fig. 6 Difference between the revised KIC extinction map and the RJCE map, in $A(K_s)$

4 Future Improvements

A number of improvements to these preliminary results are actively in progress, including incorporation of substructure parameterization into the KIC model fitting. The $\Delta E(B-V)$ residuals observed between the RJCE and the revised KIC maps are not dominated by random noise (Fig. 6). The presence of coherent clumps and gradients implies real structure in the ISM not accounted for by the KIC's exponential disk model. For example, the residual map shows a clump at $(l, b) \sim (70.5°, 14°)$, clearly visible in the RJCE and Schlegel maps but not in the smooth KIC one. This cloud corresponds to roughly 0.1 mag of $E(B-V)$ reddening *above* the background reproduced in the KIC map. Thus, identifying and parameterizing these irregular variations will have a significant impact on many stars.

Acknowledgements GZ has been supported by an NSF Astronomy & Astrophysics Postdoctoral Fellowship under Award No. AST-1203017, and DA has been supported by the National Research Foundation of Korea to the Center for Galaxy Evolution Research (No. 2010-0027910).

References

Brown, T. M., Latham, D. W., Everett, M. E., & Esquerdo, G. A. 2011, AJ, 142, 112
Casagrande, L., Ramírez, I., Meléndez, J., Bessell, M., & Asplund, M. 2010, A&A, 512, A54
Drimmel, R., Cabrera-Lavers, A., & López-Corredoira, M. 2003, A&A, 409, 205
Drimmel, R. & Spergel, D. N. 2001, ApJ, 556, 181
Gonzalez, O. A., Rejkuba, M., Zoccali, M., et al. 2012, A&A, 543, A13
Majewski, S. R. 2012, in American Astronomical Society Meeting Abstracts, Vol. 219, American Astronomical Society Meeting Abstracts #219, #205.06
Majewski, S. R., Zasowski, G., & Nidever, D. L. 2011, ApJ, 739, 25

Marshall, D. J., Robin, A. C., Reylé, C., Schultheis, M., & Picaud, S. 2006, A&A, 453, 635
Molenda-Żakowicz, J., Sousa, S. G., Frasca, A., et al. 2013, MNRAS, 434, 1422
Pinsonneault, M. H., An, D., Molenda-Żakowicz, J., et al. 2012, ApJS, 199, 30
Pinsonneault, M. H., An, D., Molenda-Żakowicz, J., et al. 2013, ApJS, 208, 12
Schlegel, D. J., Finkbeiner, D. P., & Davis, M. 1998, ApJ, 500, 525
Thygesen, A. O., Frandsen, S., Bruntt, H., et al. 2012, A&A, 543, A160
Zasowski, G., Johnson, J. A., Frinchaboy, P. M., et al. 2013, AJ, 146, 81

The APOKASC Catalog

Jennifer A. Johnson

Abstract I report on the APOKASC catalog, a joint effort between the *Kepler* Asteroseismic Science Consortium and the SDSS-III APOGEE spectroscopic survey. It will contain both seismic and spectroscopic values for stars observed by both surveys. I discuss the derivation of spectroscopic parameters and their uncertainties from the H-band spectra delivered by the APOGEE spectrograph, illustrating the sensitivity of stellar spectra to some parameters, such as T_{eff}, and lack of sensitivity to others, such as logg.

1 Contributors to the APOKASC Catalog

This catalog is the result of intensive effort by KASC and APOGEE scientists, particularly those who have been working on the analysis of *Kepler* lightcurve data, grid-based modelling, and the APOGEE spectroscopic parameters pipeline (ASPCAP), but also the broader teams from the instrument builders to lead scientists. I acknowledge here in reverse alphabetical order the former group: Gail Zasowski, Nicholas Troup, Dennis Stello, Verne Smith, Victor Silva Aguirre, Matthew Shetrone, Aldo Serenelli, Ricardo Schiavon, Marc Pinsonneault, Benoit Mosser, Andrea Miglio, Travis Metcalfe, Szabolcs Mészáros, Savita Mathur, Steven R. Majewski, Daniel Huber, Jon Holtzman, Saskia Hekker, Leo Girardi, Rafael Garcia, Ana García Pérez, Courtney R. Epstein, Yvonne Elsworth, Katia Cunha, William Chaplin, Dmitry Bizyaev, Sarbani Basu, Carlos Allende Prieto.

J.A. Johnson (✉)
Department of Astronomy, Ohio State University, 140 West 18th Avenue, Columbus, OH 43210, USA
e-mail: jaj@astronomy.ohio-state.edu

A. Miglio et al. (eds.), *Asteroseismology of Stellar Populations in the Milky Way*, Astrophysics and Space Science Proceedings 39,
DOI 10.1007/978-3-319-10993-0_10

2 Overview of APOKASC Catalog

The APOKASC catalog is a joint effort between the *Kepler* Asteroseismic Science Consortium and the SDSS-III APOGEE spectroscopic survey. For stars observed by both groups, the catalog will have the seismic parameters $\Delta\nu$ and ν_{max}, the spectroscopic parameters T_{eff} metallicity and their uncertainties. In addition, grid-based modeling values for logg, mass and radius, derived using the combination of seismic and spectroscopic parameters, will be reported. The first version of the catalog will contain the results for ∼1,900 red giant stars (Pinsonneault et al. 2014); subsequent versions of the catalog will include 1,000 of additional red giants observed in Years 2–3 of APOGEE observations as well as 100 of dwarf stars.

3 Advantages of Combining Spectroscopic and Seismic Data

Measurements of the fundamental properties of stars, such as masses, radii, ages, rotation profiles, evolutionary state, and composition, are crucial for understanding numerous issues in stellar structure and evolution, star formation histories, and stellar populations. Seismic measurements and spectroscopic measurement are very complementary in which characteristics they can measure. For example, logg is very well determined from the seismic parameters, while detailed composition measurements, such as [Mg/Fe] or [Na/Fe], will remain the purview of spectroscopy. Also, the addition of T_{eff} and metallicity information can improve the accuracy of grid-based modelling results for properties such as mass (e.g., Gai et al. 2011).

With this catalog, we plan to study a variety of areas, including the projects below, which have already been started from the preliminary version of the APOKASC catalog.

- Dependence of seismic properties on metallicity
- Surface and internal stellar rotation rates
- New identifications of stellar populations, e.g., merger remnants
- Improved distance measurements
- Tests of Galactic stellar population models from masses and radii of thousands of red giants

4 Spectroscopic Data

I focus this proceeding on describing the APOGEE spectroscopic observations and the sensitivity of near-IR spectra to stellar parameters, as this audience is most familiar with the derivation and use of seismic parameters.

4.1 Overview of APOGEE Survey

The Sloan Digital Sky Survey (SDSS) III (Eisenstein et al. 2011) uses a 2.5-m telescope with a wide field of view (seven square degrees) at Apache Point Observatory (APO) to survey the sky. The APO Galactic Evolution Experiment (APOGEE) uses a fiber-fed multiobject near-infrared spectrograph to observe 230 science targets at a time (Majewski et al. 2010). An additional 35 fibers are reserved for observing hot stars to facilitate removal of telluric lines and 35 fibers are placed on regions of black sky. The spectra are high resolution (R∼22,500), high signal-to-noise (∼ 100 per dithered resolution element) and cover the wavelength range of 1.51–1.68 μm. APOGEE began routine observations in Fall 2012. The first data release of APOGEE data, including the spectra for the stars that are part of the first APOKASC catalog, was the SDSS Data Release 10 (Ahn et al. 2014).

4.2 Derivation of Stellar Parameters from Spectra

The strengths of absorption features in the spectra of cool giants are sensitive to several properties of the atmosphere, including T_{eff} and logg, which affect the excitation and ionization balance of the electrons and the molecular equilibrium, and composition, which affects both the optical depth at the wavelengths of transitions and the continuous opacity through electron donation to form H^-.

To derive the stellar atmospheric parameters from spectra, first, the raw data are processed through the data reduction pipeline to produce combined, wavelength-calibrated, and radial-velocity-corrected spectra (Nidever et al. in prep). Next, stellar parameters are determined using ASPCAP (Garcia Perez et al. in prep), which finds the χ^2 minimum difference between the observed spectra and a 6-D grid of synthetic spectra. The parameters that are varied to create the synthetic spectra are T_{eff}, logg, [M/H], [C/M], [N/M] and [α/M]. To calculate spectra with different [M/H], the abundances of all elements except C, N, and the α elements are changed up or down in the same proportion from their solar ratios. In as much as lines of Fe are the most common out of all the elements that comprise "M", the best-fit [M/H] is an excellent proxy for [Fe/H], a fact confirmed by comparison with cluster stars (Mészáros et al. 2013). Fitting to a 6-D grid is necessary because the depth of an absorption line is never sensitive to just one parameter. A critical assessment of the systematic and random uncertainties in the ASPCAP stellar parameters was performed by comparison with parameters for stars in well-studied globular and open clusters and for stars in the "gold standard" KASC seismic sample in the *Kepler* field (Mészáros et al. 2013).

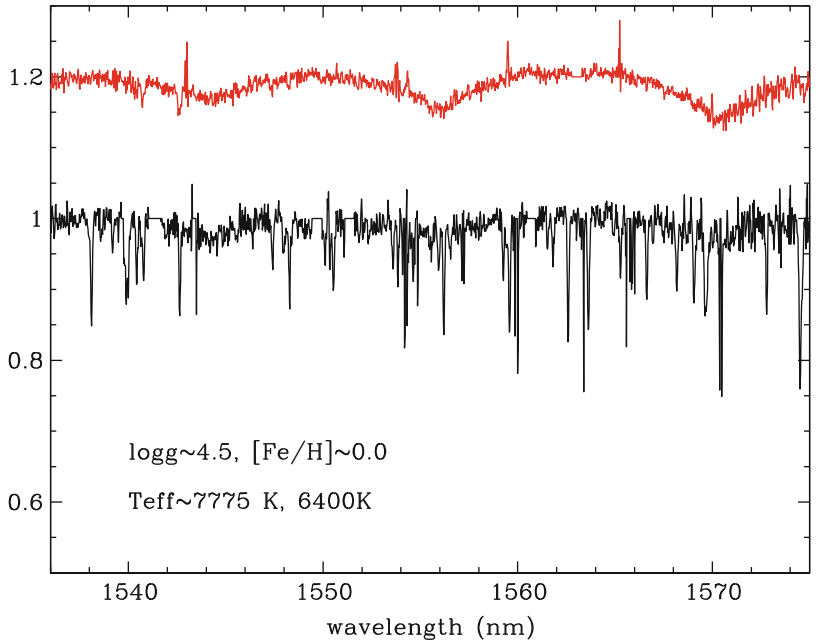

Fig. 1 This figure shows parts of the spectra of two stars in the APOKASC catalog that differ by ∼1,400 K or ∼20 % in Teff, but have similar logg and [M/H]. Despite the relative small change in the temperature, there are large differences in the appearance between the hotter star (*top*) and the cooler star (*bottom*)

4.2.1 Effective Temperature

The stellar parameter that has the most effect on the appearance of a stellar spectrum is the T_{eff}. Figure 1 shows two stars in the APOKASC catalog whose temperatures differ by a mere 20 %, yet the strength of the Brackett lines varies markedly. There are numerous lines that appear in the cooler star that are weak or non-existent in the hotter star as either the excitation or the ionization state is not appropriate for absorption of near-IR photons. The strong dependence on temperature in the Boltzmann and Saha equations and the presence of numerous lines of minority species, such as neutral atoms and molecules, means that small temperature uncertainties translate into larger uncertainties in [M/H].

To determine the accuracy of the ASPCAP-derived T_{eff}, we compared the T_{eff} from the spectroscopic pipeline to photometric temperatures derived from the IRFM-based color-T_{eff} for 2MASS filters (González et al. 2009) for cluster stars with well-determined reddenings. The ASPCAP temperatures were ∼ 150 K lower than the photometric ones on average, with a clear trend with temperature. A correction was applied to the ASPCAP temperatures to bring them into better agreement with the latter values. After the correction, the scatter in difference

between the two measurements was < 200 K, dropping to < 100 K for stars with solar-like metallicity or higher.

The advantage of determing a systematic correction to the ASPCAP temperatures, rather than using photometric temperatures for all APOGEE stars, is that a correctly calibrated spectroscopic temperature is reliable even if the reddening is uncertain. Many APOGEE fields lie in the midplane of the Galactic disk in regions of highly variable extinction, and the reddening map in the *Kepler* field itself is currently being revised (Zasowski et al. in prep; Huber et al. 2014).

4.2.2 Metallicity

As Fig. 2 shows, the composition of a star has an obvious effect on the appearance of a spectrum, as more metal-rich stars show much deeper absorption lines than a star with many fewer heavy-element atoms in its atmosphere. The problem is, of course, that temperature in particular has a much larger effect. The stars in Fig. 1 differ in T_{eff} by $\sim 20\,\%$, while the two stars in Fig. 2 differ in metal content by a factor of 100! Therefore, the uncertainties in metallicity will be much larger than the 4 % errors in T_{eff} discussed above.

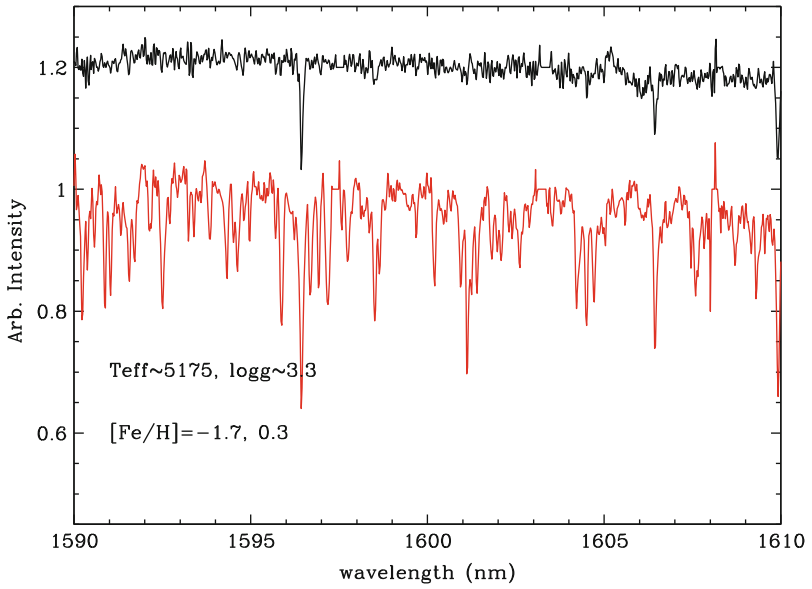

Fig. 2 This figure shows parts of the spectra of two stars in the the APOKASC catalog that differ by ~ 2 dex in [M/H], but have similar T_{eff} and logg. The number of heavy atoms in the atmosphere has a clear effect on the spectrum, as the more metal-poor star's spectrum (*top*) has considerably fewer lines than the more metal-rich star's spectrum (*bottom*)

The cluster stars provide the crucial test of the uncertainties and systematic offsets for the ASPCAP metallicity measurements, as all cluster stars should have similar metallicity, at least at the level of precision discussed here (e.g., Carretta et al. 2009), although subsequent analysis will take into account the variation in globular clusters of the light elements (e.g., Kraft 1994). We compared the [M/H] derived by ASPCAP to the [Fe/H] values reported in the literature for clusters spanning a metallicity range of $-2.3 < [Fe/H] < +0.3$ (Mészáros et al. 2013). In general, there was quite good agreement, confirming that the [M/H] value is a good proxy for [Fe/H]. For metal-rich clusters, the initial ASPCAP values are only about 0.1 too high, while they are 0.35 dex for metal-poor clusters. A metallicity-dependent correction is applied to the [M/H] values. The uncertainty in [M/H], determined by looking at the scatter in the corrected values compared to literature values, ranges from 0.15 dex for the most metal-poor clusters to ∼0.05 dex for clusters with solar metallicity and above. The strong metallicity dependence in the uncertainty in metallicity is not surprisingly, as metal-poor stars have noticeably fewer metal lines to use for the measurement.

To assess the difference that the corrected and uncorrected temperature scales and metallicity scales have on the results of the grid-based modelling, two separate computations were done. Uncorrected [M/H] were used in combination with uncorrected T_{eff} values in one case, while corrected values are used in the second case. Two sets of logg, masses and radii are reported.

4.2.3 Gravity

Logg values, unlike temperature and metallicity, can be measured by both seismic and spectroscopic techniques. However, the spectroscopic gravity measurements have larger uncertainties than the seismic measurements because the spectra of stars in the H-band are not particularly sensitive to logg changes (see Fig. 3). We compared the ASPCAP logg's with values both from seismic analysis of a few hundred stars in the *Kepler* field as well as with the logg's predicted for cluster stars from isochrones matched to the cluster distance and reddening (Mészáros et al. 2013). The values initially reported by the ASPCAP pipeline are too high compared to the seismic and isochrone stars by at least 0.2 dex, rising to 0.5 dex for metal-poor stars. A correction is again applied, leading to much better agreement. A scatter of $\sim$ 0.15 dex is present in the differences between corrected ASPCAP and calibration values, providing an estimate of the remaining uncertainty in the spectroscopic values. Part of that scatter is because it was difficult to reconcile (at the $\sim$ 0.1 dex level) the offsets between the seismic values in the *Kepler* field and the values determined from isochrones for stars with similar T_{eff} and gravity in the clusters. This difference is particularly striking for the metal-rich stars and remains under investigation by the ASPCAP team.

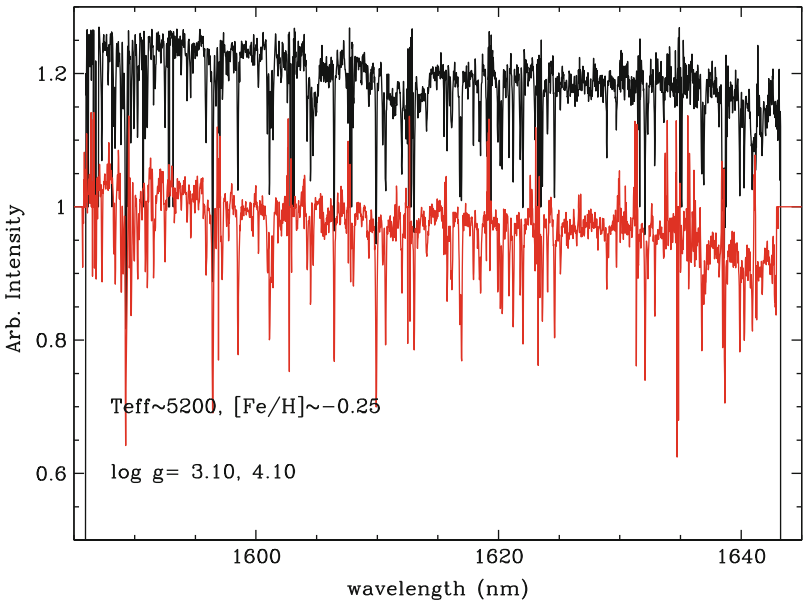

Fig. 3 This figure shows parts of the spectra of two stars in the APOKASC catalog that differ by $\sim$ 1 dex in logg, but have similar Teff and [M/H]. The differences between the lower gravity star (*top*) and higher gravity star (*bottom*) are not as obvious as for Figs. 1 and 2, demonstrating why the uncertainties in gravity are large for spectroscopically determined values

Conclusion

In this proceeding, I have summarized the APOGEE data and the derivation of stellar parameters and their uncertainties from high-resolution H-band data. These parameters, along with the seismic parameters $\Delta\nu$ and $\nu_{\rm max}$ are included in the APOKASC catalog as well as being passed to grid-based modellers for logg, mass, and radii determinations that are also included in the catalog. The publication of this catalog will, I hope, aid research in studies of stellar structure, stellar atmospheres, and stellar populations.

Acknowledgements A special thank you to Courtney Epstein, for her tireless work on targeting seismic sources in APOGEE and on gathering all the data into the catalog. And thank you to everyone who measured parameters for thousands of stars, no small task!

References

Ahn, C. P., Alexandroff, R., Allende Prieto, C., et al. 2014, ApJS, 211, 17
Carretta, E., Bragaglia, A., Gratton, R., D'Orazi, V., & Lucatello, S. 2009, A&A, 508, 695
Eisenstein, D. J., Weinberg, D. H., Agol, E., et al. 2011, AJ, 142, 72
Gai, N., Basu, S., Chaplin, W. J., & Elsworth, Y. 2011, ApJ, 730, 63
Garcia Perez, A. et al., in preparation
González Hernández, J. I. & Bonifacio, P. 2009, A&A, 497, 497
Huber, D., Silva Aguirre, V., Matthews, J. M., et al. 2014, ApJS, 211, 2
Kraft, R. P. 1994, PASP, 106, 553
Majewski, S. R., Wilson, J. C., Hearty, F., Schiavon, R. R., & Skrutskie, M. F. 2010, in IAU Symposium, Vol. 265, IAU Symposium, ed. K. Cunha, M. Spite, & B. Barbuy, 480–481
Mészáros, S., Holtzman, J., García Pérez, A. E., et al. 2013, AJ, 146, 133
Nidever, D. et al. 2014, in preparation
Pinsonneault, M., Elsworth, Y., & Epstein, C. 2014, ApJS, in press
Zasowski, G. et al. 2014, in preparation

The Red Giants in NGC 6633 as Seen with CoRoT, HARPS and SOPHIE

Ennio Poretti, Philippe Mathias, Caroline Barban, Frederic Baudin, Andrea Miglio, Josefina Montalbán, Thierry Morel, and Benoit Mosser

Abstract The open cluster NGC 6633 was observed with CoRoT in 2011 and simultaneous high-resolution spectroscopy was obtained with the SOPHIE and HARPS spectrographs. One of the four targets was not found to be a cluster member. For all stars we provide estimates of the seismic and spectroscopic parameters.

The CoRoT satellite (Convection, Rotation and planetary Transits; Baglin et al. 2006) observed the open cluster NGC 6633 in two long runs allocated from April 2011 to September 2011 (LRc07 and LRc08 in the CoRoT schedule). The red giants HD 170031 ($V = 8.20$), HD 170231 ($V = 8.69$), HD 170053 ($V = 7.30$), HD 170174 ($V = 8.31$) and the B8-star HD 170200 ($V = 5.70$) were the five stars selected to be observed in the asteroseismic channel. The Seismologic Ground-Based Working Group considered very challenging to perform simultaneous radial velocity measurements to measure the amplitude of the radial velocity variations of the solar-like oscillations occurring in red giants.

The spectroscopic runs with HARPS at European Southern Observatory were scheduled from June 23 to July 3, 2011 and from 15 to 20 July, 2011. The runs with SOPHIE at Observatoire Haute Provence from May 26 to June 6, 2011, and from June 20 to July 1, 2011. Due to long exposure time requested to provide

E. Poretti (✉)
INAF-Osservatorio Astronomico di Brera, Via E. Bianchi 46, 23807 Merate, Italy
e-mail: ennio.poretti@brera.inaf.it

P. Mathias
CNRS, IRAP, 57 Avenue d'Azereix, BP 826, 65008 Tarbes, France

C. Barban • F. Baudin • B. Mosser
LESIA, CNRS, Université Pierre et Marie Curie, Université Denis Diderot, Observatoire de Paris, 92195 Meudon Cedex, France

T. Morel • J. Montalbán
Institut d'Astrophysique et de Géophysique, Université de Liège, Liège, Belgium

A. Miglio
School of Physics and Astronomy, University of Birmingham, Edgbaston, Birmingham, B15 2TT, UK

A. Miglio et al. (eds.), *Asteroseismology of Stellar Populations in the Milky Way*, Astrophysics and Space Science Proceedings 39,
DOI 10.1007/978-3-319-10993-0_11

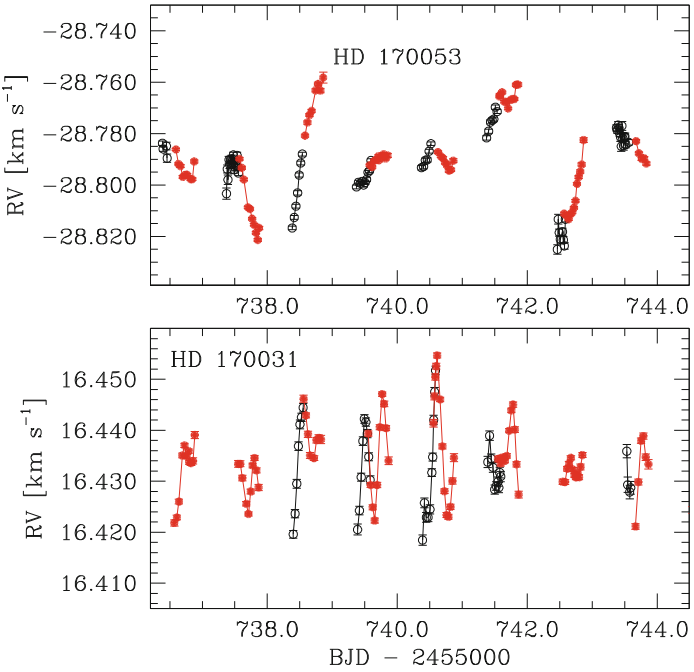

Fig. 1 Radial velocity measurements of HD 170031 and HD 170053 obtained with SOPHIE (*black empty circles*) and HARPS (*red filled circles*) (Color figure online)

the necessary accuracies, only HD 170031 and HD 170053 could be intensively observed at both observatories. Figure 1 shows the radial velocity curves obtained from June 23 to July 1, 2011. Note that error bars are reported, but often not noticeable since they have the same size of the points.

The double-site campaign clearly put in evidence the multiperiodic behaviours of the radial velocity variation in both the well-sampled red giants. Peak-to-peak amplitudes are 60 m s^{-1} for HD 170053 and 40 m s^{-1} for HD 170031. The uncertainty on a single measurement is ± 1 m s^{-1}. It also resulted that HD 170053, HD 170231, and HD 170174 have the same mean radial velocity (around -28 km s^{-1}), while HD 170031 shows a completely different value (Fig. 1). The NGC 6633 radial velocity is -25.43 km s^{-1} (Kharchenko et al. 2005) and therefore we can conclude that, unlike the other three red giants, HD 170031 is not a cluster member.

The HARPS spectra were also used to accurately estimate the atmospheric parameters (effective temperature $T_{\rm eff}$, surface gravity $\log g$, metallicity [Fe/H], microturbulent velocity ξ) and the abundances of 16 chemical species in a self-consistent manner (Morel et al. 2014), for both NGC 6633 targets and other galactic red giants. Moreover, the extensive photometric CoRoT timeseries supplied reliable estimates both for the frequency of the maximum oscillation power (ν_{max}) and for

Table 1 Physical and seismic parameters of the red giants in NGC 6633

Star	ν_{max} [μHz]	$\Delta\nu$ [μHz]	T_{eff} [K]	log g [cgs]	[Fe/H]	ξ [km s^{-1}]
HD 170174	44.56	4.17	5055	2.56	−0.07	1.58
HD 170053	9.18	1.09	4290	1.85	−0.03	1.68
HD 170231	66	5.33	5175	2.74	−0.03	1.49
HD 170031	39	3.87	4515	2.46	+0.04	1.41

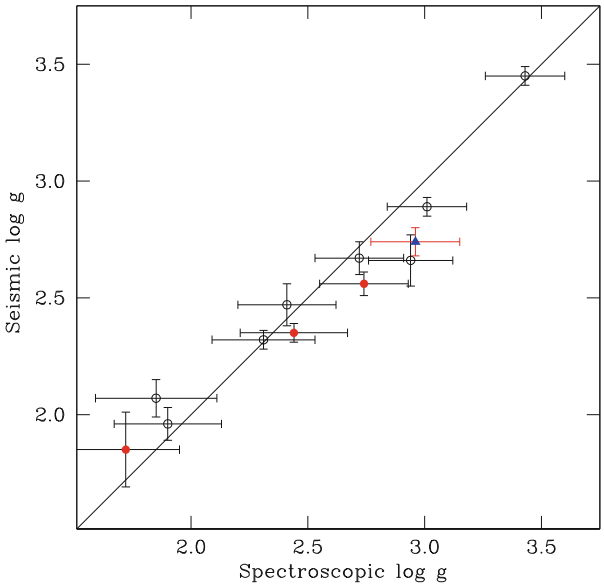

Fig. 2 Agreement between log g values obtained from seismic and spectroscopic analyses. *Red filled circles*: red giants belonging to NGC 6633; *blue filled triangle*: HD 170031; *black empty circles*: galactic red giants (Color figure online)

the large separation ($\Delta\nu$). The atmospheric parameters could be obtained from the seismic analyses, too (Table 1). The agreement is excellent, as Fig. 2 shows for the surface gravities. In particular, note the smaller error bars of the seismic values.

This study shows that spectroscopic and photometric data can be combined to describe the pulsational scenario of red giants and, in turn, make more complete models of their atmospheres.

Acknowledgements The CoRoT space mission, launched on 2006 December 27, was developed and is operated by the CNES, with participation of the Science Programs of ESA, ESA's RSSD, Austria, Belgium, Brazil, Germany and Spain. This work is based on observations collected at La Silla Observatory, ESO (Chile) under program LP185.D-0056.

References

Baglin, A., Auvergne, M., Barge, P., et al. 2006, in ESA Special Publication, Vol. 1306, ESA Special Publication, ed. M. Fridlund, A. Baglin, J. Lochard, & L. Conroy, 33

Kharchenko, N. V., Piskunov, A. E., Röser, S., Schilbach, E., & Scholz, R.-D. 2005, A&A, 438, 1163

Morel, T., Miglio, A., Lagarde, N., et al. 2014, A&A, 564, A119

"Rapid-Fire" Spectroscopy of *Kepler* Solar-Like Oscillators

Anders O. Thygesen, Hans Bruntt, William J. Chaplin, and Sarbani Basu

Abstract The NASA *Kepler* mission has been continuously monitoring the same field of the sky since the successful launch in March 2009, providing high-quality stellar lightcurves that are excellent data for asteroseismology, far superior to any other observations available at the present. In order to make a meaningful analysis and interpretation of the asteroseismic data, accurate fundamental parameters for the observed stars are needed. The currently available parameters are quite uncertain as illustrated by e.g. Thygesen et al. (A&A 543:A160, 2012), who found deviations as extreme as 2 dex in [Fe/H] and log g, compared to catalogue values. Thus, additional follow-up observations for these targets are needed in order to put firm limits on the parameter space investigated by the asteroseismic modellers. Here, we propose a method for deriving accurate metallicities of main sequence and subgiant solar-like oscillators from medium resolution spectra with a moderate S/N. The method takes advantage of the additional constraints on the fundamental parameters, available from asteroseismology and multi-color photometry. The approach enables us to reduce the analysis overhead significantly when doing spectral synthesis, which in turn will increases the efficiency of follow-up observations.

A.O. Thygesen (✉)
Zentrum für Astronomie der Universität Heidelberg, Landessternwarte, 69117 Heidelberg, Germany
e-mail: a.thygesen@lsw.uni-heidelberg.de

H. Bruntt
Department of Physics and Astronomy, Aarhus University, 8000 Aarhus C, Denmark
e-mail: bruntt@gmail.com

W.J. Chaplin
School of Physics and Astronomy, University of Birmingham, Edgbaston, B15 2TT Birmingham, UK
e-mail: w.j.chaplin@bham.ac.uk

S. Basu
Department of Astronomy, Yale University, PO Box 208101, New Haven, CT 06520-8101, USA
e-mail: sarbain.basu@yale.edu

A. Miglio et al. (eds.), *Asteroseismology of Stellar Populations in the Milky Way*,
Astrophysics and Space Science Proceedings 39,
DOI 10.1007/978-3-319-10993-0_12

1 This Project

The observations were preformed with the FIES instrument on the Nordic Optical Telescope (R= 25,000, coverage [3,700Å–7,300Å], S/N≈ 70). Eight targets were also observed by Bruntt et al. (2012) (hereafter HB12), using much higher resolution ($R = 80{,}000$) and with a much higher S/N (≥ 200). One star (KIC9025370) was found to be a double-lined binary, so this star was discarded in the analysis. The outline of our analysis method follows below.

- Use $\log g$ from asteroseismic measurements (Basu et al. 2010; Gai et al. 2011).
- Calculate $T_{\rm eff}$ from TYCHO V and 2MASS K_S photometry using the calibration from Casagrande et al. (2010), correcting for reddening using the calibration of Munari and Zwitter (1997).
- Calculate microturbulence (ξ_t) using calibration from HB12.
- Derive initial [Fe/H] from Fe II lines using the VWA software package (Bruntt et al. 2010).
- Re-iterate $T_{\rm eff}$ including metallicity dependence and subsequently redetermine ξ_t.
- Derive final value of [Fe/H] from Fe II lines, using final set of fundamental parameters.

In Fig. 1 is shown how our analysis of 23 artificially degraded spectra compare to the original results from HB12. The spectra were treated as real observations and analyzed as such. As is evident, we find very good agreement between our analysis and the comparison work, with no offset in [Fe/H] and an very small scatter. The median uncertainty on our derived metallicities is 0.10 dex, which mainly originates from line-to-line abundance scatter. We observe no clear trends of our metallicity determination with $T_{\rm eff}$, $\log g$ or [Fe/H], suggesting that our method works across the entire parameter space.

In Fig. 2 we present a comparison between the our results for the eight targets which were also observed by HB12 to allow for a direct comparison between different quality observations. Again, the agreement between a dedicated spectroscopic analysis and our proposed method is good, with an insignificant offset and a small scatter. For the observed targets we find a median uncertainty of 0.14 dex on [Fe/H] which is comparable to the typical uncertainties quoted in standard spectroscopic analyses of higher quality spectra (~ 0.15 dex).

With these results, we have illustrated how accurate metallicities can be obtained from moderate quality spectra, when constraints on $T_{\rm eff}$ and $\log g$ are available from independent sources. This provides a way of quickly deriving metallicities, requiring only measurements of a few Fe II lines and the interstellar Na-D lines, to assess reddening, which will affect the photometric $T_{\rm eff}$. Before this method can be applied in full, tests of low-metallicity targets as well as fainter targets ($V \geq 10$) need to be made, but the results presented here are encouraging. This will help reduce the overheads associated with getting accurate fundamental parameters for all *Kepler* main sequence and subgiant solar-like oscillators.

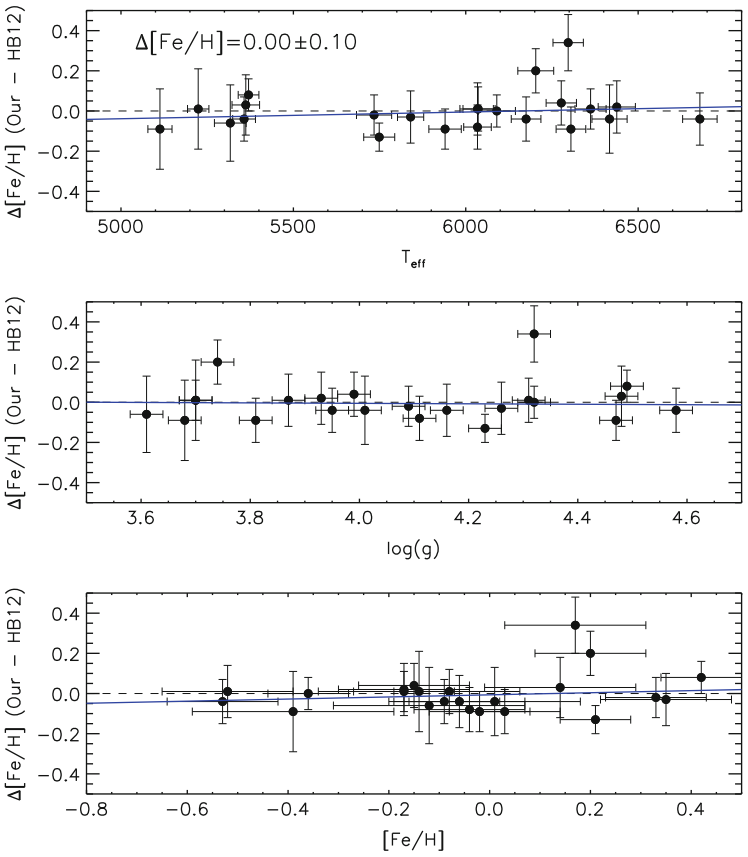

Fig. 1 Comparison of results from artificially degraded spectra to the results from HB12

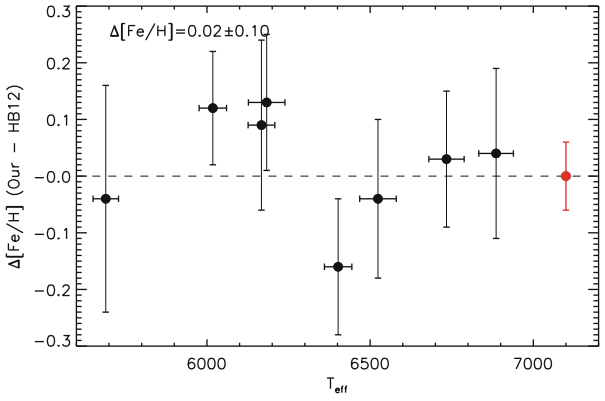

Fig. 2 Comparison of [Fe/H] derived from our observations to that of HB12. The red point at 7100K shows the typical uncertainty on [Fe/H] from HB12 (Color figure online)

Acknowledgements The authors would like to thank the entire *Kepler*-team for their continued effort to ensure the success of this mission. AOT acknowledges support from Sonderforschungsbereich SFB 881 "The Milky Way System" (subproject A5) of the German Research Foundation (DFG). SB acknowledges NSF grant AST-1105930. WJC acknowledges the financial support of the UK Science and Technology Facilities Council (STFC). This research took advantage of the SIMBAD and VIZIER databases at the CDS, Strasbourg (France), and NASA's Astrophysics Data System Bibliographic Services. Funding for this Discovery mission is provided by NASA's Science Mission Directorate.

References

Basu, S., Chaplin, W. J., & Elsworth, Y. 2010, ApJ, 710, 1596
Bruntt, H., Basu, S., Smalley, B., et al. 2012, MNRAS, 423, 122 (HB12)
Bruntt, H., Deleuil, M., Fridlund, M., et al. 2010, A&A, 519, A51
Casagrande, L., Ramírez, I., Meléndez, J., Bessell, M., & Asplund, M. 2010, A&A, 512, A54
Gai, N., Basu, S., Chaplin, W. J., & Elsworth, Y. 2011, ApJ, 730, 63
Munari, U. & Zwitter, T. 1997, A&A, 318, 269
Thygesen, A. O., Frandsen, S., Bruntt, H., et al. 2012, A&A, 543, A160

Part IV
The Milky Way, Current Uncertainties in Models of Formation and Evolution of the Galaxy, and First Results on Stellar Populations Studies Obtained Combining Seismic and Spectroscopic Constraints in the CoRoT and *Kepler* fields

New Observational Constraints to Milky Way Chemodynamical Models

Cristina Chiappini, Ivan Minchev, Friedrich Anders, Dorothee Brauer, Corrado Boeche, and Marie Martig

Abstract Galactic Archaeology, i.e. the use of chemo-dynamical information for stellar samples covering large portions of the Milky Way to infer the dominant processes involved in its formation and evolution, is now a powerful method thanks to the large recently completed and ongoing spectroscopic surveys. It is now important to ask the right questions when analyzing and interpreting the information contained in these rich datasets. To this aim, we have developed a chemodynamical model for the Milky Way that provides quantitative predictions to be compared with the chemo-kinematical properties extracted from the stellar spectra. Three key parameters are needed to make the comparison between data and model predictions useful in order to advance in the field, namely: precise proper-motions, distances and ages. The uncertainties involved in the estimate of ages and distances for field stars are currently the main obstacles in the Galactic Archaeology method. Two important developments might change this situation in the near future: asteroseismology and the now launched Gaia. When combined with the large datasets from surveys like RAVE, SEGUE, LAMOST, Gaia-ESO, APOGEE, HERMES and the future 4MOST we will have the basic ingredients for the reconstruction of the MW history in hands. In the light of these observational advances, the development of detailed chemo-dynamical models tailored to the Milky Way is urgently needed in the field. Here we show the steps we have taken, both in terms of data analysis and modelling. The examples shown here illustrate how powerful can the Galactic Archaeology method become once ages and distances are known with better precision than what is currently feasible.

C. Chiappini (✉) • I. Minchev • F. Anders • D. Brauer
Leibniz-Institut für Astrophysik Potsdam (AIP), An der Sternwarte 16, 14482 Potsdam, Germany
e-mail: cristina.chiappini@aip.de

C. Boeche
Astronomisches Rechen-Institut, Zentrum für Astronomie der Universität Heidelberg, Mönchhofstr. 12-14, 69120 Heidelberg, Germany

M. Martig
Max-Planck-Institut für Astronomie, Königstuhl 17, 69177 Heidelberg, Germany

A. Miglio et al. (eds.), *Asteroseismology of Stellar Populations in the Milky Way*,
Astrophysics and Space Science Proceedings 39,
DOI 10.1007/978-3-319-10993-0_13

1 Galactic Archaeology: How Powerful Can It Be?

The use of chemo-kinematical information of a large number of stars to understand which were the main steps in the formation of the Milky Way has been challenged when it became clear that stars can move away from their birthplaces. N-body simulations of the formation of disk galaxies have shown radial migration to be a common phenomena (see Raboud et al. 1998; Sellwood and Binney 2002; Roškar et al. 2008). Also from the observational side, there have been claims for detecting local stars that have exceedingly large metallicities to have been born in the Solar Neighbourhood (so-called super metal-rich stars). These stars are often old and show typical thin disk kinematics (see Trevisan et al. 2011, and references therein). As the metallicity of the interstellar medium (traced by HII regions and young stars near the Sun) is not expected to have increased much in the last 3–4 Gyrs (see Chiappini et al. 2003) due to a rather inefficient star formation rate at the solar Galactocentric radii during this period of time, these stars most probably came from the inner, more metal-rich, regions of the Galaxy. Indeed, chemical evolution models for the MW thin disk, which are compatible with the abundances measured in the interstellar medium at present time, cannot predict stars more metal rich than [Fe/H] $\sim$0.2 dex to be present at 8 kpc from the Galactic center (Chiappini 2009).

The age and chemical composition of the stars constitute relic informations not disturbed by the radial migration process. However, pure chemical evolution models constrained by observations derived from stars currently in a certain volume (for instance, at the Solar vicinity) are in danger of inferring wrong conclusions if the adopted observational samples turn out to have been severely contaminated by *intruder* stars. Indeed, radial migration, if important, could affect classic constraints such as the age-metallicity relation, metallicity distributions, abundance ratios vs. metallicity relations, as well as the radial abundance gradients. These stars cannot be identified by their kinematics because, as shown by Sellwood and Binney (2002) radial migration means permanent changes to the stellar angular momenta, making it possible that a migrated star shows the exact same kinematics of the ones born in situ, in a certain studied volume.

In particular, radial migration[1] has been used to challenge one of the main pillars of the two-infall model for the formation of the Milky Way (Chiappini et al. 1997). In Chiappini et al. (1997) we proposed two main epochs of star formation in the Galaxy, the first one related to the thick disk and the second one to the thin disk. This suggestion was based mostly on chemical evolution arguments (abundance ratios) given the impossibility of using ages as a constraint due to the large uncertainties at the time. A low star formation period in between the two main infall episodes would naturally explain the observed *gap* in the [α/Fe] vs. [Fe/H] diagram (Fuhrmann 1998). In Chiappini (2009) we computed a somewhat different model where the

[1]Which is different from the fact that in different samples there are some stars wandering from other regions due to eccentric orbits—those can be easily identified by calculating their orbital parameters—see, for instance Anders et al. 2014).

two infall episodes were completely disentangled and gas from the first infall did not pre-enrich the second component. One of the main conclusions of this model was that the chemical properties of the thick and thin disk (especially the shifts observed in several abundance ratios of stars kinematically classified as belonging to the thick or thin disk) can be well accounted for by a model were the thick disk formed on a short timescale (∼1–2 Gyrs) and with a larger star formation efficiency than the thin disk.

However, the reality of the observed chemical discontinuity has been challenged by Schönrich and Binney (2009), who constructed a model for chemical evolution of the MW, assuming a certain migration efficiency in order to fit the current thin disk abundance gradient and metallicity distribution at the Solar vicinity. Contrary to Chiappini et al. (1997), they find that radial migration would account for forming the thick disk, without the need of two main episodes of star formation. However, as discussed in Minchev et al. (2013), in the absence of massive mergers disk thickening due to migration is insignificant: owing to the conservation of vertical action, only extreme migrators contribute by contracting the inner disk and thickening the outskirts. This deficiency in the Schoenrich and Binney model affects their main conclusion that a thick disk can be formed in a merger-free MW disk evolution, and that the MW formation does not require two main episodes of star formation. In addition, N-body simulations where a bar is formed (as is the case in our Galaxy) suggest the efficiency of migration to vary with time and distance from the galactic center (Minchev et al. 2010; Brunetti et al. 2011; Shevchenko 2011). This fact implies that analytical approaches are not suitable to properly investigate these issues. N-body simulations are the appropriate technique to treat time-dependent non-axisymmetric systems such as our barred galaxy.

Apart from the inherent difficulties linked to the existence of radial migration and how to account for it in chemo-dynamical models, current samples of disk stars for which detailed chemical abundances and distances are known are still confined to a small volume of the Milky Way. In particular, there is always the danger that the studied stellar samples suffer from biases that could, in principle, artificially create discontinuities in the abundance ratio diagrams, as suggested by Bovy et al. (2012). While it is unclear whether the separation between the thin and thick disk in chemistry is real or due to selection effects in the SEGUE sample (Bovy et al. 2012), or inexistent as in the RAVE samples (e.g. Boeche et al. 2013a), the fact that the unbiased volume-completed (although very local) sample of Fuhrmann (2011) does show a gap argues that it may indeed be the legacy of two discrete stellar populations, or star formation episodes. Recently, Anders et al. (2014), using a sample of red giants from the first year of APOGEE data, also found a clear discontinuity in the chemical plane. As discussed in that paper, given the way this sample was selected, it was very unlike that the observed discontinuity would be produced by sample selection biases. This was now recently confirmed by Nidever et al. (2014) who has used a sample of APOGEE red clump stars, for which the sample selection was taken into account, and still report similar *gaps* as the ones seen in the Anders et al. (2014) paper. In these studies, one of the main uncertainties

remaining is the proper motions, but this should be improved soon now with the launched Gaia satellite.

Finally, an important role can be played by asteroseismology as well. Indeed, as discussed during this meeting, solar-like pulsating red giants offer a well-populate class of objects, not only spanning a large age range, but also large distances,[2] for which is now in principle possible to obtain accurate distance and ages (Valentini and Miglio, this conference; Miglio et al. 2013).

Given the suggestions in the Literature (mostly made in 2008/2009) that (a) the observed chemical discontinuity in the solar vicinity stars was due to selection biases, and (b) that radial migration could account for the observations of thick disk stars without the need for a two-infall model, we decided to proceed in the following two directions:

- develop a chemodynamical model (within the cosmological framework) and try to understand what is possible in terms of thick disk formation and if one simple disk (a single star formation episode model) can reproduce the chemo-kinematical relations in the MW.
- investigate the chemo-kinematic properties of large stellar samples in the MW, for which biases can be estimated (using data from RAVE, SEGUE and APOGEE surveys); with the goal to find new, more tight constraints to models for the MW.

In the last couple of years we have progressed in both directions and some of the results obtained so far are described in the next sections.

2 The MCM Chemodynamical Model for the Milky Way

We have recently developed an alternative way to construct a chemo-dynamical model for our Galaxy, here referred as the MCM model (Minchev et al. 2013), which is the fusion between a state-of-the-art simulation[3] in the cosmological context (Martig et al. 2012) and a detailed thin-disk chemical evolution model. The key point of our approach is the use of the exact star formation history and chemical enrichment from our chemical model to assign to the particles of the simulation. This novel approach was born from the need to avoid the known problems with chemical enrichment and star formation currently found in fully self-consistent simulations (see discussion in Minchev et al. 2013), and to focus on quantifying the

[2]Even though, only in the particular fields observed by CoRoT and *Kepler*. Hopefully, with Plato much the same data can be obtained for a larger portion of the Galaxy—see Rauer and the PLATO 2.0 collaboration (2013).

[3]The simulation builds up a galactic disk self-consistently by gas inflow from filaments and mergers and naturally takes into account radial migration processes due to early merger activity and internal disk evolution at low redshift. A central bar is developed early on, similar in size at the final simulation time to that of the MW.

radial migration and its impact on the classic MW constraints such as metallicity distribution functions (MDFs), age-metallicity relation and abundance gradients.

The main result of the MCM model for the Solar vicinity is shown in Fig. 1. The model predictions imply that stars currently at the Solar vicinity (here defined as stars with galactocentric distances $7< R <9$ kpc and height above the plane $z <3$ kpc) are a mosaic of stars born at different locations (r_0) and at different times, with a peak at $r_0 \sim 6$ kpc. We also predict more than 60 % of stars currently at the $7 < R < 9$ kpc bin to come from inner regions, whereas only around 10 % have birth radii beyond the solar circle. Because the chemical evolution at a distance of 6 kpc from the galactic center does not differ much form that at 8 kpc, the impact of radial migration on the Solar vicinity is minor. This can be seen in Fig. 2 where the predicted age-metallicity relation for stars in the Solar circle is shown, together with the same prediction for other galactocentric bins. We find in our Paper

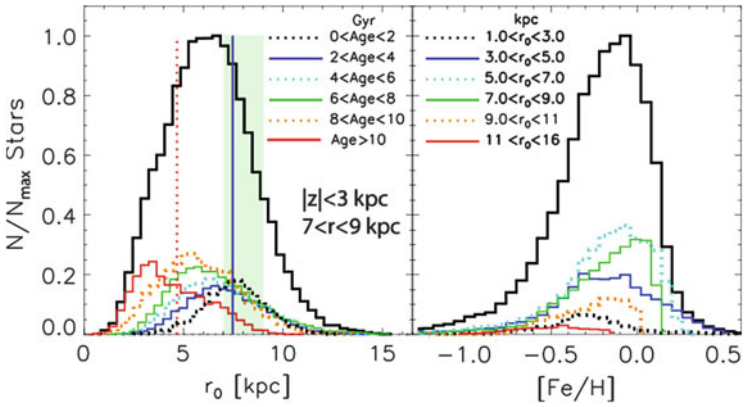

Fig. 1 For stars currently at the Solar vicinity we show: (**a**) on the *left* their age and birth radius distributions, and (**b**) on the *right* their metallicity distributions (the *solid black line* refers to the total MDF). Figure taken from Minchev et al. (2013)

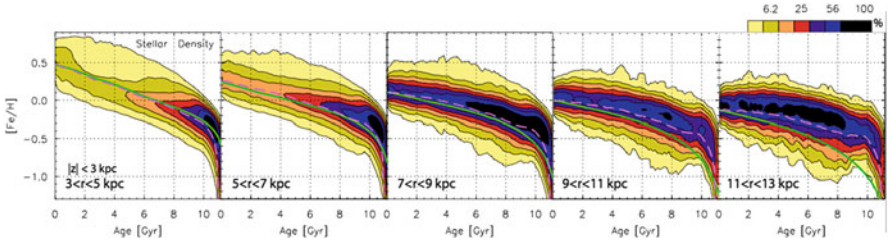

Fig. 2 The age-metallicity relation predicted at different radial bins. The *color code* indicates how the stellar density varies in each diagram. The *middle row* ($7< r < 9$ kpc) corresponds to the solar neighborhood. The input chemistry, native to each bin, is shown by the *solid-green curve*. The *dashed-pink curve* indicates the mean [Fe/H] binned by age which takes into account radial migration effects. Figure adapted from paper II (Color figure online)

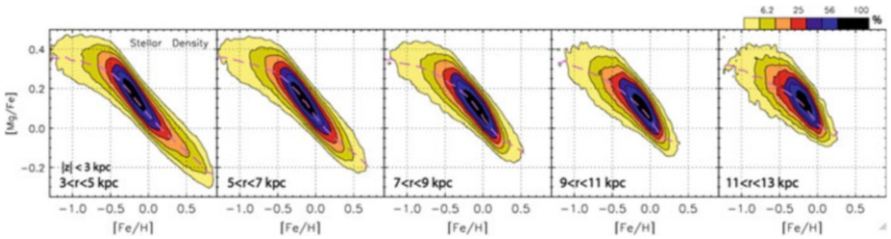

Fig. 3 The predicted density distribution of stars in a [Mg/Fe] vs. [Fe/H] diagram, at different radial bins. The *dashed-pink curve* indicates the mean [Mg/Fe] binned by [Fe/H]. The model, predict no gap in the diagram, even though several properties of its oldest stars do match several typical thick-disk kinematical, structural and chemical properties. Figure adapted from Paper II (Color figure online)

II (Minchev et al. 2014a) that the width of the r_0-distribution increases between the innermost and outermost annuli considered. The predicted increase in contamination from migration with radius is due to the exponential drop in disk surface density, where, on the average, stars migrate larger distances outwards than inwards. Inward migration is still very important, and has the effect of balancing the contribution from stars coming from the inner disk, at intermediate radii.

In Fig. 3 the same is shown for the predicted density distribution of stars in the [Mg/Fe] vs. [Fe/H] diagram. Notice that the chemo-dynamical model of a pure thin disk does not predict a gap in this diagram. On the other hand, all the other properties normally attributed to thick disk stars are met by the oldest (ages $>$ 10 Gyr) stars in our simulation. At the Solar vicinity the oldest stars show typical thick disk kinematical (as for instance, rotation velocity lag of thin disk stars, larger velocity dispersion), structural (such as shorter scale-length than younger stars), and chemical properties (such as the metallicity and [Mg/Fe] distributions). These surprising results may indicate that a discrete thick-disk component (in time, and with a high-efficiency star formation rate—as suggested in Chiappini 2009) might be still needed, which we will investigate in the near future. In other words, the discontinuity in the chemical diagram seems to be really an effect of different star formation regimes.

In our paper II (Minchev et al. 2014a) we also explain the variation of observed abundance gradients with distance from the mid-plane as due to a different mix of stars of different ages at the different slices in z. This is very important as studies using different samples (see next section) have found different metallicity and [α/Fe] gradients in the MW. Our main predictions are shown in Fig. 4. The thick black curves in the top row show the azimuthally averaged metallicity variation with galactic radius for stellar samples at different distances from the disk midplane, as marked in each panel. Different colors correspond to different age groups as indicated in the bottom-left panel. The height of rectangular symbols reflects the density of each bin. The bottom row of Fig. 4 shows the same information as above but for [Mg/Fe].

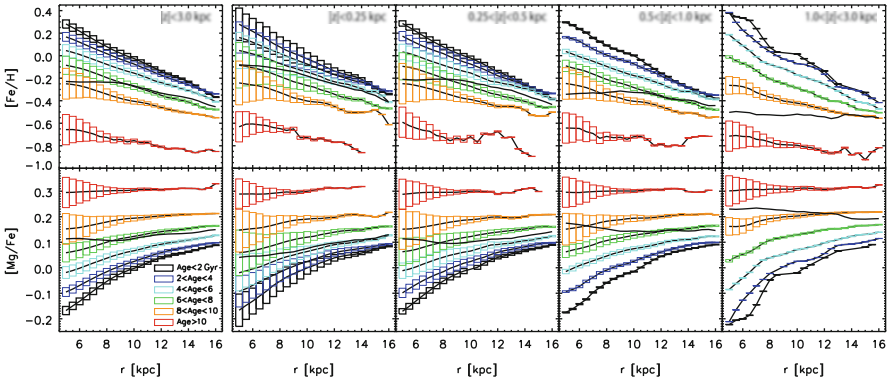

Fig. 4 The predicted density distribution of stars in a [Mg/Fe] vs. [Fe/H] diagram, at different radial bins. The *dashed-pink curve* indicates the mean [Mg/Fe] binned by [Fe/H]. The model, predict no gap in the diagram, even though several properties of its oldest stars do match several typical thick-disk kinematical, structural and chemical properties. Figure adapted from Paper II (Color figure online)

Other predictions of the MCM model can be seen in Paper I Minchev et al. (2013) and Paper II Minchev et al. (2014a).

3 New Constraints from RAVE, SEGUE and APOGEE

More detailed constraints, as for instance, sampling different heights from the galactic plane, do play a key role in constraining theoretical models. Here I give some examples of recent new constraints to chemodynamical modes we have obtained by analyzing RAVE, SEGUE and APOGEE samples. New constraints are also now coming from the Gaia-ESO survey (see contributions in this volume).

3.1 Chemodynamics with RAVE

By studying a sample of giants, we (Boeche et al. 2013a) have shown that despite RAVE's modest R = 7,000 resolution, the inferred chemical abundances and kinematical parameters can be confidently used to investigate chemodynamical properties of stars in a z_{max}-eccentricity plane (where z_{max} is the maximum height from the Galactic plane in the star's orbit). It turns out that different portions of such a diagram are more or less affected by migrators. By comparing the chemodynamical model predictions with diagrams of this kind, it is possible to look for the best parameter space in which to detect radial migrators, based on chemistry and age knowledge (hopefully feasible in the near future with CoRoT and *Kepler* data).

More recently, we discovered (Minchev et al. 2014b), that the velocity dispersion of a sample of RAVE giant stars decreases strongly for stars with large [Mg/Fe] (the oldest stars). This findings, although at odd with the classical expectations that older populations should show larger velocity dispersions, can be understood in the following way: perturbations from massive mergers in the early universe do affect more strongly the outer parts of the disk and, at the same time, lead to the subsequent radial migration of stars with cooler kinematics from the inner disk. Similar reversed trends in velocity dispersion are also found for different metallicity subpopulations. Our results suggest that the Milky Way disk merger history can be recovered by relating the observed chemo-kinematic relations to the properties of past merger events.

Finally in Boeche et al. (2013b, 2014) we computed the abundance gradients for Mg, Al, Si, Ti, and Fe at different distances from the middle plane, using RAVE samples of dwarf and giant stars, respectively (see Fig. 5). This was the first time abundance gradients for individual chemical elements have been studied in

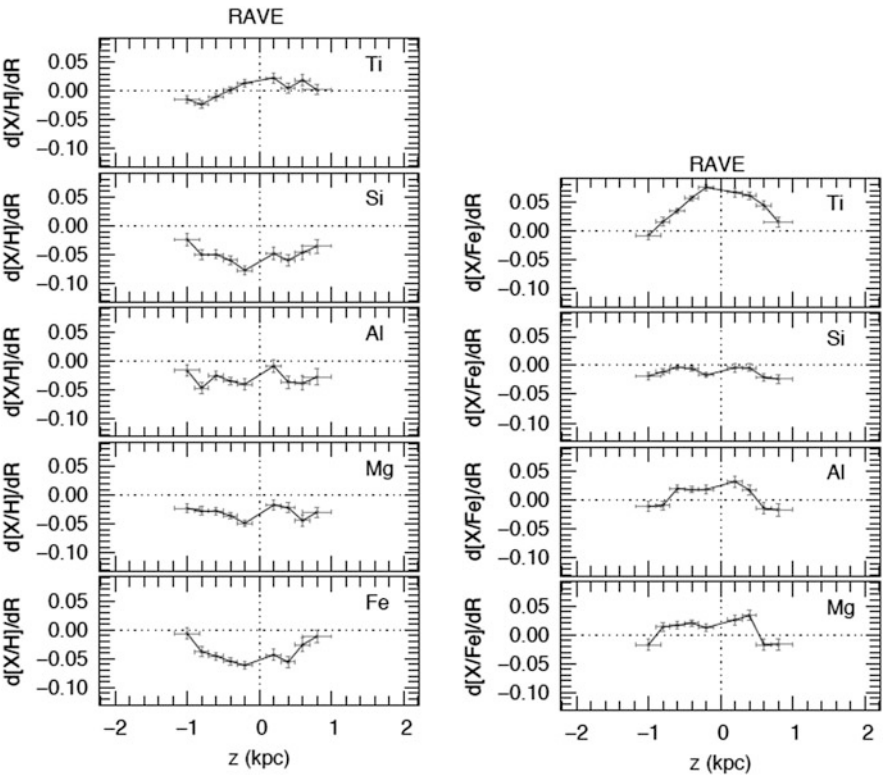

Fig. 5 Radial gradients for the RAVE red clump sample as a function of the distance from the Galactic plane z (kpc) for the elemental abundances (*left panel*) and abundance ratios [X/Fe] (*right panel*). Figure adapted from Boeche et al. (2014)

such large samples, and covering such large regions of the galactic disk. We find that (a) the radial chemical gradients are negative and become progressively flatter with increasing distance from the mid-plane; (b) the vertical chemical gradients are negative and become progressively steeper as the distance from the plane increases, until it flattens out, (c) the high [α/Fe] stars have radial chemical gradients consistent with zero; (d) the vertical chemical gradients of the low [α/Fe] stars are consistent with zero or with being slightly negative; (e) the vertical chemical gradients of the high [α/Fe] stars are consistent with zero, and negative once one approaches the middle plane. These general properties are matched by the MCM model, but a detailed comparison via mock-catalogues has to be carry out to quantitatively better constrain such models.

3.2 Chemodynamics with the First Year of APOGEE Data

More constraints were recently obtained from the study of a sample of giant stars observed by the Apache Point Observatory Galactic Evolution Experiment (APOGEE). APOGEE is the first multi-object high-resolution fiber spectrograph in the near-infrared and hence is able to peer through the dust that obscures stars in the Galactic disc and bulge in the shorter wavelengths. Therefore the APOGEE data greatly complements studies such as RAVE and SEGUE which do not cover much the mid-plane. We selected a high-quality sample in terms of chemistry (amounting to around 20,000 stars) from the first year of APOGEE data and computed distances and orbital parameters for this sample, in order to formulate constraints on Galactic chemical and chemo-dynamical evolution processes in the solar neighborhood and beyond (e.g., metallicity distributions MDFs, [α/Fe] vs. [Fe/H] diagrams, and abundance gradients).

Our sample of red giant stars covers a heliocentric distance range of 10 kpc (most of the stars are situated 1–6 kpc away from the Sun), which enabled us to increase the Galactic volume studied with spectroscopic stellar surveys with respect to the most recent chemodynamical studies based on RAVE and SEGUE by at least a factor of 8. We find excellent agreement between the MDF of the local (d $<$ 100 pc) high-resolution high-S/N HARPS sample of Adibekyan et al. (2011) and our local APOGEE sample (with d $<$ 1 kpc; see Fig. 6).

More importantly, both samples compare well in an [α/Fe] vs. [Fe/H] diagram, and in both cases a clear *gap* is observed. Figure 7 shows this chemical diagram for three different Galactocentric distance bins (inner disk, solar vicinity and outer disk). We find α-enhanced stars to be extremely rare in the outer Galactic disc, as has been suggested in the literature (e.g. Bensby et al. 2011). We have also measured gradients in [Fe/H] and [α/Fe] and their respective distribution functions over a range of 6 $<$ R $<$11 kpc in Galactocentric distance, and a 3 kpc range of distance

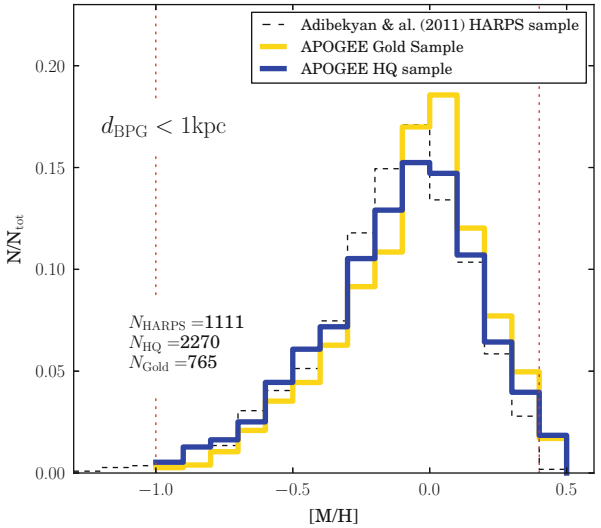

Fig. 6 The local MDF peaks slightly below solar metallicity both in the our APOGEE samples (the *gold* sample is a sub-sample with the best distances and proper motions) and in the HARPS sample. All three MDFs exhibit an extended tail towards [Fe/H] $= -1$, while showing a sharper cutoff at larger metallicities (the APOGEE sample shows a slight overabundance of stars with metallicities larger than around 0.3 dex with respect to what is observed in the HARPS sample (Color figure online)

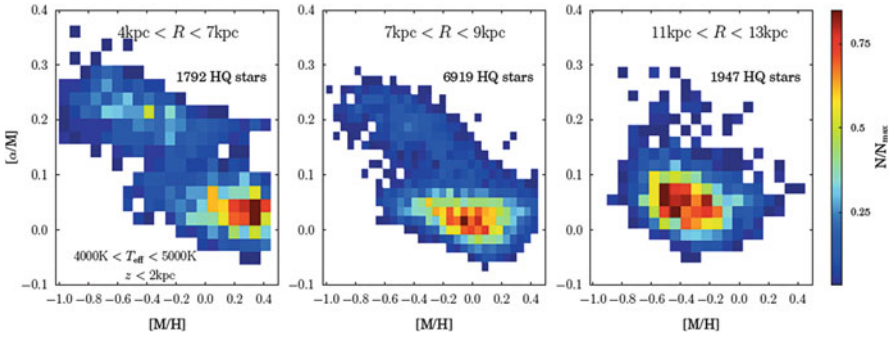

Fig. 7 Density plot of the chemical abundance plane in different radial bins for APOGEE red giant stars in the temperature range of 4,000 K < Te < 5,000 K and within z = 2 kpc. We confirm the result of Bensby et al. (2011) that the radial scale length of the thick disc is much shorter than that of the thin disc. Also important is to notice that also in the inner region there is a *gap* in the chemical plane, as observed also for the solar neighborhood

from the Galactic plane, which are in fair agreement with the gradients derived from the SEGUE, GCS and RAVE samples. For stars located at 1.5 < z < 3 kpc (which were not present in previous samples), we find a slightly positive metallicity gradient and a negative gradient in [α/Fe].

3.3 *Chemodynamics with SEGUE*

We have selected a sample of G-dwarf stars from the SEGUE survey Data Release 9 (Ahn et al. 2012). This sample (limited to distances below 3 kpc from us to keep the uncertainties in distance and proper motion at a minimum) is complementary to the RAVE giant sample discussed in Boeche et al. (2013a): both samples cover almost the same volume, whereas RAVE and SEGUE cover the southern and northern hemisphere, respectively.

Figure 8 shows the metallicity distributions obtained in both cases, RAVE and SEGUE, at the different locus of the z_{max}-eccentricity plane (Boeche et al. 2013a)

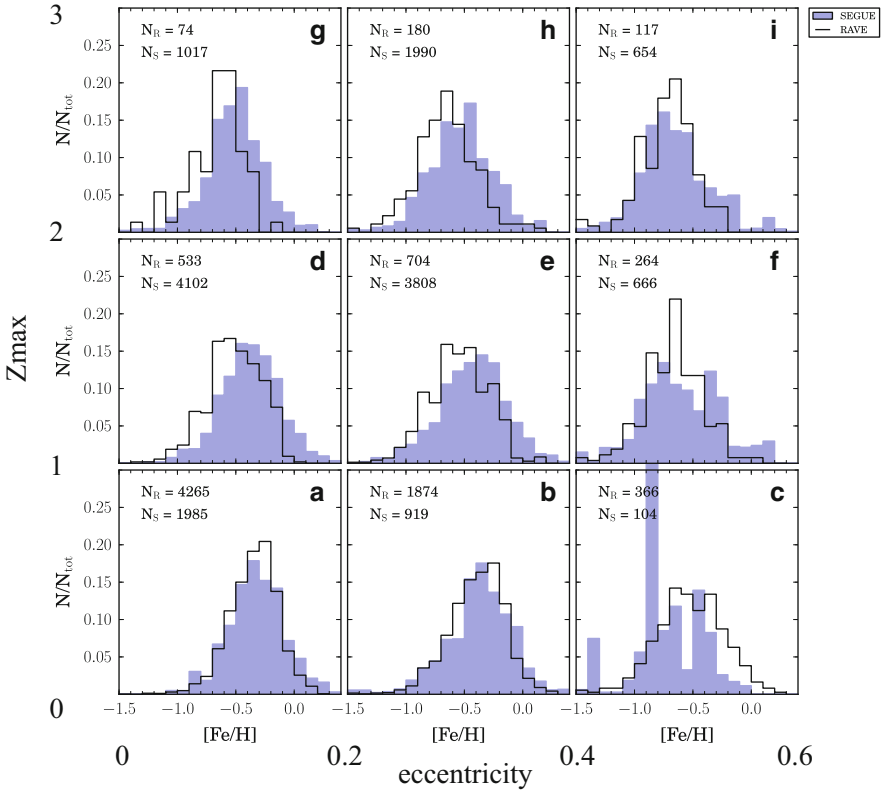

Fig. 8 This figure shows the metallicity distribution functions for a sample of RAVE giants (*solid black histograms*) and SEGUE dwarfs (*filled blue histograms*) at different ranges of z_{max} and eccentricity (indicated by the larger numbers in the x- and y-axis). The number of objects, both for RAVE and SEGUE, in each of the z_{max}-eccentricity bins are also indicated. Diagrams such as this one will also be produced for our chemodynamical models as well as for the APOGEE sample (Color figure online)

(the z_{max} and eccentricity bins are indicated in the figure). In the case of the SEGUE sample selection biases, not affecting the RAVE sample, had to be taken into account to allow a proper comparison of both surveys. Once this is done the agreement between the two samples within the different *orbital families* is encouraging. Indeed, these are completely different spectroscopic surveys, not only sampling a different hemisphere, but with different wavelength range, resolution, and different pipelines (moreover, we are here comparing a sample of dwarfs with a sample of giants). The agreement is particular good for the local thin disk dominated samples (stars in more circular orbits, not going above 1 kpc from the galactic plane—bottom left panel).

Conclusions and Outlook

Our main conclusions are summarized below:

- Stars observed here are combination of stars born hot plus radial migration bringing contribution of old stars from inner radii.
- The MW thick disc emerges naturally from (i) stars born with high velocity dispersions at high redshift, (ii) stars migrating from the inner disk early on due to strong merger activity, and (iii) further radial migration driven by the bar and spirals at later times.
- The oldest population in our chemodynamical model has the properties of what has been called thick disk, but not a clear gap in chemical plane. When applying to the simulated particles similar observational biases as it is the case in some of the high-resolution observed samples, one can recover the chemical discontinuity. However, there are samples that seem to be free from biases and still show a gap (as for instance the APOGEE sample studied in Anders et al. 2014). This might indicate the need for the two star formation episodes as in the model of Chiappini (2009).
- For now we are using [α/Fe] as proxy for age. Tighter constraints will be obtained once ages will be available.
- New observational constraints to theoretical models are now available from surveys like SEGUE, APOGEE, RAVE (some of the most recent summarized here) and Gaia-ESO. However, for a proper comparison with chemodynamical models one has to build *observed theoretical samples* (or mock catalogues). We plan to employ a newly developed selection interface (Piffl et al. in preparation) to create mock surveys from a full chemo-dynamical MW model to be able to better constrain the models.
- New constraints involving age knowledge are also now feasible thanks to the recent spectroscopic follow-ups of CoRoT and *Kepler* targets by both APOGEE and Gaia-ESO.

Acknowledgements C.C. would like to thank SDSS-III (and in particular the Brazilian and German Participation Groups) for the work done in APOGEE and SEGUE, and in particular Basilio Santiago and Leo Girardi. The RAVE collaboration is greatly acknowledged as well. Finally, I would like to thank the organizers for the invitation and for the patience in waiting for this contribution.

References

Adibekyan, V. Z., Santos, N. C., Sousa, S. G., & Israelian, G. 2011, A&A, 535, L11
Ahn, C. P., Alexandroff, R., Allende Prieto, C., et al. 2012, ApJS, 203, 21
Anders, F., Chiappini, C., Santiago, B. X., et al. 2014, A&A, 564, A115
Bensby, T., Alves-Brito, A., Oey, M. S., Yong, D., & Meléndez, J. 2011, ApJ, 735, L46
Boeche, C., Chiappini, C., Minchev, I., et al. 2013a, A&A, 553, A19
Boeche, C., Siebert, A., Piffl, T., et al. 2014, A&A, 568, A71
Boeche, C., Siebert, A., Piffl, T., et al. 2013b, A&A, 559, A59
Bovy, J., Rix, H.-W., & Hogg, D. W. 2012, ApJ, 751, 131
Brunetti, M., Chiappini, C., & Pfenniger, D. 2011, A&A, 534, A75
Chiappini, C. 2009, in IAU Symposium, Vol. 254, IAU Symposium, ed. J. Andersen, J. Bland-Hawthorn, & B. Nordström, 191–196
Chiappini, C., Matteucci, F., & Gratton, R. 1997, ApJ, 477, 765
Chiappini, C., Romano, D., & Matteucci, F. 2003, MNRAS, 339, 63
Fuhrmann, K. 1998, A&A, 338, 161
Fuhrmann, K. 2011, MNRAS, 414, 2893
Martig, M., Bournaud, F., Croton, D. J., Dekel, A., & Teyssier, R. 2012, ApJ, 756, 26
Miglio, A., Chiappini, C., Morel, T., et al. 2013, MNRAS, 429, 423
Minchev, I., Boily, C., Siebert, A., & Bienayme, O. 2010, MNRAS, 407, 2122
Minchev, I., Chiappini, C., & Martig, M. 2013, A&A, 558, A9
Minchev, I., Chiappini, C., & Martig, M. 2014a, arXiv:1401.5796
Minchev, I., Chiappini, C., Martig, M., et al. 2014b, ApJ, 781, L20
Nidever, D.L., Bovy, J., Bird, J. 2014, ApJ, in press (arXiv:1409.3566)
Raboud, D., Grenon, M., Martinet, L., Fux, R., & Udry, S. 1998, A&A, 335, L61
Rauer, H. & the PLATO 2.0 collaboration. 2013, ArXiv e-prints
Roškar, R., Debattista, V. P., Quinn, T. R., Stinson, G. S., & Wadsley, J. 2008, ApJ, 684, L79
Schönrich, R. & Binney, J. 2009, MNRAS, 399, 1145
Sellwood, J. A. & Binney, J. J. 2002, MNRAS, 336, 785
Shevchenko, I. I. 2011, ApJ, 733, 39
Trevisan, M., Barbuy, B., Eriksson, K., et al. 2011, A&A, 535, A42

The Expected Stellar Populations in the *Kepler* and CoRoT Fields

Léo Girardi, Mauro Barbieri, Andrea Miglio, Diego Bossini, Alessandro Bressan, Paola Marigo, and Thaíse S. Rodrigues

Abstract Using the stellar population synthesis tool TRILEGAL, we discuss the expected stellar populations in the *Kepler* and CoRoT fields.

1 Introduction

Kepler and CoRoT asteroseismic observations are providing us with precious information about the properties and structure of stars displaced widely across the Galaxy. Observations of these fields will not be repeated any time soon with instrumentation of comparable precision and efficiency. Since both missions were primarily driven by the goal of "finding the most planets", they applied complex target selection criteria which are not ideal for the stellar populations and Galaxy archeology applications which were devised later. Therefore, what can be extracted from this data depends on a good understanding of the data selection, and of our ability to model the entire samples with population synthesis tools. This contribution will concentrate on the latter aspect.

L. Girardi (✉) • T. Rodrigues
INAF – Osservatorio Astronomico di Padova, Vicolo dell'Osservatorio 5, Padova, Italy

LIneA – Laboratório Interdepartamental de e-Astronomia, Rua José Cristino, Rio de Janeiro, Brazil
e-mail: leo.girardi@oapd.inaf.it

M. Barbieri • P. Marigo
Dipartimento di Fisica e Astronomia, Università di Padova, Padova, Italy

A. Miglio • D. Bossini
University of Birmingham, Birmingham, UK

A. Bressan
SISSA, Via Bonomea 265, 34136 Trieste, Italy

A. Miglio et al. (eds.), *Asteroseismology of Stellar Populations in the Milky Way*,
Astrophysics and Space Science Proceedings 39,
DOI 10.1007/978-3-319-10993-0_14

2 Population Synthesis of the Milky Way

Population synthesis models of the Milky Way are the successors of the "star counts" models introduced in the 1980s (e.g. Bahcall and Soneira 1980; Bahcall 1986) to model the luminosity and color distribution of stars across the sky. The main novelty introduced by the population synthesis approach is the use of extended databases of stellar models to describe the intrinsic luminosity distribution of stars in given pass-bands, $\mathscr{L}_\lambda$, instead of recurring to empirical data. More exactly, $\mathscr{L}_\lambda$ are derived from grids of stellar evolutionary tracks suitable converted into isochrones, which are then "colored" by using synthetic photometry applied to extended grids of model spectra, and later weighted by assuming some star formation and chemical enrichment history (SFH), and the initial mass function (IMF). The all process is detailed in (e.g. Girardi et al. 2002, 2005). The advantages of the theoretical over the empirically-derived $\mathscr{L}_\lambda$ are evident: there are almost no limits to the kind of stellar populations to be tested; moreover very different databases (e.g. comprising many passbands) can be modeled in a consistent way, and the models can be more reliably extrapolated to larger photometric depths. On the other hand, the population synthesis approach introduces many additional parameters and functions, like those describing the SFH and IMF for each Galactic component, that apparently complicate the problem. Moreover, using the population synthesis approach implies trusting on the predictive capability of the underlying stellar models.

But the necessity of the population synthesis approach becomes dramatically more evident when we consider the present asteroseismic data: empirical data simply cannot replace the stellar models in this case, simply because there is not enough empirical information to build the asteroseismic versions of $\mathscr{L}_\lambda$ starting from star clusters of from stars with parallaxes. In this case, the asteroseismic data is helping to test the stellar models in a very detailed way, star by star, and helping to test the galactic models at the same time.

2.1 TRILEGAL

TRILEGAL is a population synthesis code started with the initial goal of simulating deep and wide multi-band photometric data (Groenewegen et al. 2002; Girardi et al. 2005; Vanhollebeke et al. 2009). More recently, the code has become a fundamental tool to test stellar evolutionary tracks from the Padova-Trieste group (e.g. Girardi et al. 2009, 2010; Bianchi et al. 2011; Rosenfield et al. 2014). With the recent/ongoing addition of new quantities in the code, like the surface chemical composition and asteroseismic parameters, it is ready to be applied in the simulation and interpretation of large databases like those provided by CoRoT and *Kepler*.

2.2 Expectations for CoRoT

Miglio et al. (2013a,b) provide a detailed description of the model expectations in CoRoT fields. CoRoT eyes are directed towards very different lines-of sight, probing a large range of both galactocentric radii and heights above/below the Galactic Plane. The main result in Miglio et al. (2013b) was the detection of a significant difference in the mass distribution of stars towards the CoRoT fields LRc01 and LRa01, which was interpreted as being mainly due to the different stellar ages being sampled at two different heights below the Galactic Plane. Similar differences are expected for all other CoRoT lines-of-sight, but are of harder interpretation given their more complex target selection.

2.3 Expectations for Kepler

Figure 1 is extracted from a large simulation of the *Kepler* field, including many of the filter systems of interest. The simulation scales down the Schlegel et al. (1998) extinction values down to the distance of each simulated star, distributing it along the

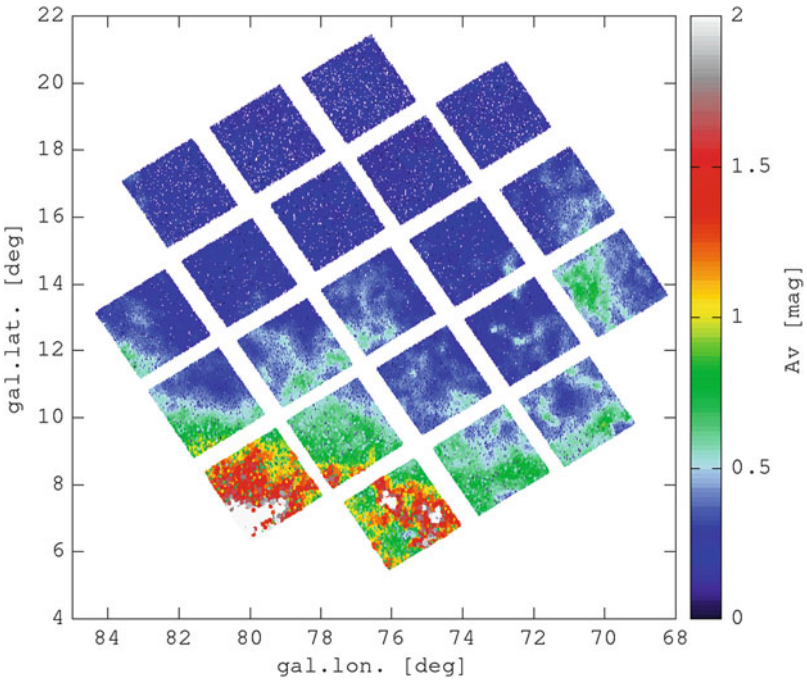

Fig. 1 Barbieri et al. (in preparation) large simulation of the *Kepler* field, including many of the filter systems of interest (e.g. SDSS, DOO51, 2MASS, and the wide Kp filter). The plot simply shows the stellar location in the sky (galactic coordinates) color coded by their extinction A_V

line-of-sight by assuming an exponential dust layer with $h_z = 110$ pc. A correction for the Local Bubble is also made.

One of the main novelties in the simulation are the more complex way the binaries are simulated: their mass ratio, orbital period and eccentricity, inclination etc., are derived for the system at birth following a series of reasonable assumptions. The binary evolution is then followed with the BSE code (Hurley et al. 2002), which considers mass transfer and accretion, common-envelope evolution, collisions, supernova kicks, angular momentum loss mechanisms, circularization and synchronization of orbits by tidal interactions. Of course there are many tunable parameters involved in these models, like the strength of tidal damping in radiative, convective and degenerate regions, the Reimers (1975) mass-loss coefficient, the binary enhanced mass loss, the common envelope efficiency.

Any simulation of the *Kepler* field will be of limited use if not including a simulation of the *Kepler* target selection criteria. The best study of these criteria so far has been by Farmer et al. (2013), who built a software that tries to mimic all the steps involved in building the *Kepler* input catalogue and prioritization (Brown et al. 2011; Batalha et al. 2010). For asteroseismic studies, we should also consider the addition of targets not coming from the original planet-detection plan, and estimate the probability of actually measuring the asteroseismic parameters and their errors (e.g. Chaplin et al. 2011, for dwarfs).

Figure 2 provides some basic information about the expected distribution of these stars across the Galaxy, in particular evincing the modest coverage in $R_{\rm GC}$, and the large range in z. Since younger stars are concentrated at smaller heights, the model predicts strong differences between the distributions stellar masses observed at the latitude extremes of this field, as evidenced in Fig. 3. These differences are large enough to be easily measurable in the *Kepler* data, although their interpretation is somewhat complicated by the patchy extinction in the low-latitude fields. Work is ongoing to transform these distributions of stellar mass in clear constraints to the increase of scale-height with stellar age, hence complementing the earlier suggestions derived from CoRoT data.

It is hoped that *Kepler* data will help to solve the dramatic problem pointed out by Reylé and Robin (2001), that is: when attempting to fit star counts only, there is a strong degeneracy between scale height and surface density of thick disk, with models favoring either high scale height and small local density (for example, the $h_z = 1{,}400$ pc and 2 % of disk density favoured by Reid and Majewski 1993, against the 910 pc and 5.9 % from Buser et al. 1999). Although the problem can be relieved with more photometric data, a clearcut distinction between thick and from old thin disk (if any exists, e.g. Bovy et al. 2012) would help. That is where *Kepler* data can be critical.

Additional information is store in *Kepler* data in the form of chemical abundances and kinematics of stars of different masses and ages. The secondary red clump (Girardi 1999), for instance, contains a pure population of $\sim$1 Gyr stars and which is

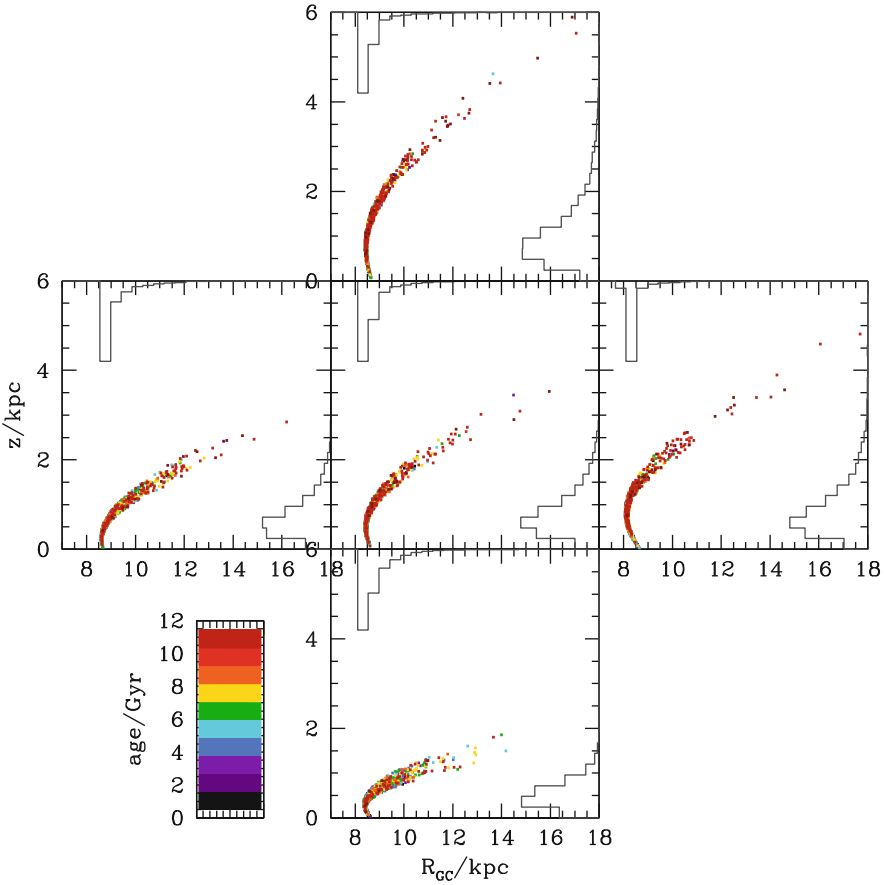

Fig. 2 The expected ranges of galactocentric radius, R_{GC}, and height above the Plane, z, for subsamples located in the N, S, W and E extreme corners of the *Kepler* field, and for the center as well. It evidences the modest coverage in R_{GC}, and the large range in z. Younger stars are concentrated at smaller heights

easily identifiable in a log g versus log $T_{\rm eff}$ plot (Fig. 4), especially when additional information from mixed modes (period spacing) is available. Stellar metallicities for these stars, as measured e.g. by APOKASC (Pinsonneault et al. 2014) can provide a direct probe of the intrinsic metallicity spread, and a solid point along the age-metallicity relation, across the Galaxy.

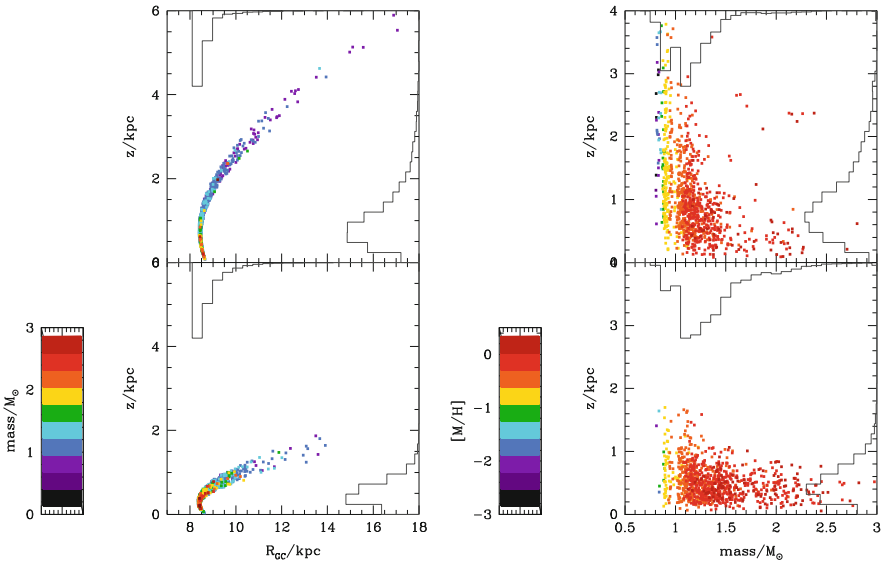

Fig. 3 *Left panel*: distribution of heights above the plane for the two extreme fields of *Kepler* (*top* for $b = 20°$, *bottom* for $b = 6°$). *Right panel*: The expected distribution of stellar masses for stars in these fields

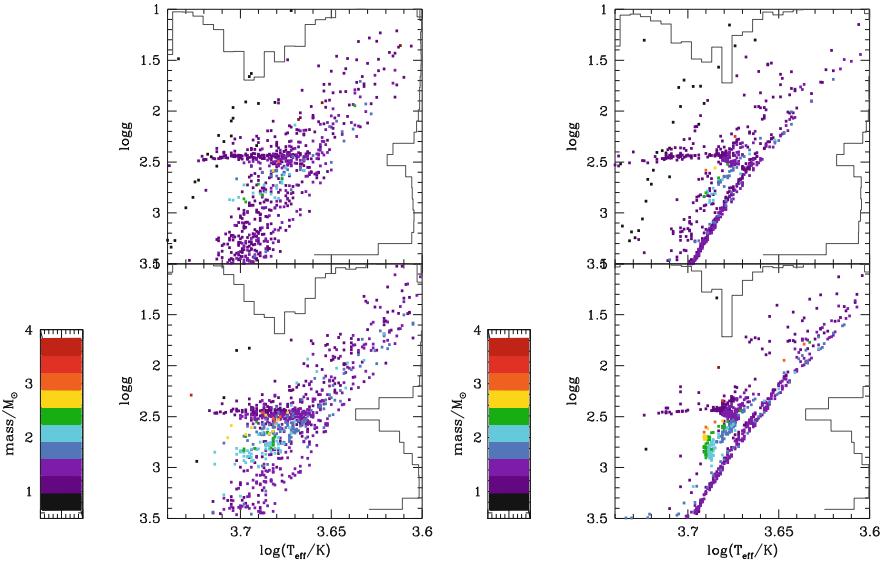

Fig. 4 *Left panel*: red clump with default metallicity dispersion. *Right panel*: without metallicity dispersion (Color figure online)

Concluding Remarks

The population synthesis approach has revealed to be a powerful technique, very useful for the interpretation of wide-area surveys in terms of the MW structure and evolution. Present applications to CoRoT and *Kepler* asteroseismic samples are still limited, but with their direct measurements of ages and evolutionary stages, they provide excellent hopes for imposing tight constrains in the models.

While dwarfs in *Kepler* fields seem to have their radii well reproduced by models, there is a discrepancy for masses, still to be clarified (Chaplin et al. 2011). Giants in *Kepler* represent the ideal sample for testing the variation of stellar properties with z, and hopefully will provide long-awaited constraints to disk-heating and accretion scenarios, and complement the kinematical information either already available (e.g. from proper motions, GCS) or being collected by APOKASC. The expected variation of mean mass (age) with z is detected in the CoRoT giants (Miglio et al. 2013b), but those results may be affected by the large range of galactocentric radii probed by CoRoT. Of course, it is expected that once the vertical structure is revealed by the *Kepler* sample, CoRoT results will have to be reevaluated.

Acknowledgements We thank all participants in the Sexten meeting for the stimulating discussions, and the *Kepler* and CoRoT teams for providing such wonderful and promising databases.

References

Bahcall, J. N. 1986, ARA&A, 24, 577
Bahcall, J. N. & Soneira, R. M. 1980, ApJS, 44, 73
Batalha, N. M., Borucki, W. J., Koch, D. G., et al. 2010, ApJ, 713, L109
Bianchi, L., Efremova, B., Herald, J., et al. 2011, MNRAS, 411, 2770
Bovy, J., Rix, H.-W., & Hogg, D. W. 2012, ApJ, 751, 131
Brown, T. M., Latham, D. W., Everett, M. E., & Esquerdo, G. A. 2011, AJ, 142, 112
Buser, R., Rong, J., & Karaali, S. 1999, A&A, 348, 98
Chaplin, W. J., Kjeldsen, H., Christensen-Dalsgaard, J., et al. 2011, Science, 332, 213
Farmer, R., Kolb, U., & Norton, A. J. 2013, MNRAS, 433, 1133
Girardi, L. 1999, MNRAS, 308, 818
Girardi, L., Bertelli, G., Bressan, A., et al. 2002, A&A, 391, 195
Girardi, L., Groenewegen, M. A. T., Hatziminaoglou, E., & da Costa, L. 2005, A&A, 436, 895
Girardi, L., Rubele, S., & Kerber, L. 2009, MNRAS, 394, L74
Girardi, L., Williams, B. F., Gilbert, K. M., et al. 2010, ApJ, 724, 1030
Groenewegen, M. A. T., Girardi, L., Hatziminaoglou, E., et al. 2002, A&A, 392, 741
Hurley, J. R., Tout, C. A., & Pols, O. R. 2002, MNRAS, 329, 897
Miglio, A., Chiappini, C., Morel, T., et al. 2013a, in European Physical Journal Web of Conferences, Vol. 43, European Physical Journal Web of Conferences, 3004
Miglio, A., Chiappini, C., Morel, T., et al. 2013b, MNRAS, 429, 423
Pinsonneault, M., et al., ApJS in press, arXiv1410.2503

Reid, N. & Majewski, S. R. 1993, ApJ, 409, 635
Reimers, D. 1975, Memoires of the Societe Royale des Sciences de Liege, 8, 369
Reylé, C. & Robin, A. C. 2001, A&A, 373, 886
Rosenfield, P. et al., 2014, ApJ, 790, 22
Schlegel, D. J., Finkbeiner, D. P., & Davis, M. 1998, ApJ, 500, 525
Vanhollebeke, E., Groenewegen, M. A. T., & Girardi, L. 2009, A&A, 498, 95

Early Results from APOKASC

Courtney Epstein

Abstract Asteroseismology and spectroscopy provide complementary constraints on the fundamental and chemical properties of stars. I describe the first results from APOKASC, a collaboration between the *Kepler* asteroseismic science consortium (KASC) and the SDSS-III APOGEE survey. These include (1) the first test of asteroseismic scaling relationships in the metal-poor regime using halo and thick disk stars identified in the APOKASC sample; and (2) the calibration of spectroscopic parameters using precise asteroseismic measurements of surface gravity. I also highlight future research avenues that are made possible by this unique sample of thousands of well-characterized red giant stars.

1 Introduction

To understand galaxy formation and evolution, one can either study numerous high-redshift galaxies or examine in detail one nearby galaxy, like the Milky Way. Reconstructing the star formation history of the Milky Way requires detailed knowledge of the fundamental and chemical properties of its constituent stars.

To achieve this goal, the Apache Point Observatory Galaxy Evolution Experiment (APOGEE; Majewski et al. 2010) partnered with the *Kepler* asteroseismic science consortium (KASC) to form APOKASC. APOGEE is a high-resolution, high signal-to-noise, H-band spectroscopic survey that is part of the Sloan Digital Sky Survey III (Eisenstein et al. 2011). APOGEE provides measurements of effective temperature ($T_{\rm eff}$), surface gravity ($\log g$), metallicity ([M/H]), rotation ($v \sin i$), and radial velocity. In the *Kepler* field, these spectroscopic measurements will be complemented by asteroseismic constraints on mass, radius, and $\log g$, and evolutionary state information, when available (e.g., Bedding et al. 2011; Mosser et al. 2012; Stello et al. 2013).

C. Epstein (✉)
The Ohio State University, Department of Astronomy, McPherson Laboratory,
140 W 18th Avenue, Columbus, OH 43210-1173, USA
e-mail: epstein@astronomy.ohio-state.edu

A. Miglio et al. (eds.), *Asteroseismology of Stellar Populations in the Milky Way*,
Astrophysics and Space Science Proceedings 39,
DOI 10.1007/978-3-319-10993-0_15

In the first year of observations (Ahn et al. 2014), APOGEE observed $\sim$ 1,900 red giants with asteroseismically determined parameters. These data will be made publicly available in the APOKASC catalog (Pinsonneault et al. in prep.). I will describe two early results where the APOKASC dataset has been used to test the asteroseismic (Sect. 2) and spectroscopic (Sect. 3) determination of stellar parameters. I conclude by outlining future areas of investigation.

2 Testing Asteroseismic Scaling Relationships

The APOKASC sample is useful for testing the asteroseismic mass scale. Two asteroseismic observables can be extracted from the power spectrum of oscillating red giants, namely the frequency of maximum power, $\nu_{\rm max}$, and the large frequency separation, $\Delta\nu$. The masses and radii of stars with oscillations driven by surface convection may be estimated using empirical scaling relationships (Ulrich 1986; Brown et al. 1991; Kjeldsen and Bedding 1995):

$$\frac{\Delta\nu}{\Delta\nu_\odot} \simeq \left(\frac{\rm M}{\rm M_\odot}\right)^{1/2}\left(\frac{\rm R}{\rm R_\odot}\right)^{-3/2} \quad (1)$$

$$\frac{\nu_{\rm max}}{\nu_{\rm max,\odot}} \simeq \left(\frac{\rm M}{\rm M_\odot}\right)\left(\frac{\rm R}{\rm R_\odot}\right)^{-2}\left(\frac{\rm T_{eff}}{\rm T_{eff,\odot}}\right)^{-1/2}, \quad (2)$$

where $\Delta\nu_\odot = 135.0 \pm 0.1$ μHz, $\nu_{\rm max,\odot} = 3140 \pm 30$ μHz, and $\rm T_{eff,\odot} = 5777$ K (Pinsonneault et al. in prep.).

These scaling relationships are calibrated based on the Sun and are therefore not guaranteed to work for more evolved stars, like red giants, which have a different internal structure. The accuracy of radii derived with asteroseismic scaling relationships have been examined using interferometry (Huber et al. 2012), *Hipparcos* parallaxes (Silva Aguirre et al. 2012), and RGB stars in the open cluster NGC6791 (Miglio et al. 2012; see Miglio et al. 2013 for a review of constraints).

Eclipsing binaries provide a test of scaling relationships masses. In particular, the metal-rich ([Fe/H]$\sim +0.4$ dex) open cluster NGC 6791 serves as a prime test case. From measurements of eclipsing binaries near the cluster's main sequence turn-off, the mass of red giant branch stars is inferred to be $\rm M_{RGB} = 1.15 \pm 0.02\ M_\odot$ (Brogaard et al. 2012). Asteroseismic oscillations have been detected for red giant branch stars in this cluster. Scaling relationships yield mass estimates of $\rm M_{RGB} = 1.20 \pm 0.01\ M_\odot$ and $1.23 \pm 0.02\ \rm M_\odot$ from Basu et al. (2011) and Miglio et al. (2012). These mass estimates are sensitive to, for example, the choice of temperature scale. Wu et al. (2014) defined an additional scaling relationship and determined a mass of $\rm M_{RGB} = 1.24 \pm 0.03\ M_\odot$, consistent with previous results.

2.1 Current Results: Probing the Metal-Poor Regime

These tests of the standard scaling relationships have been confined to metallicities close to solar ($-0.5 \lesssim$ [Fe/H] $\lesssim +0.4$). However, the scaling relationships take no account of metallicity. Because metallicity could potentially influence mode excitation and damping and opacity-driven changes in convective properties, stellar properties derived using scaling relationships need to be verified over a wide range of metallicities. The APOKASC sample enabled the first test of mass estimates from asteroseismic scaling relationships in the low-metallicity regime (Epstein et al. 2014).

In the first year of APOGEE observations in the *Kepler* field, there were nine stars with measured asteroseismic parameters, reliable spectroscopic measurements, and [M/H]< -1 dex. We differentiated between halo and disk stars by computing the 3D space velocities and adopting $v_{\rm tot,LSR} = 180$ km/s as the kinematical division between stars classified as halo and disk populations (Venn et al. 2004). We considered metal-poor stars with disk kinematics to be members of the thick disk.

Halo and metal-poor thick disk stars have a variety of independent constraints on their mass and age. The combined evidence from isochrone fits to globular clusters, e.g., Gratton et al. (1997), the white dwarf cooling sequence, e.g., Hansen et al. (2002), the radioactive decay of uranium and thorium, e.g., Sneden et al. (1996), and the imprint left by the MSTO on the stellar temperature distribution function (Jofré and Weiss 2011), places halo stars as being 10 Gyr or older. Metal-poor, α-enhanced members of the Galactic disk have been found to be 8 Gyr or older (Bensby et al. 2013; Haywood et al. 2013). We converted these age constraints into mass constraints using Dartmouth stellar isochrones (Dotter et al. 2008). The mass range associated with these age constraints is shown as the gray bands in Fig. 1. These mass ranges are consistent with the mass measurements of the eclipsing binary found in the metal-poor thick disk globular cluster 47 Tuc (Thompson et al. 2010). The width of these bands includes uncertainties in the input physics, including the assumed helium abundance, heavy element mixture, nuclear reaction rates, equation of state, opacity, model atmosphere, and heavy element diffusion rate (see van Saders and Pinsonneault 2012 for details).

Figure 1 shows that the masses determined using asteroseismic scaling relationships, asteroseismic parameters from the APOKASC catalog, and spectroscopic temperatures are a weighted average of ΔM$= 0.17 \pm 0.05$ M$_\odot$ higher than expectations. Possible explanations for this mass discrepancy are fully detailed in Epstein et al. (2014). For example, shifts in the temperature scale and contamination of this red giant branch sample by more evolved (e.g., horizontal branch or asymptotic giant branch) stars work to increase the mass difference. Two published theoretically motivated corrections (White et al. 2011; Mosser et al. 2013) reduce the mass estimates by as much as ~ 5 %. Differences between methods of determining $\Delta\nu$ and $\nu_{\rm max}$ can shift ΔM by as much as 0.04 M$_\odot$ for these stars. Epstein et al.

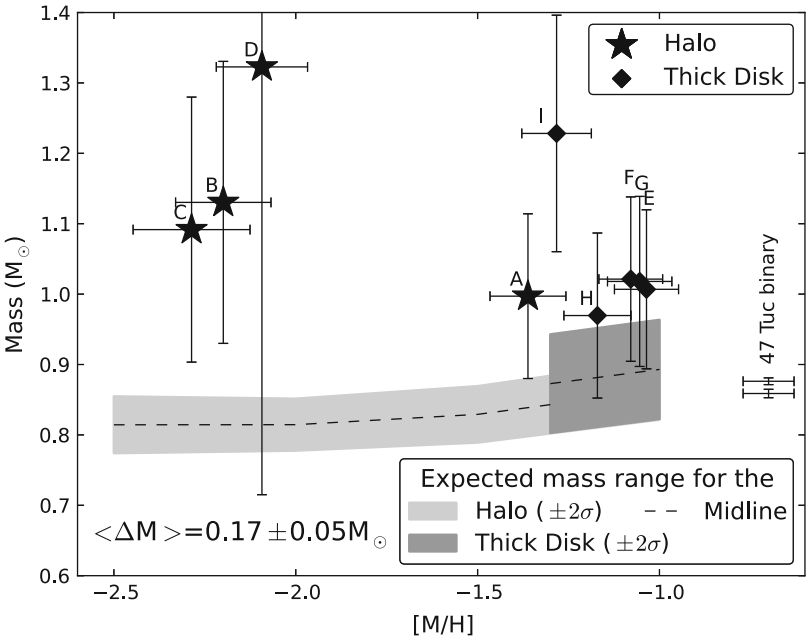

Fig. 1 Mass determined using standard asteroseismic scaling relationships [see Eqs. (1) and (2)], asteroseismic parameters from the APOKASC Catalog (Pinsonneault et al. in prep.), and spectroscopic temperatures from APOGEE. The expected mass ranges based on astrophysical priors for halo and thick disk stars are indicated by the *light* and *dark gray bands*, respectively. See Pinsonneault et al. (in prep.) for a description of the method used to determine $\Delta\nu$ and $\nu_{\max}$ and their uncertainties

also note a difference between masses derived using scaling relationships compared with $\nu_{\max}$-independent techniques (Bedding et al. 2006; Deheuvels et al. 2012).

2.2 *Upcoming Work*

The second year of APOGEE observations will include additional metal-poor stars, enabling a better statistical test of the mass offset at low-metallicity. Detailed frequency modeling of metal-poor stars in the APOKASC sample will help to calibrate masses derived using scaling relationships. The influence of Eq. (2) on asteroseismic mass estimates also merits investigation. Theoretical corrections, e.g., White et al. (2011), have been computed for $-0.2 <$[Fe/H]$< +0.2$; work is underway to extend similar models to lower metallicity.

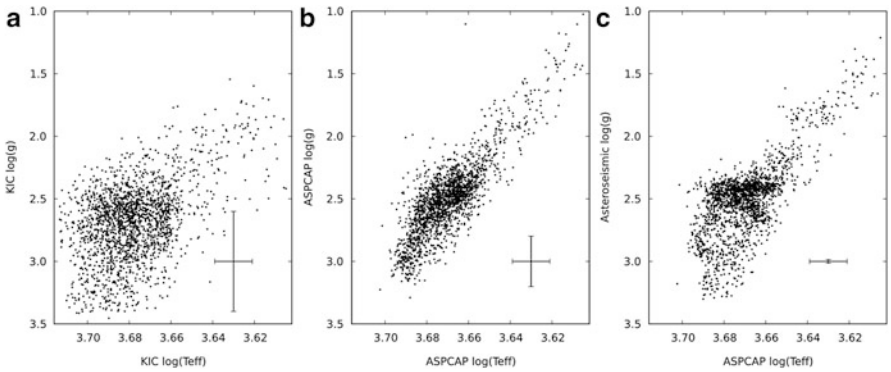

Fig. 2 A comparison of the ASPCAP sample's log g and T_{eff} distribution on the red giant branch, as determined using different measurement techniques. (**a**) Parameters were taken from the Kepler Input Catalog, which is based on photometric inputs Brown et al. (2011). (**b**) Spectroscopic parameters were derived using the ASPCAP. (**c**) Spectroscopic T_{eff} and asteroseismic log g from the APOKASC Catalog (Pinsonneault et al. in prep.). The typical uncertainty is shown in the *lower right*

3 Calibrating Stellar Parameters from Atmospheric Models

Many studies have investigated the accuracy of asteroseismic gravities for evolved stars and have found good agreement between asteroseismic and spectroscopic techniques (e.g., Morel and Miglio 2012; Thygesen et al. 2012). Asteroseismic log g have been shown to be largely model independent (Gai et al. 2011) and robust to using different approaches to derive oscillation parameters and incorporating corrections to the $\Delta\nu$ scaling relationship [Eq. (1)] (Hekker et al. 2013).

The APOGEE survey used the asteroseismic log g as an independent check on the log g derived using the APOGEE Stellar Parameters and Chemical Abundances Pipeline (ASPCAP) (Mészáros et al. 2013). The ASPCAP determines stellar parameters (including log g) and abundances by performing a χ^2 minimization in a grid of synthetic spectra. Mészáros et al. defined an empirical correction to the ASPCAP log g based on combined constraints from asteroseismology and open/globular cluster stars for application to the larger APOGEE sample (Mészáros et al. 2013).

Future Applications and Conclusions
The APOKASC sample represents the largest set of joint asteroseismic and spectroscopic constraints available to date. Figure 2 shows the impact of these improved constraints on the H-R diagram. The precise asteroseismic log g measurements make possible the identification of features, like the red clump and red bump, in a sample of field stars.

(continued)

The detection of mixed-modes (Bedding et al. 2011; Mosser et al. 2012; Stello et al. 2013) can distinguish between helium-core-burning and hydrogen-shell-burning stars. This information will be useful for identifying stellar populations and probing their properties as a function of a Galactic position and age. Bayesian estimates of stellar age (e.g., Serenelli et al. 2013) based on APOKASC's and asteroseismic constraints will help to reconstruct the star formation history of the Milky Way through diagnostics, such as the age-metallicity relationship.

Additionally, the locus of the red giant branch will provide an excellent test of stellar interior models. For example, we can test whether adopting a solar mixing-length for stars is consistent with asteroseismic measurements across a range of mass, [M/H], and $\log g$ (e.g., Bonaca et al. 2012). The power of precise asteroseismic $\log g$ (Sect. 3) could also be harnessed to constrain stellar model atmospheres.

The APOKASC collaboration offers a treasure trove of information that will enable studies of both stellar physics and stellar populations for years to come.

References

Ahn, C. P., Alexandroff, R., Allende Prieto, C., et al. 2014, ApJS, 211, 17
Basu, S., Grundahl, F., Stello, D., et al. 2011, ApJ, 729, L10
Bedding, T. R., Butler, R. P., Carrier, F., et al. 2006, ApJ, 647, 558
Bedding, T. R., Mosser, B., Huber, D., et al. 2011, Nature, 471, 608
Bensby, T., Feltzing, S., & Oey, M. S. 2013, ArXiv e-prints
Bonaca, A., Tanner, J. D., Basu, S., et al. 2012, ApJ, 755, L12
Brogaard, K., VandenBerg, D. A., Bruntt, H., et al. 2012, A&A, 543, A106
Brown, T. M., Gilliland, R. L., Noyes, R. W., & Ramsey, L. W. 1991, ApJ, 368, 599
Brown, T. M., Latham, D. W., Everett, M. E., & Esquerdo, G. A. 2011, AJ, 142, 112
Deheuvels, S., García, R. A., Chaplin, W. J., et al. 2012, ApJ, 756, 19
Dotter, A., Chaboyer, B., Jevremović, D., et al. 2008, ApJS, 178, 89
Eisenstein, D. J., Weinberg, D. H., Agol, E., et al. 2011, AJ, 142, 72
Epstein, C. R., Elsworth, Y. P., Johnson, J. A., et al. 2014, ApJ, 785, L28
Gai, N., Basu, S., Chaplin, W. J., & Elsworth, Y. 2011, ApJ, 730, 63
Gratton, R. G., Fusi Pecci, F., Carretta, E., et al. 1997, ApJ, 491, 749
Hansen, B. M. S., Brewer, J., Fahlman, G. G., et al. 2002, ApJ, 574, L155
Haywood, M., Di Matteo, P., Lehnert, M., Katz, D., & Gomez, A. 2013, ArXiv e-prints
Hekker, S., Elsworth, Y., Mosser, B., et al. 2013, A&A, 556, A59
Huber, D., Ireland, M. J., Bedding, T. R., et al. 2012, ApJ, 760, 32
Jofré, P. & Weiss, A. 2011, A&A, 533, A59
Kjeldsen, H. & Bedding, T. R. 1995, A&A, 293, 87
Majewski, S. R., Wilson, J. C., Hearty, F., Schiavon, R. R., & Skrutskie, M. F. 2010, in IAU Symposium, Vol. 265, IAU Symposium, ed. K. Cunha, M. Spite, & B. Barbuy, 480–481
Mészáros, S., Holtzman, J., García Pérez, A. E., et al. 2013, AJ, 146, 133
Miglio, A., Brogaard, K., Stello, D., et al. 2012, MNRAS, 419, 2077

Miglio, A., Chiappini, C., Morel, T., et al. 2013, in European Physical Journal Web of Conferences, Vol. 43, European Physical Journal Web of Conferences, 3004
Morel, T. & Miglio, A. 2012, MNRAS, 419, L34
Mosser, B., Goupil, M. J., Belkacem, K., et al. 2012, A&A, 540, A143
Mosser, B., Michel, E., Belkacem, K., et al. 2013, A&A, 550, A126
Pinsonneault, M. H., Elsworth, Y., Epstein, C., et al. 2014, arXiv:1410.2503
Serenelli, A. M., Bergemann, M., Ruchti, G., & Casagrande, L. 2013, MNRAS, 429, 3645
Silva Aguirre, V., Casagrande, L., Basu, S., et al. 2012, ApJ, 757, 99
Sneden, C., McWilliam, A., Preston, G. W., et al. 1996, ApJ, 467, 819
Stello, D., Huber, D., Bedding, T. R., et al. 2013, ApJ, 765, L41
Thompson, I. B., Kaluzny, J., Rucinski, S. M., et al. 2010, AJ, 139, 329
Thygesen, A. O., Frandsen, S., Bruntt, H., et al. 2012, A&A, 543, A160
Ulrich, R. K. 1986, ApJ, 306, L37
van Saders, J. L. & Pinsonneault, M. H. 2012, ApJ, 746, 16
Venn, K. A., Irwin, M., Shetrone, M. D., et al. 2004, AJ, 128, 1177
White, T. R., Bedding, T. R., Stello, D., et al. 2011, ApJ, 743, 161
Wu, T., Li, Y., & Hekker, S. 2014, ApJ, 781, 44

The Metallicity Gradient of the Old Galactic Bulge Population

Sara Alejandra Sans Fuentes and Joris De Ridder

Abstract Understanding the structure, formation and evolution of the Galactic Bulge requires the proper determination of spatial metallicity gradients in both the radial and vertical directions. RR Lyrae pulsators, known to be excellent distance indicators, may hold the key to determining these gradients. Jurcsik and Kovacs (A&A 312:111, 1996) has shown that RR Lyrae light curves and the phase difference of their Fourier decomposition, ϕ_{31}, can be used to estimate photometric metallicities. The existence of galactic bulge metallicity gradients is a currently debated topic that would help pinpoint the Galaxy's formation and evolution. A recent study of the OGLE-III Galactic Bulge RR Lyrae Population by Pietrukowicz et al. (ApJ 750:169, 2012) suggests that the spatial distribution is uniform. We investigate how small a gradient would be detectable within the current S/N levels of the present data set, given the random and systematic errors associated with the derivation of a photometric metallicity versus spatial position relationship.

1 Introduction

The eleventh part of the Optical Gravitational Lensing Experiment (OGLE-III) contains the most complete and up-to-date photometric data set of Galactic Bulge RR Lyrae pulsating stars currently available. The sample contains photometric light curves in the I and V bands for a total of 11,756 fundamental mode RR Lyrae (RRab) (Soszyński et al. 2011; Udalski et al. 2008). This extensive data set has proven useful in investigating the Galactic interstellar extinction, metallicity gradients, and 3-D spatial distributions (Pietrukowicz et al. 2012; Nataf et al. 2013; Smolec 2005). The work presented here uses 10,456 RRab stars from the OGLE-III Galactic Bulge RR Lyrae catalog to investigate the detection limits of galactic bulge metallicity gradients.

S.A.Sans Fuentes (✉) • J. De Ridder
KU Leuven, Instituut voor Sterrenkunde, Celestijnenlaan 200D, 3001 Leuven, Belgium
e-mail: Alejandra.Sans@ster.kuleuven.be

A. Miglio et al. (eds.), *Asteroseismology of Stellar Populations in the Milky Way*,
Astrophysics and Space Science Proceedings 39,
DOI 10.1007/978-3-319-10993-0_16

2 Methodology

The present sample includes RRab stars with I magnitudes between $13 + (V - I)$ and $16 + (V - I)$, in order to exclude foreground and background stars. Background stars are likely to belong to the Sgr dSph Galaxy (Soszyński et al. 2011; Pietrukowicz et al. 2012). From this sample, we create 1,000 population samples by assuming Gaussian distributions centered on the observed OGLE values and standard deviations equal to the respective errors for each star's Period, ϕ_{31}, I and V. For each of these population samples, the photometric metallicities are estimated using the P-ϕ_{31}-[Fe/H] relationship given in Smolec (2005):

$$[\mathrm{Fe/H}] = -3.142 - 4.903P + 0.824(\phi_{31} + \pi), \tag{1}$$

where a phase shift is necessary due to sine/cosine fitting differences in Smolec (2005) and Soszyński et al. (2011). The galactocentric distances for each sample are calculated following the methodology presented in Pietrukowicz et al. (2012):

$$\log Z = [\mathrm{Fe/H}] - 1.765 \tag{2}$$

$$M_V = 2.288 + 0.882 \log Z + 0.108(\log Z)^2 \tag{3}$$

$$M_I = 0.471 - 1.132 \log P + 0.025 \log Z \tag{4}$$

$$R_I = A_I / E(V - I) \tag{5}$$

$$\log R = 1 + 0.2\,(I_0 - M_I) \tag{6}$$

$$R_{GCD} = \left[R_0^2 + R^2 - 2RR_0\cos(l)\right]^{0.5}. \tag{7}$$

We estimate the mean sample barycenter to be $R_0 = 8.48 \pm 0.01$ Kpc and a mean sample metallicity of -0.994 ± 0.327 for the OGLE-III Galactic Bulge RR Lyrae magnitude limited sample.

The effects that introducing a small synthetic gradient in the metallicity versus galactocentric distance plane would have on our observed variables are tested by introducing a Δ [Fe/H] to each stars metallicity based on its position. A backwards propagation of the Δ [Fe/H] perturbation is performed, under the assumptions that

- The distance to each star remains fixed,
- The ratio of total to selective extinction, R_I, remains unchanged,
- In cases of degeneracies, the induced perturbations are equally distributed between the fractional perturbations of all involved variables,

A synthetic data set is created for which new values of [Fe/H] and R_{GCD} and associated error distributions are calculated. In the case where Δ [Fe/H] values are introduced to create a synthetic gradient of -0.01 [dex/Kpc], our mean sample barycenter and mean sample metallicity become $R_0 = 8.47 \pm 0.01$ Kpc and

[Fe/H]$= -0.992 \pm 0.329$. Sampling through the defined [Fe/H] and R_{GCD} distributions of each star, 1,000 least-squares (LS) fits are performed. An F-test, to a confidence level of 0.05, is performed on each LS fit to determine the significance of derived trends. The mean fit coefficients and their standard deviations are obtained for both samples.

3 Preliminary Results

Re-deriving the OGLE-III Galactic Bulge RR Lyrae metallicities with the latest methodology, and fitting the R_{GCD} - [Fe/H] plane suggests that there exists a small but statistically significant galactic bulge metallicity gradient within the OGLE-III Galactic Bulge RR Lyrae database of strength -0.0239 ± 0.0006 [dex/Kpc]. In addition, using simulated data with an artificial trend of -0.01 [dex/Kpc] and realistic noise, a least squares fit results in an also statistically significant metallicity gradient of -0.012 ± 0.0006 [dex/Kpc]. In both cases the significance of the gradient is tested to a confidence level of 0.05. Therefore, we conclude that with the current methodology and data sample, a gradient as small as -0.01 [dex/Kpc] can be detected within the OGLE-III Galactic Bulge RR Lyrae.

Acknowledgements The authors would like to thank Igor Soszynski and Marcio Catelan for providing necessary fit and calibrations errors. This work was carried out, in whole or in part through the Gaia Research for European Astronomy Training (GREAT-ITN) network. The research leading to these results has received funding from the European Union Seventh Framework Programme ([FP7/2007–2013]) under grant agreement n°—264895.

References

Jurcsik, J. & Kovacs, G. 1996, A&A, 312, 111
Nataf, D. M., Gould, A., Fouqué, P., et al. 2013, ApJ, 769, 88
Pietrukowicz, P., Udalski, A., Soszyński, I., et al. 2012, ApJ, 750, 169
Smolec, R. 2005, Acta Astron. , 55, 59
Soszyński, I., Dziembowski, W. A., Udalski, A., et al. 2011, Acta Astron. , 61, 1
Udalski, A., Szymanski, M. K., Soszynski, I., & Poleski, R. 2008, Acta Astron. , 58, 69

Part V
Future Spectroscopic, Astrometric and Seismic Surveys, and Synergies with Gaia

4MOST: 4m Multi Object Spectroscopic Telescope

Éric Depagne and The 4MOST Consortium

Abstract 4MOST (4m Multi Object Spectroscopic Telescope) is a spectroscopic facility that will be installed on ESO's VISTA around 2020. The science rationale of this facility are to be found in the ASTRONET Science Vision for European Astronomy (de Zeeuw & Molster, (eds) A Science Vision for European Astronomy, Astronet 2007. ISBN 978-3-923524-62-4). Specifically fundamental contribution can be made to the Extreme Universe (Dark Energy & Dark Matter, Black holes), Galaxy Formation & Evolution, and the Origin of Stars science cases in the ASTRONET Science Vision. The unique capabilities of the 4MOST facility are due to by its large field-of-view, high multiplex, its broad optical spectral wavelength coverage

1 History

In 2010, ESO issued a Call for Letters of Interest (LoI) for the Conceptual Design of a Multi-Object Spectroscopic instrument or facility. AIP, leading a consortium of 11 (at that time) institutes in Europe, answered this call by proposing 4MOST. The main science drivers for this proposal, was to allow a complete exploitation of the data to be provided to the astronomical community by two spacecrafts:

– Gaia
– E-rosita.

The proposal was made with an unchosen location at that time, and the concept could be installed on both the NTT and VISTA. ESO then chose in may 2012 that the telescope of choice for such an instrument would be VISTA located at the Paranal Observatory. The Conceptual Design Phase was completed in May 2013, with the official selection by ESO, alongside the other project selected during this call for LoI: MOONS, which will be installed on the VLT. The official starting date as an ESO project is January 2015, with an installation planned on VISTA in 2019.

É. Depagne (✉)
Leibniz-Inisitut für Astrophysik Potsdam, Potsdam, Germany
e-mail: edepagne@aip.de

A. Miglio et al. (eds.), *Asteroseismology of Stellar Populations in the Milky Way*,
Astrophysics and Space Science Proceedings 39,
DOI 10.1007/978-3-319-10993-0_17

2 Science Drivers

The call for LoI made it explicit that the facility should allow ESO's astronomers to open up new areas in research that would be left unexplored otherwise. But let the proposer choose any other science goal they wish.

This lead the 4MOST consortium to define 6 Design Reference Surveys (DRS) that will be the main scientific drivers for the design of the facility, with the clear understanding that the decision they implied should not , as much as possible, hinder the possibility of other science to be done. The 6 DRS are:

- Milky Way Stellar Halo (High and Low Resolution)
- Milky Way Bulge and Disk (High and Low Resolution)
- Cluster of Galaxies (Low Resolution)
- AGN (Low Resolution)

The main constraint for these DRS, is that they have to be finished within 5 years. Finished, for the DRS has a special meaning. For each DRS, we have defined a Figure of Merit (FoM) that allows to measure the progress over time of the observations. For each DRS, we required that the FoM be 1 at the end of the 5 years. al

2.1 Milky Way

There are of course many questions that 4MOST will allow to tackle, and it is not possible to list them all (since we know some will come up with ideas to use the data in ways we did not foresee), but here is a list of what we already plan to do:

- Determine the MW 3D potential from streams to $\sim$100 kpc
- Measure the effects of baryons
- Map out the mass spectrum of Dark Matter halo, substructure by the kinematic effects on cold streams of 10^3–$10^5 M_\odot$
- Identify moving groups in velocity distribution up to 10 kpc (Hipparcos did it only up to 200 pc). 4MOST will allow to go half-way through the Galaxy.
- Derive abundances on an unparalleled scale. The High Resolution channel will allow a determination down to a precision of 0.1–0.2 dex (Caffau et al. 2013) for all the major nucleosynthesis channels:
  - Light elements
  - α elements
  - Iron-peak elements
  - r-Process elements
  - Heavy and light s-process elements
  - Odd Z elements (such as Na, Al)

– Observe 10^5 halo stars, leading to the most accurate determination of the Metallicity Distribution Function, allowing the identification of chemo-dynamical substructure (such as streams of tidally disrupted dwarves galaxies) and most importantly, understanding for those substructure, if the formation is done in-situ of mostly by accretion.
– Observe 1.5×10^5 bulge giants, allowing to understanding the effects of reddening and the existence of substructure (with a very good overlap with what MOONS will be doing at the VLT), disentangle the bulge formation scenarios: Collapse or merging of proto-galaxies.

2.2 AGN and Galaxies Clusters

3 Data Policy

The raw data gathered by 4MOST during its lifetime (which is currently expected to be around 10 years) will be made immediately public. The calibrations will also be made public, so that anyone interested in reducing and using the data will have the opportunity to do so. But the 4MOST consortium will develop in-house a data reduction pipeline, that will produce not only calibrated spectra, but also an analysis of those spectra, to produce a catalog that will contain, for each object, the stellar parameters, but also a chemical analysis.

4 Concept Design

4MOST is an instrument that will be installed on VISTA. It will be available for observations 100 % of the time (which is a major difference with instrument of the same kind to be installed at other observatories).

The main characteristics of the instruments are as follows:

– Large Field of View. The current design allows for a FoV of 2.5° in diameter, providing an area of 4.06 deg^2 on sky. The design of the correcting optics (that includes an Atmospheric Dispersion Corrector) allows for the whole field of view to be seeing limited.
– Fibre Positioner. The current design of this critical part of the system, is for an Echidna-style positioner. An Echidna-style positioner (named AESOP) allows a quick set-up of the fibres on the focal plane, opening the possibility to reconfigure the spines on a short timescale (basically, it can be done every 20 mn). It allows an efficient coverage of the FoV, and a high density of fibres. The fibre pitch (describing how far from the center of a spine, the next spine center is located) is as small as 10 mm, with a patrol radius (indicating how far from its center a spine can move), is 12 mm. The accuracy of the positioning of each spine is

Table 1 Details of each spectroscopic channel

	High resolution	Low resolution
Number of fibers	800	1,600
Resolution	> 20,000	> 5,000
Wavelength coverage	390–457 595–950	390–950 nm

very good and allows for 99 % of the spines to be located within 0.1″ of their requested position. The current design allows 2,400 fibres to be positioned on the focal surface.
– Spectrographs. 4MOST will observe simultaneously in its two spectroscopic channels a High-Resolution and a Low-Resolution. The details of each channel can be found in Table 1

4.1 Expected Performances

5 4MOST Facility Simulator (4FS)

5.1 Description

The 4MOST Facility Simulator is a set of tools that we use in the project to ensure the science goals will be reachable. It has been designed to be very versatile, allowing us to check the impact of design changes, but also observing strategy changes. Thus, it has become a crucial tool for the evolution of the project. For an ease of use, and to ensure a very good efficiency of the simulator, it has been designed as a modular tool, comprised of the following three main parts:

– a throughput simulator (TPS)
– a data quality control tool (DQCT)
– and an operation simulator tool (OpSim).

The input for the 4FS consists in the catalogs that have been prepared for each DRS. These catalogs contain a list of objects, and among other information, their coordinates, their magnitudes their type and the requested observing time to consider the observation a success. Along these catalogs comes a series of spectral templates that will be used to produce a simulated observation with 4MOST.

5.2 Workflow

The 4FS Workflow has been devised in order to maximise the efficiency of the simulations. We describe it briefly in the coming section (see Figs. 1 and 2).

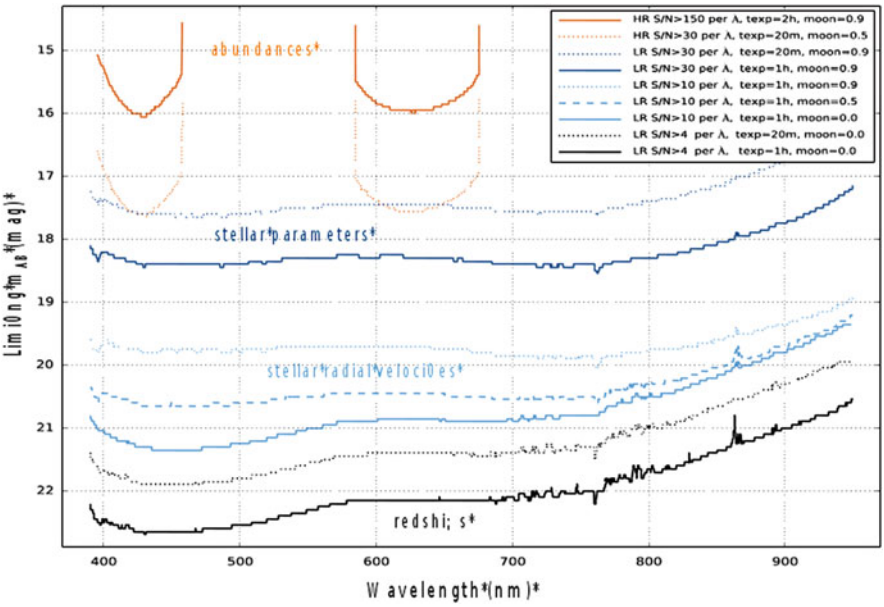

Fig. 1 This figure shows the magnitude as a function of wavelength, that can be reached for various scenarios, by 4MOST. This plot shows how efficient this facility will be, and how versatile it will be, allowing to tackles key astrophysical problems both in Galactic and Extra-galactic Astrophysics

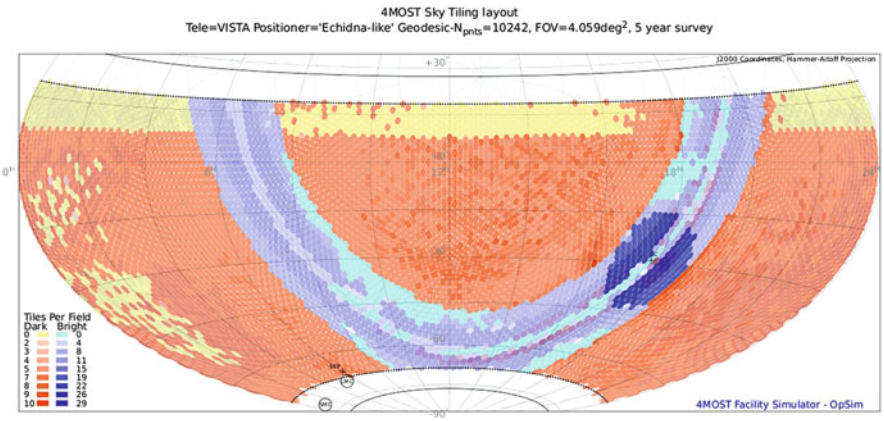

Fig. 2 This figure shows the observed sky during the first 5 years of the survey. The *color code* indicates how frequently each tile has been observed. The whole sky is covered at least once, but there are important parts of the sky, such as the South Galactic Pole, which are seriously underobserved. This will be fixed with a more sophisticated Observing Strategy, but the RA pressure on this region is significant (Color figure online)

– TPS:
  - The first step is to fold a noise-free template spectrum with a simulated instrument response, in order to obtain a noisy "observed" spectrum. This is done for a variety of exposure times: from 10 to 240 mn.
  - Then a simulated sky background, corresponding to the three observing period we have defined: bright-, grey- and dark-time is added.
  - This procedure is repeated in 1 magnitudes step, to cover the whole magnitude range of the expected observed targets. This leads to approximatively 4,000 templates to analyse.
– DQCT:
  - Once the simulated spectra have been produced, the Signal to Noise ratio for each exposure is computed.
  - According to this S/N evaluation, the exposure time for each template is computed, and this parameter is included in the Operations Simulator.
– OpSim
  - With the updated list of targets, a new list of targets to be observed is produced, and a new field configuration is generated. The process is repeated until the first 5 years of operations are over.

5.3 Survey Strategy

We have defined various possibilities for the 4MOST facility, with different number of fibres, spectrographs, etc. We have defined what we call a "Baseline" facility, which is defined as follows (the Moon phases and the predominant Northern Winds are taken into account):

– AESOP Fibre positioner, 1,624 LR + 812 HR fibres, 4.06 $\deg^2$ FoV (hex), 5 % overlap between tiles, 100 (LR) + 50 (HR) sky fibres reserved
– Exposure times: everywhere 6 × 20 min, more repeats on Bulge and fewer (3 × 20 min) in selected areas on-Disk
– Thousand eight hundred and twenty seven nights, with 5 (sched.) + 6 (unsched.) nights of technical downtime p.a., and 20

6 Observed Targets and Fiber Efficiency

The number of targets that will be observed by 4MOST during the first 5 years of operations is round 35 millions, all DRS included. The computation of the observed target is made using the Baseline, defined previously, setting for 4MOST. Table 2

Table 2 This table summarizes the simulation for 5 years of operations of 4MOST

DRS	Observed targets	Successful targets	Success rate
Halo LR	1, 746, 500	150, 100	0.86
Halo HR	113, 800	70, 500	0.62
Disk LR	10, 996, 800	10, 689, 300	0.97
Disk LR	2, 508, 300	2, 508, 300	0.82
Galaxy clusters	72, 300	55, 300	0.76
Cluster galaxies	1, 563, 400	1, 403, 700	0.90
AGN	763, 700	669, 800	0.88
BAO	15, 804, 100	12, 801, 000	0.81
All	33, 496, 600	29, 096, 300	0.87

It is important to note that, for instance, in 10 years, SDSS has collected 2.4 million spectra, and our estimates are made on very conservative throughput estimates

Table 3 This table summarizes the efficiency of each spectroscopic channel of 4MOST

Channel	Allocated fiber	Unallocated fiber
High resolution	2, 969, 100	6, 430, 600
Low resolution	15, 338, 000	3, 465, 500

gives the number of targets for each individual DRS while Table 3 summarizes the predicted efficiency of 4MOST.

Conclusion

4MOST is a very powerful spectroscopic facility, that will be installed on VISTA in 2019. It will allow the astronomical community to have access to a unique instrument, that will be able to deliver cutting edge data both in the Galactic and the extra-Galactic field. It is currently in a Conceptual Design Phase, and will enter the Preliminary Design Phase early 2015.

Currently, 7 Design Reference Surveys have been identified, that have helped shape the design of the instrument. But there is a lot of room for other Surveys, be they large or small, in order to maximize the scientific output of the facility. As a survey facility, all data obtained at the telescope will be made public immediately.

The 4FS, a very powerful and truly unique tool, allows for the exploration of various observing strategies, to optimize the coverage of the sky, but also allows to test various technical solutions, such as the effect of modifying the number of fibers. As such, it is a virtual 4MOST Instrument, and it is planned to transform it into what will the ETC be.

Reference

Caffau, E., Koch, A., Sbordone, L., et al. 2013, Astronomische Nachrichten, 334, 197

Mapping the Stellar Populations of the Milky Way with Gaia

Carla Cacciari

Abstract Gaia will be ESA's milestone astrometric mission, and is due for launch at the end of 2013. Gaia will repeatedly map the whole sky measuring about one billion sources to V = 20–22 mag. Its data products will be μ as accuracy astrometry, optical spectrophotometry and medium resolution spectroscopy. A description of the Gaia space mission and its characteristics and performance is given. The expected impact on Galactic stellar population studies is discussed, with particular attention to the sources of interest for CoRoT and *Kepler*.

1 Gaia

Gaia is a major ESA mission with astrometric, photometric and spectroscopic capabilities. It is currently scheduled for launch in December 2013 from Kourou, to be placed at the Lagrangian point L2, 1.5 million km from the Earth in the direction opposite the Sun, for a planned lifetime of 5 years.[1]

Gaia represents the natural continuation and a huge improvement with respect to the Hipparcos mission: it will extend the V magnitude limit from 12 to about 20–22 (for blue and red objects respectively), observe a factor 10^4 more sources (including objects such as galaxies and quasars unobservable by Hipparcos), reach a factor ∼100 better astrometric accuracy, and provide spectrophotometric information for all of the observed objects, as well as spectroscopy for a large fraction of them.

These characteristics are summarized in Table 1, and are described in some more detail in the following.

[1]For a detailed description of the satellite and system, payload and telescope, functioning and operations see http://www.cosmos.esa.int/web/gaia/mission-overview

C. Cacciari (✉)
INAF—Osservatorio Astronomico, Via Ranzani 1, Bologna, Italy
e-mail: carla.cacciari@oabo.inaf.it

A. Miglio et al. (eds.), *Asteroseismology of Stellar Populations in the Milky Way*,
Astrophysics and Space Science Proceedings 39,
DOI 10.1007/978-3-319-10993-0_18

Table 1 From Hipparcos to Gaia

	Hipparcos[a]	Gaia[b]
Magnitude limit	$V_{lim} = 12$	V_{lim} =20–22 (blue–red sources, respectively)
Number of objects	1.2×10^5	$\geq10^9$ (2.5×10^7 to V = 15, 2.5×10^8 to V=18)
Quasars	None	$\sim5\times10^5$
Galaxies	None	$\sim 10^6$–10^7
Astrometric accuracy	∼1 mas	∼7–10 μas at V≤12 10–25 μas at V=15, 100–300 μas at V=20
Broad-band phot.	2 (B,V)	3 (to V_{lim}) + 1 (to V=17)
Spectrophotometry	None	2 bands (B/R) to V_{lim}
Spectroscopy (CaT)	None	1–15 km/s to V=16–17
Obs. programme	Pre-selected targets	All-sky complete and unbiased

[a]Final catalogue: Perryman (1997); New reduction of the raw data: van Leeuwen (2007)
[b]Expected final catalogue: 2020–22

1.1 Satellite, Payload, Instruments

The satellite spins around its axis, which is oriented 45° away from the Sun, with a period of 6 h, and the spin axis has a precession motion around the solar direction with a period of 63 days. The combination of these two motions results in the scanning law that allows the entire sky to be observed on average 70 times over the 5 year mission lifetime (see the transit map in Fig. 1).

The payload is a toroidal structure holding two primary 1.45×0.50 m rectangular mirrors (field of view FoV = 1.7° × 0.6°) whose lines of sight are separated by an angle of 106.5° (Basic Angle, BA). The BA needs to be known with extremely high precision to ensure Gaia's expected astrometric accuracy, and therefore a BA monitoring system is hosted on the payload, as well as all the optical components which allow to superpose the FoVs of the two mirrors and combine them on the focal plane.

The focal plane contains several arrays of 4.5×2.0 K CCDs:

i) the sky mapper (SM), 2 × 7 CCDs for detection and confirmation of source transit;
ii) the astrometric field (AF), 9 × 7 CCDs corresponding to 40 × 40 arcmin, for astrometric measurements and white light (G-band, 330–1,050 nm) photometry;
iii) the blue (BP) and red (RP) photometers, 2×7 CCDs for low resolution (R<100) slitless prism spectro-photometry in the ranges 330–680 nm and 640–1,050 nm, respectively. From the spectra the G_{BP} and G_{RP} integrated magnitudes are derived.
iv) the radial velocity spectrometer (RVS), 3 × 4 CCDs for slitless spectroscopy at the Ca II triplet (847–870 nm) with R∼11,000.

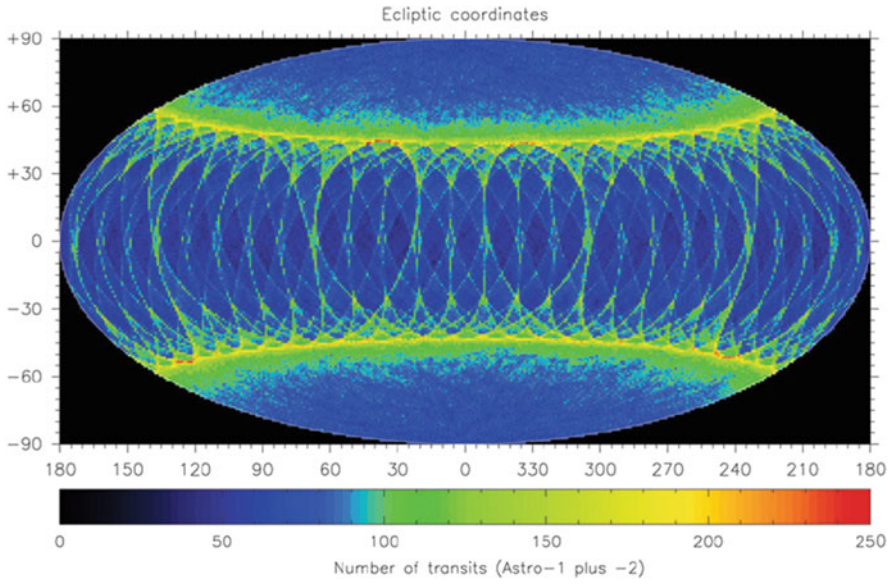

Fig. 1 Dependence of the end-of-mission number of focal plane transits on position on the sky. Shown is an all-sky equal-area Hammer projection in ecliptic coordinates. The maximum number of transits will occur in a $\sim 10^{\circ}$ wide strip around ecliptic latitudes $+/-45^{\circ}$

Measurements are made in time-delayed-integration mode, reading the CCD at the same speed as the source trails across the focal plane, i.e. 60 arcsec/s, corresponding to a crossing/reading time of 4.4 s per CCD.

1.2 Astrometry: Measuring Principles

The mission is designed to perform global (wide field) astrometry as opposed to local (narrow field) astrometry. In local astrometry, the star positions can only be measured with respect to neighbouring stars in the same field. Even with a very accurate instrument the propagation of errors is prohibitive when making a sky survey. The principle of global astrometry is to link stars with large angular distances in a network where each star is connected to a large number of other stars in every direction.

Global astrometry requires the simultaneous observation of two fields of view in which the star positions are measured and compared. This is provided by the two lines of sight of the primary mirrors. Then, like with Hipparcos, the two images are combined, slightly spaced, on a unique focal plane assembly. Objects are matched in successive scans, attitude and calibration parameters are updated, and object positions are solved and fed back into the system. This procedure is iterated as more scans are added. In this way the system is self-calibrating by the use of isolated non

variable point sources, which will form a sufficiently large body of reference objects for most calibration purposes, including the optical definition of the International Celestial Reference System (ICRS) by observing about half a million QSOs.

Therefore Gaia's astrometry will be not only unprecedently accurate as far as internal rms errors are concerned, because derived from an all-sky solution, but also unprecedently precise in *absolute* values, because obtained with *direct reference to the ICRS*.

1.3 Expected Performance

1.3.1 Astrometry

Astrometric errors are dominated by photon statistics. Sources at V∼6 mag represent the bright magnitude limit for Gaia observations, as saturation sets in at that level. The predicted sky-averaged end-of-mission standard errors on the parallax are summarized in Table 2.[2] We note that the standard errors on position and proper motion are about 0.74 and 0.53 of those on parallax, respectively.

1.3.2 Photometry

Gaia's photometric data include the integrated white light (G-band) from the AF, and the BP/RP prism spectra from which the G_{BP} and G_{RP} integrated magnitudes are derived. The expected end-of-mission errors are shown in Table 2.

Table 2 End-of-mission expected standard errors of astrometric, photometric and spectroscopic data as a function of Johnson V magnitude for three unreddened reference spectral types

V (mag)	σ_π (μas)			σ_{phot} (mmag)			σ_{RV} (km/s)		
	B1V	G2V	M6V	B1V	G2V	M6V	A0V	G5V	K4V
6–12	7	7	7	1–4–4	1–4–4	1–4–4	1−2	1	1
13	11	10.5	7.5	1–4–4	1–4–4	1–4–4	3	1	1
15	27	26	10	1–4–5	1–4–4	1–6–4	16	3	2
16	41	41	15	1–4–5	1–5–5	1–9–4		7–8	4
17	70	66	23	2–5–7	2–5–5	2–20–5		20	10
18	110	107	40	2–7–14	2–9–8	2–49–5			
20	340	333	100	3–29–83	3–43–43	3–301–17			

Left: sky-averaged parallax errors (in units of μas) for B1V, G2V, and M6V. *Middle*: photometric errors in the $G–G_{BP}-G_{RP}$ bands, in units of milli-magnitude, for B1V, G2V, and M6V. *Right*: radial velocity errors (in units of km/s) for A0V, G5V and K4V

[2]July 2014 updated estimates can be found at http://www.cosmos.esa.int/web/gaia/science-performance

From the BP/RP spectral energy distributions it will be possible to estimate astrophysical parameters using pattern recognition techniques (Bailer-Jones 2010). For example, one may expect to obtain: (i) T_{eff} to $\leq$5 % (15 %) for a wide range of spectral types brighter (fainter) than V=16; (ii) log$g$ to 0.2–0.3 dex (0.2–0.5 dex) for hot (SpT$\leq$A) stars brighter (fainter) than V=16; (iii) $[Fe/H]$ to $\sim$0.2–0.4 dex (0.5–0.7 dex) down to [Fe/H]= -2.0 for cool stars (SpT>F) brighter (fainter) than V=16; (iv) A_V to $\sim$0.05–0.2 mag (0.05–0.3 mag) for hot stars brighter (fainter) than V=16.

Ranges in errors reflect the influence of spectral type and metallicity. It is also to be noted that at V=15 the degeneracy between T_{eff} and A_V amounts to about 3–4 % and 0.1–0.2 mag respectively.

1.3.3 Spectroscopy

The RVS provides the third component of the space velocity for red (blue) sources down to about magnitude 17 (16). Radial velocities are the main product of the RVS, with typical end-of-mission errors as shown in Table 2. For sources brighter than $\sim$14 mag the RVS spectra will provide information also on rotation and chemistry, and combined with the prism BP/RP spectra will allow us to obtain more detailed and accurate astrophysical parameters.

2 Science with Gaia

"The primary objective of Gaia is the Galaxy: to observe the physical characteristics, kinematics and distribution of stars over a large fraction of its volume, with the goal of achieving a full understanding of the MW dynamics and structure, and consequently its formation and history." (Concept and Technology Study Report, ESA-SCI-2000-4).

Gaia will provide a complete census of all Galactic stellar populations down to 20th magnitude. Based on the Besançon Galaxy model (Robin et al. 2003; Robin et al. 2004) Gaia is expected to measure more than 10^9 stars belonging to the thin and thick disk, the bulge and the spheroid. Binaries, variable stars and rare (i.e. fast-evolving) stellar types will be well sampled, as well as special objects such as Solar System bodies ($\sim 10^5$), extra-solar planets ($\sim 2 \times 10^4$), WDs ($\sim 2 \times 10^5$), BDs ($\sim 5 \times 10^4$).

One billion stars in 5-D (6-D if the radial velocity is available, and up to 9-D if the astrophysical parameters are know as well) will allow us to derive the spatial and dynamical structure of the Milky Way, its formation and chemical history (e.g. by detecting evidence of accretion/merging events), and the star formation history throughout the Galaxy. The huge and accurate database will provide a powerful testbench for stellar structure and evolution models. The superb astrometric and photometric accuracy will allow us to obtain proper-motion-cleaned Hertzprung–

Russell diagrams throughout the Galaxy, and hence complete characterization and dating of all spectral types and Galactic stellar populations. The dark matter distribution will be mapped by the distribution and rate of microlensing events. The cosmic distance scale will be accurately defined on a reliable ground thanks to the distance (i.e. luminosity) calibration of the primary standard candles, RR Lyraes and Cepheids.

2.1 MW Stellar Population Studies with Gaia: A Few Examples

2.1.1 The Bulge: $\sim 1.7 \times 10^8$ Stars

Our knowledge of the Galactic bulge has greatly improved in the last decade(s), and presently the structure of the bar is constrained from modelling of gas dynamics, stellar surface brightness and stellar dynamics. However many questions remain open, for example (just to quote a few) on the formation mechanism (single enrichment event or merging from chemically distinct subcomponents?), on the chemical evolution timescale (less than 1 Gyr or more extended?), on the presence of chemodynamical subpopulations, on the relation with other Galactic populations, especially the inner disk (see Rich (2013) for a review).

Gaia will make a major contribution to the solution of these problems by measuring accurate distances and proper motions of several millions of stars, as well as a huge number of radial velocities (to V=17 mag), especially in bulge fields at $b < -6^\circ$ where the X-shaped structure is important. The northern bulge will also be observable, because red clump stars can be reached by Gaia even with ∼3–4 mag extinction. Simulations show that, at the reference distance of 8 kpc, a typical tracer such as a red clump star (M0III, $M_V = -1$ mag) dimmed by 4 mag extinction would have V=17.5. Gaia will measure its parallax with an rms error of ∼50 μas and proper motion to ∼1 km/s, as well as the radial velocity to ≤15 km/s, and obtain useful information on its astrophysical parameters (and hence age and chemical properties). Complementary high-dispersion spectroscopy, e.g. by the Gaia-ESO Survey (GES), HERMES and 4MOST, will provide more detailed information on chemistry and kinematics.

2.1.2 The Disk(s): $\geq 10^9$ Stars

In recent years several photometry and spectroscopy surveys have greatly increased the number of stars with good distances, radial and transverse velocities, and abundance estimates. However, an enormous amount of practical and conceptual work needs to be done to answer the many questions still open in this field (see Rix & Bovy (2013) for a review).

Based on current simulations, the effective volume that Gaia will explore will be limited to only a quadrant of the Galactic disk, because of dust extinction and image

crowding. Assuming as a typical tracer a K3III star ($M_V = 0$ mag) dimmed by 2 mag extinction, the disk can be mapped as far as 10 kpc with individual distance errors $\leq$50 μas, proper motion errors $\leq$1.5 km/s, radial velocity errors $\leq$10 km/s, and with additional information on astrophysical parameters and ages. The huge number and high accuracy of these data will provide a major breakthrough in the understanding of the many aspects related to the disk formation, structure and evolution (see K. Freeman's contribution, this meeting).

2.1.3 The Halo: $\sim 2 \times 10^7$ Stars

Typical tracers of the field halo population, which have been used in several studies, are red giants (K3III, $M_V = -1$), HB stars (A5III, $M_V = +0.5$), and MS-TO stars (G2V, $M_V = +4.5$). With the former two stellar types Gaia will map the inner halo as far as 10 kpc with proper motion errors $\leq 1\,\mathrm{km\,s^{-1}}$, and the outer halo as far as 30 kpc with proper motion errors of $\sim$3–7 $\mathrm{km\,s^{-1}}$, respectively. The much fainter (but more numerous) MS-TO stars can be used to map the inner halo as far as 4 kpc with proper motion errors $\leq 1\,\mathrm{km\,s^{-1}}$ (as far as 10 kpc to 6–7 $\mathrm{km\,s^{-1}}$). By these in situ measurements it will be possible to settle questions such as the inner/outer halo dichotomy, their origins and mechanisms of formation (if different) and hence the merger history of the Galaxy, and derive the gravitational potential of the Milky Way's dark matter halo. The synergy with LSST will be especially fruitful to extend these results at fainter magnitudes (see Ivezić et al. (2012) for a review).

2.2 CoRoT and Kepler Targets

The study of the dynamical and chemical evolution of stellar populations in the Galaxy requires accurate data on kinematics (velocities), chemical properties (abundances) and ages (distances, astrophysical parameters) for a significant fraction of MW stars. Gaia, in synergy with the large ongoing or forthcoming photometric and spectroscopic surveys, will provide enormous amounts of such data in the next decade. Accurate ages for individual field stars, however, are quite difficult to acquire, and asteroseismology can make a fundamental contribution by estimating ages, e.g. for individual red giants. These stars are bright and allow us to probe the evolution of populations across the whole Galaxy as far as its more distant parts.

During their searching campaigns for exoplanets around late type (mostly F–M) dwarf stars, CoRoT and *Kepler* found thousands of red giants with solar-like oscillations, which could be analyzed with asteroseismology techniques to derive their physical parameters, distances and ages. As an example, we consider the work by Miglio et al. (2013) who analyzed about 2,000 red giants with solar-like oscillations in two exofields of the CoRoT survey extending about 8–10 kpc each, on opposite directions with respect to the Sun. The stars are selected to be brighter than R=16. For our simulations of Gaia observations we have assumed as templates

Table 3 CoRoT red stars with solar-like oscillations: expected end-of-mission errors on parallax, transverse velocity (from proper motions) and radial velocity (from the RVS) from Gaia measures, at the magnitude limit R_{lim} =16 assuming zero reddening

Sp. type	V–R (mag)	V (mag)	M_V (mag)	Dist–Par (kpc)–(μas)	σ_π (μas)	p.m. σ_{TV} (km/s)	RVS σ_{RV} (km/s)
G8III	0.50	16.50	+0.6	15–66	40	1.5	11
K3III	0.64	16.60	+0.1	20–50	40	2.0	5
M0III	0.88	16.90	−0.4	29–35	39	2.9	7
F6V	0.29	16.30	+3.5	3.6–275	39	0.3–0.4	15
G2V	0.37	16.40	+4.8	2.1–480	39	0.2	12

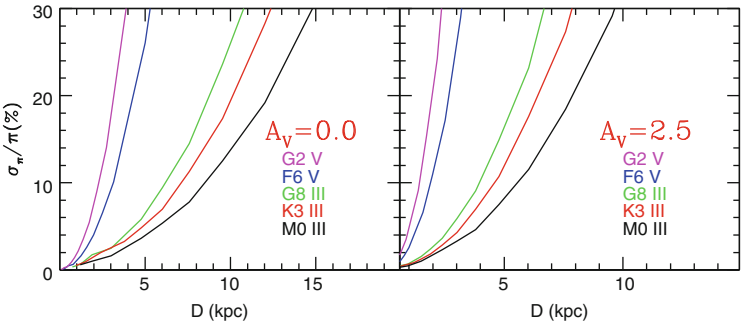

Fig. 2 The *lines* show Gaia's expected accuracy on parallax measures as a function of distance, for the same spectral types listed in Table 3

the spectral types G8III, K3III and M0III. For the sake of completeness, we have performed simulations also for two template red dwarfs, i.e. F6V and G2V, which are targets of the CoRoT and *Kepler* surveys as well.

The characteristics of these stars, and the expected astrometric and kinematic performance of Gaia at the adopted R_{lim} =16 are summarized in Table 3.[3] The Gaia photometric errors at these levels of magnitude are a few mmag (see Table 2). As mentioned in Sect. 1.3, for stars brighter than ∼16 mag the spectrophotometric data are expected to give good information on stellar astrophysical parameters such as temperature, gravity, metallicity and reddening; somewhat less accurate, but still useful estimates of these parameters can be obtained down to ∼18 mag.

To complement the information given in Table 3, we plot in Fig. 2 the detailed behaviour of the expected astrometric accuracy (i.e. percent error on parallax) as a function of distance, which shows the range of distances that can be reached by the various spectral types to ≤30 %, for two values of reddening.

The results of these simulations indicate that there is an area of overlap where the combined use of Gaia's data and asteroseismology techniques can be very fruitful.

[3] Astrometric simulations are based on de Bruijne (2009).

On the one hand, Gaia will provide a complete census and very accurate multi-fold information for the nearest and brightest stars accessible to asteroseismology, and hence facilitate the selection of targets and initial input parameters. On the other hand, the cross-verification of Gaia's results by the very detailed and independent asteroseismology techniques, even if applicable only to a small subsample of stars, will help understand in finer detail Gaia's results and calibrate them on physical grounds. Possible discrepancies, if any, only promise to open the path to deeper understanding.

Acknowledgements The support by the INAF (Istituto Nazionale di Astrofisica) and the ASI (Agenzia Spaziale Italiana) under contracts I/037/08/0 and I/058/10/0 dedicated to the Gaia mission is gratefully acknowledged.

References

Bailer-Jones, C. 2010, MNRAS, 403, 96
de Bruijne, J. 2009, GAIA-CA-TN-ESA-JDB-055 (Gaia Livelink Internal Report)
Ivezić, Z., Beers, T., & Jurić, M. 2012, ARA&A, 50, 251
Miglio, A., Chiappini, C., Morel, T., et al. 2013, MNRAS, 429, 423
Perryman, M. 1997, ESA-SP, 402
Rich, R. 2013, in *Planets, Stars and Stellar Systems: Galactic Structure and Stellar Populations* eds. T.D. Oswalt, G. Gilmore, Springer, 5
Rix, H. & Bovy, J. 2013, arXiv:1301.3168
Robin, A. C., Reylé, C., Derrière, S., & Picaud, S. 2003, A&A, 409, 523
Robin, A. C., Reylé, C., Derrière, S., & Picaud, S. 2004, A&A, 416, 157
van Leeuwen, F. 2007, Astrophysics and Space Science Library , Springer, 350

Part VI
Discussions

Uncertainties in Models of Stellar Structure and Evolution

Arlette Noels and Angela Bragaglia

Abstract Numerous physical aspects of stellar physics have been presented in Session 2 and the underlying uncertainties have been tentatively assessed. We try here to highlight some specific points raised after the talks and during the general discussion at the end of the session and eventually at the end of the workshop. A table of model uncertainties is then drawn with the help of the participants in order to give the state of the art in stellar modeling uncertainties as of July 2013.

1 Introduction

After three opening talks on galactic astrophysics, age estimates and ensemble asteroseismology, Session 2 was devoted to uncertainties in stellar structure and evolution, constraints from asteroseismic analyses and tests of the determination of stellar properties in well-constrained systems. We have tried to put together the questions and answers raised after the talks and during the general discussion following the presentations of Session 2. We do not follow the order of the presentations but we rather have selected a number of physical subjects differently approached in several talks. In order to ease the lecture we have tentatively linked the different subjects through a thin Ariane thread, whenever possible, and we give the names of the speakers in an attempt to render the vividness of the discussions that took place in the beautiful Sesto environment.

A. Noels (✉)
Institut d'Astrophysique et de Géophysique, Liège University, Allée du 6 Août 17, B-4000 Liège, Belgium
e-mail: Arlette.Noels@ulg.ac.be

A. Bragaglia
INAF-Osservatorio Astronomico di Bologna, via Ranzani 1 40127 Bologna, Italy
e-mail: angela.bragaglia@oabo.inaf.it

A. Miglio et al. (eds.), *Asteroseismology of Stellar Populations in the Milky Way*, Astrophysics and Space Science Proceedings 39,
DOI 10.1007/978-3-319-10993-0_19

2 Galactic Astrophysics, Age Estimates and Ensemble Asteroseismology

In order to draw a realistic picture of our Galaxy and its evolution, we are desperately waiting for spectroscopic analyses of huge numbers of stars. The problem of metallicity is indeed crucial to all aspects of the evolution of stars and of the Galaxy. The helium abundance is also obviously an issue, as well as effective temperatures and gravities. Gaia will provide parallaxes and proper motions with unprecedented accuracy. Moreover our great hope is to have soon precise stellar ages derived from asteroseismic analyses of stellar populations but this first requires a good knowledge of the metallicity of these stars. This will in turn provide the long awaited for detailed $3D$, or directional, age-metallicity relation in our Galaxy, i.e. a relation taking into account the location of each analyzed object in the Galaxy (distance to the galactic center as well as galactic latitude and longitude). This is extensively discussed in Sessions 3 and 4, which report on ongoing spectroscopic surveys, namely Gaia-ESO Survey (GES), Apache Point Observatory Galactic Evolution Experiment (APOGEE) and Galactic Archaeology with Hermes Survey (GALAH). Ongoing and future large photometric surveys, such as Strömgren survey for Asteroseismology and Galactic Archaeology (SAGA), SkyMapper Southern Sky Survey and Large Synoptic Survey Telescope (LSST), will also offer an important contribution especially in term of target selection.

2.1 Age-Metallicity Relation

– *Arlette Noels*—An important issue in the talk presented by Gerry Gilmore was the rather large dispersion in metallicity at a given age in our Galaxy, coupled with only a very small spread in $[\alpha/Fe]$ at any given $[Fe/H]$.
– *Alessandro Bressan*—The spread in metallicity in the Galaxy may be due to a fast enrichment with small difference in ages with respect to billion years.
– *Gerry Gilmore*—The early enrichment of the local Galaxy up to near solar seems to have indeed been very fast. In the last $\sim$8 Gyr the mean value of $[Fe/H]$ has changed only by perhaps a factor of two. When we have reliable ages we will be able to quantify the discrepancy between the apparent factor of two scatter in $[Fe/H]$ at any time, and only a tiny range of $[\alpha/Fe]$ at any $[Fe/H]$.
– *Nicolas Grevesse*—The spread in the plots $[Fe/H]$ vs age comes from the uncertainties in the ages. But could it not be also very much due to the spread in the abundances themselves?

– *Gerry Gilmore*—Yes of course! These are preliminary results only. We are still working at making the error bars quantitative, including both random and systematic effects.
– *Jennifer Johnson*—Once Sagittarius blends into the halo of our Galaxy, should we think of the halo as being α-poor and metal-rich? The mass of Sagittarius compared to the mass of the halo is not overwhelming and not all Sagittarius stars are α-poor and metal-rich.
– *Gerry Gilmore*—We need to go beyond the concept of a *halo*. The "inner halo" is old, metal-poor and α-rich. The "outer halo" is young, metal-rich and α-poor. It needs another name.

2.2 Age Indicators

– *Arlette Noels*—In some cases, more than one age indicator can be used. Is there an agreement in the age determinations in such a case?
– *David Soderblom*—The agreement among different age indicators for a given star is generally good, qualitatively at least, n the sense that if a star looks young, or old, in one way, it looks young, or old, in other ways. But quantitative agreement is usually not as good.
– *Jennifer Johnson*—Chromospheric activity is used as an age estimator for solar type dwarfs, although revealing some important spread. Is mass a possible source for scatter in a plot of activity in binaries?
– *David Soderblom*—We do not know in detail how activity depends on fundamental stellar parameters such as mass and composition, so that could contribute to scatter. But, at the same time, if mass effects dominated the scatter in the $Ca\ II\ H\&K$ emission index R'_{HK} vs $(B-V)$ for binaries, I would expect the lines joining members of binaries to be slanted, but not to go every which way, like they do.

2.3 Asteroseismic Age Estimation and Ensemble Asteroseismology

– *Arlette Noels*—It was clear from Andrea Miglio's talk that asteroseismology can be a powerful tool to estimate stellar ages but since this is inherently model dependent, it urgently requires a careful testing of stellar models.
– *Jennifer Johson*—What causes the differences in age at the same luminosity for the different models and is there another parameter other than $\log L$ that could reduce the scatter?
– *Andrea Miglio*—The discrepancies in age shown in the comparisons are due both to differences in the choice of micro and macro physics in the codes and, to a lesser extent, to differences in the numerics. Additional observational constraints

will likely reduce the scatter. This is e.g. the case for age predictions of the $2M_{\odot}$ models: models computed with and without overshooting during the MS give significantly different ages, but when the period spacing of gravity modes is considered an additional constraint, then some of the models can be ruled out (see Josefina Montalbán's talk).
– *Ken Freeman*—For some purposes age ranking, i.e. differential ages estimation, is already very useful. However from Andrea's luminosity/age graphs, it seems that even the ranking can be uncertain.
– *Andrea Miglio*—Age ranking may indeed be uncertain, in particular when our limited understanding of say, transport of chemicals (diffusion, mixing near energy generating cores) has a different impact depending on the age and the mass of the star. A quantitative appraisal of the robustness of relative and absolute ages is one of the goals of the hares & hounds exercises we will conduct as one of the outcomes of this meeting.
– *Arlette Noels*—The discrepancy between synthesis population with TRILEGAL and the *Kepler* data could perhaps be due to differences in the selection criteria. Could such differences be also responsible for the dissimilarity in the mass distribution relative to the CoRoT C (galactic center direction) and AC (galactic anticenter direction) data?
– *Andrea Miglio*—We have applied to the synthetic populations selection criteria designed to reproduce the CoRoT target selection, hence we expect this effect to be largely accounted for. Since the criteria applied to select CoRoT targets are not the same in all the observed fields, understanding and correction of selection biases on a field-by-field basis will be a crucial step also for future analyses.

3 Uncertainties in Stellar Modeling, Asteroseismic Constraints and Tests of Stellar Properties in Well-Constrained Systems

To the question: Are the surface abundances the initial ones, the answer is definitely: No! Various physical phenomena are responsible for this, among which are extra-mixing, as a result of convective overshooting and/or rotation, semi-convection, thermohaline convection, dredge-ups and mass loss. Asteroseismology can help draw a profile of chemicals within the stars and thus constrain the efficiency of those processes but theoretical studies as well as hydrodynamical simulations are urgently needed to help creating a new generation of stellar models, which in turn, through population synthesis analyses, will enrich our understanding of the evolution of our Galaxy.

3.1 Overshooting

Stars never forget the amount of overshooting they had on the main sequence — A. Bressan

– *Arlette Noels*—The problem of overshooting during MS in low mass stars is quite different from its counterpart in massive stars. In the latter, the convective core mass continuously decreases during main sequence and overshooting bubbles penetrate layers which chemical composition is identical to that of the convective core material. Bubbles are then slowed down and thermalized until they reach the same density than the surrounding material and, at that point, do not move backwards. In low mass stars heavy enough to keep a convective core on the main sequence, on the contrary, convective cores grow in mass during part of core hydrogen burning while nuclear reactions still take place outside the convective core. Overshooting bubbles enter lighter material and are rapidly stopped by buoyancy forces. Even if they partly mix with the surrounding material they remain heavier and are forced backwards even after thermalization. This probably implies only a very small extent of overshooting in low mass stars. For even less massive stars, the convective core induced by the accumulation of ${}^3_2He$ rapidly disappears once the equilibrium value is reached. If some overshooting layers are added to the mixed region, the equilibrium value might never be reached and a convective core might be present during part of or all core hydrogen burning. This can change the turn-off morphology as well as the MS lifetime and may be incompatible with observations.
– *Alessandro Bressan*—Contrary to many years ago when I began together with Cesare Chiosi and Paolo Bertelli the first systematic investigation of the effects of non local overshoot in a very skeptic scientific environment, it is nowadays widely accepted that a more extended mixing beyond the formal unstable convective core is needed. Asteroseismology is putting firm constraints on the presence of this extended mixing.

3.1.1 Red Giants: Overshooting in MS Stars

– *Arlette Noels*—In addition to the ability of asteroseismology to probe the internal structure of stars, it is true that it is a powerful tool to assess the amount of overshooting, especially from the seismic analysis of low mass red giants. In particular, for red giants belonging to the secondary red clump, there is a well defined relation between the period spacing, ΔP, of g-dominated modes and the mass of the *He* core. Since the latter is affected by the amount of overshooting present during core H-burning, a direct constraint on the *MS extra-mixing* immediately follows. The asteroseismic determination of the total mass (from $\Delta\nu$ and ν_{max} and the scaling relations) together with the mass of the *He* core obtained from ΔP is indeed a direct clue to the amount of MS overshooting (Montalbán et al. 2013; Montalbán and Noels 2013). This is however dependent on the chemical composition and a precise determination of the metallicity is required before reaching firm conclusions.

Interestingly enough an attempt at determining the amount of overshooting during MS by this asteroseismic method was under way by Dennis Stello during this workshop. Quite soon after his talk and just before the general discussion, he was able to present his preliminary results.

– *Dennis Stello*—In order to derive the amount of overshooting during the MS from the mass of secondary clump stars identified from their observed period spacings, we have tested different degrees of extra-mixing by means of an exponential overshoot parametrized by f. Our chosen f value and their counterparts for the usual overshooting parameter α_{ov} were:

$$\begin{aligned} \mathrm{f} = 0.0 \quad &\rightarrow \quad \alpha_{ov} \sim 0.0 \\ \mathrm{f} = 0.008 \quad &\rightarrow \quad \alpha_{ov} \sim 0.1 \\ \mathrm{f} = 0.015 \quad &\rightarrow \quad \alpha_{ov} \sim 0.2. \end{aligned}$$

The best match with the observed mass of secondary clump stars in "public" RG sample, which is 2.2 $M_{\odot}$ from pure scaling relations (no corrections), is obtained with MESA models computed with $f = 0.008$. It is important that we either take care of any corrections in scaling or even better we model individual frequencies for these secondary red clump red giants, before we proclaim a lower than usual overshoot.

– *Josefina Montalbán*—This must be taken with caution since an extra-mixing during MS is not the only factor which can affect the mass at the secondary red clump. A decrease of Z and/or an increase of Y lead to a decrease of this mass. This is due to the higher luminosity on the ZAMS for a given mass, which "mimics" a more massive MS star. Such an exercise should only be done if the stellar metallicities of all the stars in the sample are known.

– *Jennifer Johnson*—With 2 % errors on T_{eff} (combining systematics and random) and 0.1 dex metallicity errors, what is the largest source of error? What about errors in the scaling relations?

– *Dennis Stello*—This depends on the location in the HR diagram and on the stellar quantity to be determined. The scaling relation for $\Delta\nu$ is known to be off by a few percentage depending on T_{eff}. For ν_{max}, the scaling relation is good to the level we have been able to test it but νmax is ill defined for some stars. It could also still hide or allow systematics that we, in the end, care about.

– *Jennifer Johnson*—What are the possibilities of forward modeling, i.e. of computing a large grid of RGB models with predicted frequency spectra and doing a comparison with the observed individual frequencies?

– *Dennis Stello*—This might be feasible for low luminosity RGB but near and above the bump, I would think it is less feasible. Calculation of one track takes hours up to days. Computation of all the frequencies along that track in small enough time steps of evolution takes days. To make a grid in M, Z, Y, α_{MLT}, α_{ov} that is dense enough requires thousands of tracks. It is obvious that some sort of interpolation and scaling will be needed.

– *Arlette Noels*—As was shown in the seismic analysis of the Sun, the presence of a periodic component in the large frequency separation is a signature of a "glitch" in the stellar structure located at the basis of the convective envelope and/or the *HeII*

ionization zone (see for example Houdek and Gough 2007). This in turn can lead to an estimation of the superficial helium abundance. Do we already have an idea of the surface helium abundance in red giants from similar analyses of the red giant *Kepler* data?
– *Andrea Miglio*—While robust detections of the signature of *He* ionization will be possible with *Kepler* data, inferences on the *He* abundance are likely to be limited to distinguishing between helium rich and helium poor giants. Results of tests on artificial data will soon appear in Broomhall et al. (2014).
– *Victor Silva Aguirre*—Although important constraints will indeed come on the MS overshooting from clump stars, we should not forget using directly main sequence and sub-giant stars to calibrate MS overshooting, as we have much better understanding of seismic diagnosis in those phases than for post sub-giant branch evolution.
– *Josefina Montalbán*—I disagree with the fact that we better understand the seismic diagnostic for MS sequence or sub-giants than for red giants. As shown in talks in this meeting and references therein, simple predictions from models are able to explain observational results and interpret them in a consistent way, and that for a large number of red giants. So, in my opinion, period spacing together with the large separation $\Delta\nu$ and ν_{max} are powerful seismic diagnostics for understanding red giants as well as MS and sub-giant stars. Moreover the mass of the stars in the secondary clump is around 2 $M_{\odot}$, too massive to present solar like oscillations during MS. The stars for which solar like oscillations allow us to derive the extension of the extra-mixing region during MS have a mass around 1.3 $M_{\odot}$. Therefore, both approaches are complementary and could eventually allow us to answer the question about the dependence of overshooting on stellar mass.

3.1.2 MS Stars

– *Jennifer Johnson*—Victor Silva Aguirre presented an interesting result at KASC which showed that fits to individual frequencies quite frequently give solutions for MS stars that have very low Y. From Martin Asplund's talk (see also Asplund et al. 2009), the solar abundances Z could be decreased from 0.021 to 0.014. Would adjusting Z help give more reasonable values of Y?
– *Victor Silva Aguirre*—I think the biggest impact would be caused by the change in opacities required to reconcile the new solar abundances with results from helioseismology. At a given luminosity, an increase in the opacities would produce a decrease in mass that would need to be compensated by an increase in the helium abundance.
– *Arlette Noels*—It has been shown by Bonaca et al. (2012) that using the solar calibrated value of α_{MLT} in the analysis of a large sample of dwarfs and subgiants observed by *Kepler* very often led to Y values smaller than the primordial helium abundance. With α_{MLT} as a free parameter they obtained more reasonable Y values. Moreover they were able to show that α_{MLT} increases with the metallicity. On the other hand, if α_{MLT} depends on the stellar mass (see for example Ludwig and

Salaries 1999; Yıldız et al. 2006), how would this affect the seismic properties of stellar models?
– *Josefina Montalbán*—The dependence of α_{MLT} on the stellar mass, mainly for main sequence stars, such as δ Scuti and γ Doradus pulsators, can modify the location of the corresponding instability strips. For solar-like pulsators like red giants, the changes of α_{MLT} will modify the radius of the star, but not the global properties of pulsations. What really affects the frequency values for these pulsators is the different $dP/d\rho$ that $3D$ models predicts for their superadiabatic region. One of the main problems to use individual frequencies as seismic constraints is the description of this layer in $1D$ and time independent models of convection. $3D$-average models of the external regions would improve the computation of frequencies and reduce or bring some light about the so-called "surface effects".
– *Arlette Noels*—It is indeed important to have as many $3D$ model atmospheres as possible, first to map the *HR* diagram with *realistic* α_{MLT} values, to better understand the excitation of solar-like oscillations in MS and red giant pulsators, to obtain a more realistic temperature distribution in the superadiabatic region and last but not least to check the surface abundances obtained wit $1D$ model atmospheres
– *Alessandro Bressan*—Victor has used asterosesimology to estimate the amount of extra-mixing in low mass stars (Silva Aguirre et al. 2013). The star analyzed is just above the limit between stars that should possess a convective core, as predicted by current evolutionary stellar models, but it cannot be excluded that this is due to efficient shear mixing induced by differential rotation. It would be interesting to try to extend the same test to main sequence stars just below this limit. Of course in this case an extended mixing could be more difficult to assess because of the longer lifetime required to change the chemical composition.

3.1.3 *He*-Burning Stars

– *Arlette Noels*—The average value of the asymptotic period spacing of *He*-burning red giants is closely related to the mass of the convective core or more precisely to the mass of the mixed central layers. The comparison of theoretical values with the asymptotic period spacings derived from *Kepler* red clump stars seems to suggest an extra-mixing during core *He*-burning (Montalbán et al. 2013; Montalbán and Noels 2013).

It is however important to stress some problems related to the numerical determination of the convective core boundary in *He*-burning stars (see Gabriel et al. 2014). In such stars the convective core grows in mass during a rather large fraction of the core *He*-burning phase. This means that a μ-discontinuity builds in as time goes on.
– *Alessandro Bressan*—Local overshoot arising from a discontinuity in composition, first discussed by (Schwarzschild 1958, see p. 168) was already well studied in the 1970s (Castellani et al. 1971). During the central *He*-burning phase it arises because matter around the border of the convectively unstable region is dominated by free–free opacity, which grows at increasing $C - O$ abundance as the

discontinuity of chemical composition gets larger. Not all evolutionary codes take this instability into account, but it is worth recalling that a proper consideration of these effects increases the *He*-burning lifetime by a significant fraction, drastically affecting the ratio of core *He*-burning lifetime to the asymptotic phase duration.
– *Arlette Noels*—When the convective boundary is searched for through a change of sign of the $\nabla_{rad} - \nabla_a$, where ∇ stands for $dlnT/dlnP$ and *rad* and a, for radiative and adiabatic respectively, the presence of a μ-discontinuity in the interval where the change of sign seems to occur, prevents any correct determination of the boundary. The convective core mass is then too small and when the μ-discontinuity reaches a significant level, it is even impossible to allow any further increase in the convective core mass (see for example Fig. 15 in Paxton et al. 2013).

This problem was indeed already encountered and discussed by Castellani et al. (1971) who showed that an *induced* overshooting was required to correctly assess the location of the convective boundary. Instead of wrongly locating the boundary through a search for a change of sign in an interval including a μ-discontinuity, the correct procedure, consisting in extrapolating $\nabla_{rad} - \nabla_a$ from points *within the convective core only*, must be applied.

3.2 Rotation

– *Maurizio Salaris*—In your computation of a rotating 1 $M_\odot$ star, you used an initial velocity of 50 km/s. To which evolutionary phase does this initial velocity correspond? Is this value an extreme one or a typical one?
– *Patrick Eggenberger*—The initial velocity corresponds to the velocity on the ZAMS. This corresponds to a typical value for a solar-type star on the ZAMS, which is sensitive to the rotational history of the star during the PMS and in particular to the duration of the disc-locking phase. The surface velocity of a solar-type star model rapidly decreases during the MS evolution due to magnetic braking.
– *Nicolas Grevesse*—You showed that rotation counteracts atomic diffusion. So, what happens to diffusion in the Sun if you include rotation? What about the solar helium abundance?
– *Patrick Eggenberger*—Rotational mixing counteracts the effects of atomic diffusion and thus a rotating model of a solar-type star will exhibit a higher value of the surface helium abundance at a given age than a non-rotating model including only atomic diffusion. Consequently, a rotating solar model will be characterized by a higher surface abundance of helium at the solar age compared to a non-rotating one, which is not in good agreement with helioseismic determinations of the helium abundance in the solar convective zone. However, a moderate efficiency of rotational mixing can transport light elements to deeper and hotter stellar layers in order to predict surface abundances of lithium in better agreement with the solar values.
– *Arlette Noels*—What would be the outcome in population synthesis if models computed with rotation were used?

– *Patrick Eggenberger*—It is clear that the effects of rotation on the global and asteroseismic properties of low-mass stars will have an impact on the properties of a given stellar population. Starting from the discussion of the changes induced by rotation on the evolutionary track of a given stellar model, it is however not straightforward to deduce the effects on a whole stellar population without doing a detailed population synthesis computation. For instance, rotational mixing simultaneously changes the location of the star in the HR diagram and increases its main-sequence lifetime leading to isochrones that can be very similar to the ones of non-rotating models (see for example Girardi et al. 2011). Interestingly, the increase of the luminosity during the post-main sequence evolution of a rotating model leads to a decrease of the mass of a red giant at a given luminosity. Asteroseismic observations of red giants in clusters are thus particularly valuable to determine a precise mass for these stars and to investigate thereby the possible need and efficiency of rotational mixing. Moreover, rotational mixing can change the chemical composition at the stellar surface, which can be constrained by spectroscopic determination of surface abundances. All these photometric, asteroseismic and spectroscopic constraints must be simultaneously satisfied by stellar models and it will thus be particularly useful to develop population synthesis tools for rotating models to compare in more details the prediction of these models with the numerous observational constraints that are now available.
– *Arlette Noels*—If we need internal gravity waves or magnetic fields to flatten the rotation profile, do we still need to build models with rotation?
– *Patrick Eggenberger*—A flat rotation profile does not mean that there is no mixing. Rotational mixing is due to the shear instability and to the transport of chemicals by meridional circulation. The rotation profile of models including internal gravity waves or magnetic fields being flatter, there is a decrease of the efficiency of shear mixing and an increase of the transport of chemicals by meridional circulation. In the case of low-mass stars with a radiative core and a convective envelope, the strong decrease of the efficiency of shear mixing is not compensated by the limited increase of the transport of chemicals by meridional circulation resulting in a global decrease of the efficiency of rotational mixing (Eggenberger et al. 2010). For more massive models with a convective core, the situation is quite different. For these stars, the increase of the efficiency of the transport of chemicals by meridional circulation is larger than the decrease of the shear turbulent mixing resulting in a global increase of the efficiency of rotational mixing (Maeder and Meynet 2005).

3.3 Semi-convection

– *Arlette Noels*—Semi-convection in low mass stars occurs when the convective core mass increases during MS, i.e. when the $p - p$ chain nuclear reactions are still an important fraction of the total nuclear energy rate. This affects a rather narrow

mass range contained between $\sim 1.1\ M_{\odot}$ and $\sim 1.5\ M_{\odot}$. Because of this, a μ-discontinuity together with a μ-gradient discontinuity build up at the convective core border, which leads to a discontinuity in the opacity, larger outside the convective core. At the convective boundary, the condition $\nabla_{rad} = \nabla_a$ is necessarily fulfilled and the layers located just outside are then such than $\nabla_{rad} > \nabla_a$. However, due to the strong stabilizing effect of the μ-gradient, one still has $\nabla_{rad} < \nabla_{Ldx}$ where ∇_{Ldx} stands for the Ledoux temperature gradient containing the term in ∇_{μ}. These layers are definitely not convective and only a partial adjustment of the chemical composition is assumed to take place into what is called a semi-convective region.
– *Alessandro Bressan*—Regarding the criterion to be used for the neutrality against convective instability in the semi-convective region (Schwarzschild, $\nabla_{rad} = \nabla_a$, or Ledoux, $\nabla_{rad} = \nabla_{Ldx} = \nabla_a + \beta/(4-3\beta)(dln\mu/dlnP)$) it is instructive to read the discussion in Kato (1966). He finds that the Ledoux criterion is not stable against overstable convection, i.e. growing oscillatory convection because the medium is thermally dissipative. So the Schwarzschild condition should be applied even in presence of a gradient of molecular weight.
– *Arlette Noels*—According to Kato (1966), this results indeed in a chemical adjustment such that $\nabla_{rad} = \nabla_a$ in the semi-convective region, which means a neutrality towards the Schwarzschild criterion. It is important to recall that, on the other hand, for a radiative layer to become convectively unstable, the condition $\nabla_{rad} > \nabla_{Ldx}$ must imperatively be met.

Semi-convection in *He*-burning stars has a different origin. It occurs when the distribution of ∇_{rad} with increasing fractional mass starts showing a minimum in the convective core. It is thus impossible to fix the boundary, neither at the minimum itself since ∇_{rad} would be larger outside the convective core than inside, nor at a larger mass value than the mass at the discontinuity since some layers inside the core would be radiative (Castellani et al. 1971). Again the actual outcome of the so-called semi-convective mixing is not known.

3.4 Thermohaline Convection

– *Nadège Lagarde*—Thermohaline instability develops along the red giant branch (RGB) at the bump luminosity in low-mass stars and on the early-AGB in intermediate-mass stars, when the gradient of molecular weight becomes negative ($dln\mu/dlnP < 0$) in the external wing of the thin hydrogen-burning shell surrounding the degenerate stellar core (Charbonnel and Zahn 2007a,b; Siess 2009; Stancliffe et al. 2009; Charbonnel and Lagarde 2010). This inversion of molecular weight is created by the ${}^{3}_{2}He({}^{3}_{2}He, 2p){}^{4}_{2}He$ reaction (Ulrich 1971; Eggleton et al. 2006, 2008). In Charbonnel and Lagarde (2010), we showed that its efficiency increases with the decrease of the initial stellar mass. During this phase thermohaline mixing induces the changes of surface abundances of ${}^{3}He$, ${}^{7}Li$, C and N for stars brighter

than the bump luminosity. Our model predictions are compared to observational data for lithium, $^{12}C/^{13}C$, $[N/C]$, $[Na/Fe]$, $^{16}O/^{17}O$, and $^{16}O/^{18}O$ in Galactic open clusters and in field stars with well-defined evolutionary status, as well as in planetary nebulae. Thermohaline mixing simultaneously reproduces the observed behavior of $^{12}C/^{13}C$, $[N/C]$, and lithium in low-mass stars that are more luminous than the RGB bump. Moreover, ^{3}He is strongly depleted by thermohaline mixing on the RGB, although low-mass stars remain net ^{3}He producers. As a result, the contribution of low-mass stars to the Galactic evolution of ^{3}He is strongly reduced compared to the standard framework.

In Lagarde et al. (2012), we have included in the galactic chemical evolution code (see for example Chiappini et al. 2001), new stellar yields of ^{3}He as well as ^{4}He and D taking into account effects of thermohaline instability and rotation-induced mixing. We have compared these new prescriptions with their primordial values and abundances derived from observations of different galactic regions. The inclusion of thermohaline instability in stellar models provides a solution to the long standing "^{3}He problem" on Galactic scale. In addition, stellar models including rotation and thermohaline instability reproduce very well observations of D and ^{4}He in our Galaxy.

Although thermohaline instability cannot be characterized by asteroseismic parameters, it can be identified by its effects on spectroscopic studies, and must be included in theoretical models to better understand stellar evolution of low- and intermediate-mass stars.

3.5 Mass Loss

– *Alessandro Bressan*—Mass loss during the Red Giant Branch has been described by a universally known empirical relation (Reimers 1975)

$$\dot{M} = 4 \times 10^{-13} \frac{L}{gR} \quad \text{in solar units} \quad .$$

This relation has been subsequently calibrated on Globular Clusters through the famous multiplicative η parameter, with $\eta \sim 0.35$. This relation has more recently been revisited on a physical approach by Schröder and Cuntz (2005), always aiming at reproducing the blue part of the horizontal branch of GCs.

In the recent years it has become clear that the blue edge of GCs is not due to strong mass loss but to a high initial *He* content of some fraction of member stars (see for example D'Antona et al. 2002, 2005). In the meantime Miglio et al. (2012), from asteroseismology of the old metal rich open cluster NGC 6791 with Kepler, obtained a best smaller value $\eta \sim 0.2$. Recent claims by Origlia et al. (2007) on

impulsive stochastic mass loss along a large fraction of the RGB of 47 Tuc have not been confirmed. Instead McDonald et al. (2011) find that a significant mass loss rate is detected only in the most luminous stars of this cluster. It thus seems that there is no need for a high value for the η parameter in the Reimers relation.
– *Arlette Noels*—What is the explanation for such a large helium abundance in low metallicity stars in clusters?
– *Alessandro Bressan*—We need stars with strong second dredge-up (to produce the large *He* enrichment), slow stellar winds (to prevent material from being lost by the star cluster) and no metal production (to avoid metal enrichment which is not observed). The most appealing solution is thus a population of massive AGB stars.
– *Carla Cacciari*—In globular clusters the mass loss prior to the HB phase is indeed only mildly dependent on metallicity, and mostly on luminosity. The few GCs that are metal-rich and have a blue HB can be generally explained by a higher *He* abundance, but a higher mass loss is still needed to account for the bluest HB stars. The Reimers mass loss law was found and calibrated on PopI stars mostly of the AGB type, and may not be adequate for PopII RGs.
– *Leo Girardi*—Maurizio Salaris did not mention the presence of a significant population of extremely hot HB stars in NGC 6791. They have a very small envelope mass, hence have lost much more mass than expected from Reimers' law. And if you have those, you should also have a population of He white dwarfs, which completely missed the horizontal branch.
– *Karsten Brogaard*—The extreme horizontal branch (EHB) stars in the cluster NGC 6791 are very unlikely to arise from a dispersion in mass loss. This cluster has stars only on the EHB and in the RC with nothing in between (Brogaard et al. 2012). The EHB stars are much more likely to be formed by binary evolution. One out of three stars on the EHB, observed by Kepler, is a confirmed binary (Pablo et al. 2011).
– *Maurizio Salaris*—I completely agree that there must be a substantial population of He core white dwarfs. My worry is that you need a very fine-tuning of their initial–final mass relation to have (almost) all of these at the observed magnitude of the bright peak of the white dwarfs luminosity function.
– *Corinne Charbonnel*—Is the old open cluster NGC 6791 "very" massive? Does it show evidence of multiple populations, like in globular clusters?
– *Maurizio Salaris*—There is a recent paper by Geisler et al. (2012) that finds evidence of multiple populations also in this cluster: a "normal" homogeneous $Na - O$ population and a population with a spread that follows the $Na - O$ anticorrelation observed so far only in globular clusters.
– *Angela Bragaglia*—In NGC 6819 there seems to be some differences between distance and age from EB (eclipsing binary) and stellar models (Jeffries et al. 2013) at variance with NGC 6791. Is there some reason or am I remembering wrong?

– *Karsten Brogaard*—As I recall, the age and distance are consistent between both methods :

CMD alone $\rightarrow$ $(m - M)_V = 12.37 \pm 0.10$

Eclipsing binary $\rightarrow$ $(m - M)_V = 12.44 \pm 0.07$.

The small difference in ages between these two methods is mainly due to difference in the adopted distance modulus. For NGC6791 we (Brogaard et al. 2012) did not compare to, or derive, an age from the CMD alone.

4 A Table of Uncertainties in Global Stellar Properties and Theoretical Models Parameters as of July 2013

This table is an attempt at setting up a benchmark for the uncertainties on stellar models structure *as of July 2013*. This was carried out during the discussions at Sesto and in the following weeks, by e-mail exchanges. We heartily thank all those who participated to this project. This is probably a too optimistic *state of the art as of July 2013*. Thanks to ongoing exploitation of CoRoT and *Kepler* results, to a promised harvest of beautiful Gaia data and the outcome of the ongoing large spectroscopic surveys GES, APOGEE and GALAH, and thanks to theoretical progress in stellar model computations, we do hope that it will soon be obsolete and be replaced by a striking new version with much smaller error bars.

RG property	Uncertainty
R	$\sim$5 %[1]
M	$\sim$10 %[1]
$T_{\rm eff}$	20 K[2] and 70 − 80 K at $Z_{\odot}$[3]—much larger at low Z (Molenda-Żakowicz et al. 2013) Towards 1 % accuracy (Casagrande et al. 2014)
$\log g$	0.15–0.20 dex from spectroscopy, $<$ 0.1 dex when seismic constraints are available[3]
L	Depends on π_{Gaia} and BC (Bruntt et al. 2010)
Y	$Y_{\odot,Helio} = 0.2485 \pm 0.0034$ (envelope, see Basu and Antia 2004) – Spread towards larger Y (see Sect. 3.5)[4] – Spread towards smaller Y (see Sect. 3.1.2)
Z	$Z_{\text{“}new\text{”}\odot} = 0.014$ (Asplund et al. 2009) $Z_{\text{“}old\text{”}\odot} = 0.020$ (Grevesse and Noels 1993)[5]—low Z—high Z
Age	40 % $\Rightarrow$ 15 % if Z and evolutionary state are known[6]
α_{MLT}	1.7 ± 0.5 (Bonaca et al. 2012) (see also Sect. 3.1.2)

[1] From scaling relations (see e.g. A. Miglio et al. these proceedings).

[2] Values as low as 20 K can only be obtained for stars similar to the Sun and using a differential analysis (Meléndez et al. 2012).

[3] T. Morel, private communication (see also T. Morel, these proceedings).

[4] See M. Salaris, these proceedings.

[5] See also B. Plez & N. Grevesse, these proceedings.

[6] See also the discussion in A. Miglio et al. these proceedings, and references therein.

References

Asplund, M., Grevesse, N., Sauval, A. J., & Scott, P. 2009, ARA&A, 47, 481
Basu, S. & Antia, H. M. 2004, ApJ, 606, L85
Bonaca, A., Tanner, J. D., Basu, S., et al. 2012, ApJ, 755, L12
Brogaard, K., VandenBerg, D. A., Bruntt, H., et al. 2012, A&A, 543, A106

Broomhall, A.-M., Miglio, A., Montalbán, J., et al. 2014, MNRAS, 440, 1828
Bruntt, H., Bedding, T. R., Quirion, P.-O., et al. 2010, MNRAS, 405, 1907
Casagrande, L., Portinari, L., Glass, I. S., et al. 2014, MNRAS, 439, 2060
Castellani, V., Giannone, P., & Renzini, A. 1971, Ap&SS, 10, 340
Charbonnel, C. & Lagarde, N. 2010, A&A, 522, A10
Charbonnel, C. & Zahn, J.-P. 2007a, A&A, 476, L29
Charbonnel, C. & Zahn, J.-P. 2007b, A&A, 467, L15
Chiappini, C., Matteucci, F., & Romano, D. 2001, ApJ, 554, 1044
D'Antona, F., Bellazzini, M., Caloi, V., et al. 2005, ApJ, 631, 868
D'Antona, F., Caloi, V., Montalbán, J., Ventura, P., & Gratton, R. 2002, A&A, 395, 69
Eggenberger, P., Meynet, G., Maeder, A., et al. 2010, A&A, 519, A116
Eggleton, P. P., Dearborn, D. S. P., & Lattanzio, J. C. 2006, Science, 314, 1580
Eggleton, P. P., Dearborn, D. S. P., & Lattanzio, J. C. 2008, ApJ, 677, 581
Gabriel, M., Noels, A., Montalbán, J., & Miglio, A. 2014, A&A (submitted)
Geisler, D., Villanova, S., Carraro, G., et al. 2012, ApJ, 756, L40
Girardi, L., Eggenberger, P., & Miglio, A. 2011, MNRAS, 412, L103
Grevesse, N. & Noels, A. 1993, in Origin and Evolution of the Elements, ed. N. Prantzos, E. Vangioni-Flam, & M. Casse, 15–25
Houdek, G. & Gough, D. O. 2007, MNRAS, 375, 861
Jeffries, Jr., M. W., Sandquist, E. L., Mathieu, R. D., et al. 2013, AJ, 146, 58
Kato, S. 1966, PASJ, 18, 374
Lagarde, N., Romano, D., Charbonnel, C., et al. 2012, A&A, 542, A62
Ludwig, H.-G. & Salaries, M. 1999, in Astronomical Society of the Pacific Conference Series, Vol. 173, Stellar Structure: Theory and Test of Connective Energy Transport, ed. A. Gimenez, E. F. Guinan, & B. Montesinos, 229
Maeder, A. & Meynet, G. 2005, A&A, 440, 1041
McDonald, I., Boyer, M. L., van Loon, J. T., et al. 2011, ApJS, 193, 23
Meléndez, J., Bergemann, M., Cohen, J. G., et al. 2012, A&A, 543, A29
Miglio, A., Brogaard, K., Stello, D., et al. 2012, MNRAS, 419, 2077
Molenda-Żakowicz, J., Sousa, S. G., Frasca, A., et al. 2013, MNRAS, 434, 1422
Montalbán, J., Miglio, A., Noels, A., et al. 2013, ApJ, 766, 118
Montalbán, J. & Noels, A. 2013, in European Physical Journal Web of Conferences, Vol. 43, European Physical Journal Web of Conferences, 3002
Origlia, L., Rood, R. T., Fabbri, S., et al. 2007, ApJ, 667, L85
Pablo, H., Kawaler, S. D., & Green, E. M. 2011, ApJ, 740, L47
Paxton, B., Cantiello, M., Arras, P., et al. 2013, ApJS, 208, 4
Reimers, D. 1975, Memoires of the Societe Royale des Sciences de Liege, 8, 369
Schröder, K.-P. & Cuntz, M. 2005, ApJ, 630, L73
Schwarzschild, M. 1958, Structure and evolution of the stars. (Princeton University Press)
Siess, L. 2009, A&A, 497, 463
Silva Aguirre, V., Basu, S., Brandão, I. M., et al. 2013, ApJ, 769, 141
Stancliffe, R. J., Church, R. P., Angelou, G. C., & Lattanzio, J. C. 2009, MNRAS, 396, 2313
Ulrich, R. K. 1971, ApJ, 168, 57
Yıldız, M., Yakut, K., Bakış, H., & Noels, A. 2006, MNRAS, 368, 1941

Photospheric Constraints, Current Uncertainties in Models of Stellar Atmospheres, and Spectroscopic Surveys

Bertrand Plez and Nicolas Grevesse

Abstract We summarize here the discussions around photospheric constraints, current uncertainties in models of stellar atmospheres, and reports on ongoing spectroscopic surveys. Rather than a panorama of the state of the art, we chose to present a list of open questions that should be investigated in order to improve future analyses.

1 Introduction

We summarize here the questions that were raised during the discussion session following the talks on *Photospheric constraints, current uncertainties in models of stellar atmospheres, and reports on ongoing spectroscopic surveys.* Many of the issues that were discussed could not be settled, and most are also addressed in this volume's contributions. We refer to them in the text. This paper remains therefore mainly as a collection of questions, and tracks to be explored, in order to provide us with more definite answers on which we can rely for future work.

B. Plez (✉)
Laboratoire Univers et Particules de Montpellier, CNRS, Université Montpellier 2, Montpellier, France
e-mail: bertrand.plez@univ-montp2.fr

N. Grevesse
Centre Spatial de Liège, Université de Liège, avenue Pré Aily, B-4031 Angleur-Liège, Belgium

Institut d'Astrophysique et de Géophysique, Université de Liège, Allée du 6 Août, 17, B-4000 Liège, Belgium
e-mail: nicolas.grevesse@ulg.ac.be

A. Miglio et al. (eds.), *Asteroseismology of Stellar Populations in the Milky Way*,
Astrophysics and Space Science Proceedings 39,
DOI 10.1007/978-3-319-10993-0_20

2 Model Atmospheres

It was shown by M. Asplund that present 3D models outperform all 1D models, despite their coarser description of the radiation field. Solar abundances derived with 3D models, all indicators, atomic and molecular, being consistent, are at present in conflict with helioseismology. The predicted sound speed, the depth of the convection zone, and the He/H surface abundance, all are in error. The solution of this problem will probably affect all stars. This is a burning question, and its solution, either through a modification of the opacities, or some other mechanism is eagerly awaited. Could the solar 3D surface abundances increase again with further refinements of the models? This is unlikely, but a surprise is not to be excluded. Still, 3D models, obviously superior to 1D models, should be used in a broader range of studies, although the ease of use of 1D models make them hard to throw away from our toolboxes. A first approach is to use 1D averaged $\langle 3D \rangle$ models. They do not capture all the physics of full 3D atmospheres, but are as easy to use as a classical 1D model, in particular they can be used in NLTE studies. Grids should become available soon (M. Asplund).

3 Abundances and Stellar Parameters

T. Morel showed how the use of seismic gravities in 1D, LTE abundance analyses lead to discordances between neutral and ionized iron abundances. NLTE effects are of the order of 0.2 dex for dwarfs, and 0.4 dex for giants, the effect being greater at low metallicity, and lower gravity. Fe II lines seem to be a better iron abundance indicator, however, we know that iron lines are sensitive to 3D effects and to $T_{\rm eff}$. So far no 3D NLTE analysis of iron lines has been carried out. Reliable collisional cross sections with hydrogen and electrons are still missing for NLTE calculations. Progress will be made in the years to come that will probably improve the abundance determinations. For the time being we still don't know if Fe I or Fe II are reliable iron abundance indicators (T. Morel).

It is important here to recall that spectroscopists will more and more use asteroseismic gravity (and $T_{\rm eff}$) determinations in order to avoid using the iron ionization balance, or to test spectroscopic methods. Asteroseismologists on the other hand use spectroscopic gravities to test their inversion algorithms. We must be careful here not to go in circles, and be aware of the limitations on both sides. From what was quoted at this conference (e.g. D. Stello, and K. Brogaard) gravities from asteroseismology are more accurate than spectroscopic gravities, and this will remain true in the years to come. We must strive to understand the systematics behind this difference in gravity, using 3D and NLTE studies on representative samples of stars. The determinations of $T_{\rm eff}$ are not all in agreement. G. Zasowski showed the systematic differences between photometric and spectroscopic determinations. These must also be understood. Finally we should not forget uncertainties

in atomic and molecular data (oscillator strengths, partition functions, ionization and dissociation potentials, etc.).

4 The Contribution of Large Surveys

The numerous on-going and planned surveys require a transition from detailed hand-made analyses of a few stars, using a few lines, to automated fits of very large samples using thousands of lines. In the questions raised, the above detailed surveys will undoubtedly help. The large number of stars with parameters spanning a large range of values helps highlight the errors, and delineate their causes (3D, NLTE, reddening, general calibration, ...). However, they must be completed by dedicated studies on smaller samples of well observed, well known objects, e.g. nearby stars with well-known distances, luminosities, diameters, masses. These detailed studies must be carried out with the best possible ensemble of techniques, models, and data. Current surveys do indeed include such studies in their design.

5 Atmospheres as Boundaries

Model atmospheres can also, and are used as boundary conditions for stellar structure and evolution models. It was shown by P. Marigo that the surface properties of RGB models depend critically on that boundary condition and on the adopted convection theory. The effective temperatures can shift by almost 100 K in response to a change of the mixing-length parameter of only 0.1. Detailed 3D model atmospheres, after proper 1D averaging, could be used to provide either a calibration of the mixing-length parameter, or better, thermal and pressure profiles (or whatever thermodynamical variable is appropriate) for inclusion in stellar evolution models. Maybe these 3D models should be calculated to deeper depths (M. Asplund). The same 3D models can be used to provide recipes for turbulent pressure and overshoot, or to better quantify mode excitation and damping rates (M. Asplund).

Conclusion
Confronting our results from asteroseismology and spectroscopy/photometry is an absolutely crucial step in our quest for better constrained stellar parameters, leading to our understanding of stellar and galactic evolution. Conferences like this one greatly contribute to making us all aware of the limitations of the various methods, encouraging us to join in our efforts to understand and resolve systematics and errors.